Many-Body Localization for Decoherence Protected Quantum Memory

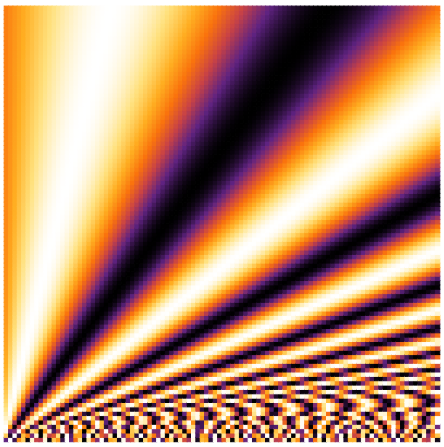

Von der Fakultät für Mathematik, Informatik und Naturwissenschaften der RWTH Aachen University zur Erlangung des akademischen Grades eines Doktors der Naturwissenschaften genehmigte Dissertation

vorgelegt von

Evangelos Varvelis, M. Sc.
aus
Veroia, Griechenland

Berichter: Prof. Dr. David DiVincenzo
Prof. Dr. Fabian Hassler

Tag der mündlichen Prüfung: 22.08.2023

Diese Dissertation ist auf den Internetseiten der Universitätsbibliothek verfügbar.

Eidesstattliche Erklärung

Declaration of Authorship

I, Evangelos Varvelis

declare that this thesis and the work presented in it are my own and has been generated by me as the result of my own original research.

Hiermit erkläre ich an Eides statt / I do solemnely swear that:

1. This work was done wholly or mainly while in candidature for the doctoral degree at this faculty and university;
2. Where any part of this thesis has previously been submitted for a degree or any other qualification at this university or any other institution, this has been clearly stated;
3. Where I have consulted the published work of others or myself, this is always clearly attributed;
4. Where I have quoted from the work of others or myself, the source is always given. This thesis is entirely my own work, with the exception of such quotations;
5. I have acknowledged all major sources of assistance;
6. Where the thesis is based on work done by myself jointly with others, I have made clear exactly what was done by others and what I have contributed myself;
7. Parts of this work have been published before as: list references below

[1] C. Berke, E. Varvelis, S. Trebst, A. Altland and D. P. DiVincenzo:
'Transmon platform for quantum computing challenged by chaotic fluctuations',
Nature communications 13, 1–10 (2022).

[2] E. Varvelis and D. P. DiVincenzo:
'Perturbative analysis of quasi-periodic patterning of transmon quantum computers: enhancement of many-body localization',
arXiv preprint arXiv:2212.03805 (2022)

Date:

Signature:

Abstract

In recent years, the field of quantum information has witnessed remarkable progress through the utilization of superconducting qubits. Nonetheless, despite these advancements, significant hurdles persist when it comes to scaling up these systems. One critical challenge that this thesis aims to tackle is the phenomenon of decoherence, whereby a quantum system behaves akin to a classical system in thermal equilibrium. However systems can avoid thermalization if they are in the many-body localized phase.

The main objective of this thesis is to investigate the potential of MBL in protecting quantum memories from decoherence. We pursue a two-fold approach: firstly, we establish the existence of a thermal to MBL phase transition in disordered transmon arrays. To achieve this, we employ well-established diagnostics such as level spacing distribution and inverse participation ratio (IPR). Additionally, we introduce a new diagnostic tool called the Walsh-Hadamard coefficients, which reinforce the findings of IPR in a basis-independent manner. We apply these diagnostics to both 1D and 2D transmon arrays with Gaussian disorder, as well as chains with designed frequency patterns using the LASIQ technique.

Furthermore, we demonstrate that disorder-free systems can also exhibit MBL by compensating for the absence of disorder through the utilization of quasi-periodic frequency patterns. Surprisingly, we find that these systems not only achieve localization, but also surpass the localization observed in comparable systems with Gaussian disorder. Finally, we develop a perturbation theory scheme that enables the determination of the Walsh-Hadamard coefficients for large transmon lattices, which are comparable to experimental devices.

Keywords: Quantum Information, Qubits, Transmons, Dephasing, Quantum Chaos, Thermalization, Random Matrix Theory, Anderson Localization, Many-Body Localization, Walsh-Hadamard Transformation, Local Integral of Motion, Quasi-Periodic Potential

Abstrakt

In den letzten Jahren wurden auf dem Gebiet der Quanteninformation durch die Nutzung supraleitender Qubits bemerkenswerte Fortschritte erzielt. Dennoch bestehen trotz dieser Fortschritte weiterhin erhebliche Hürden bei der Skalierung dieser Systeme. Eine entscheidende Herausforderung, die in dieser Arbeit diskutiert wird, ist das Phänomen der Dekohärenz, bei dem sich ein Quantensystem ähnlich wie ein klassisches System im thermischen Gleichgewicht verhält. Allerdings können Systeme eine Thermalisierung vermeiden, wenn sie sich in der lokalisierten Vielkörperphase befinden.

Das Hauptziel dieser Arbeit besteht darin, das Potenzial von Vielkörperlokalisierung zum Schutz von Quantenspeichern vor Dekohärenz zu untersuchen. Wir verfolgen einen dualen Ansatz: Zuerst weisen wir die Existenz eines thermischen Phasenübergangs zur MBL-Phase in ungeordneten Transmon-Arrays nach. Um dies zu erreichen, verwenden wir bewährte Diagnoseverfahren wie die Verteilung der Niveauabstancle und das inverse Participation Ratio (IPR). Darüber hinaus stellen wir ein neues Diagnosetool namens Walsh-Hadamard-Koeffizienten vor, das die Ergebnisse von IPR auf basisunabhängige Weise untermauert. Wir wenden diese Diagnostik sowohl auf 1D- als auch auf 2D-Transmon-Arrays mit Gaußschen Störungen sowie auf Ketten mit designten Frequenzmustern unter Verwendung der LASIQ-Technik an.

Darüber hinaus zeigen wir, dass auch störungsfreie Systeme MBL aufweisen können, indem sie das Fehlen von Störungen durch die Nutzung quasiperiodischer Frequenzmuster kompensieren. Überraschenderweise stellen wir fest, dass diese Systeme nicht nur eine Lokalisierung erreichen, sondern auch die in vergleichbaren Systemen mit Gaußschen Störungen beobachtete Lokalisierung übertreffen. Abschließend entwickeln wir ein Störungstheorieschema, das die Bestimmung der Walsh-Hadamard-Koeffizienten für große Transmongitter ermöglicht, die mit experimentellen Aufbauten vergleichbar sind.

Acknowledgements

I would like to take a few lines to thank everyone that contributed to the completion of this thesis one way or another.

I would like to thank the person without whom none of this would have been possible. David DiVincenzo thank you for providing such an interesting topic and for being an excellent supervisor. I have the utmost respect for you as a scientist and person. It has been an incredible experience collaborating with you. You have shaped my thinking as a physicist, and I will always remember your advice for approaching research by following my curiosity rather than an "assembly line production schedule".

I would also like to thank Fabian Hassler for being an unofficial mentor and a great friend. I will cherish the wonderful discussions we had for physics and beyond. It has also been great fun hanging out with you for a drink after work. At this point I would also like to thank Daniel Zeuch who has been a great support during my early years in Aachen. Of course I could not forget Helen Barton for her infinite patience in helping me with the bureaucratic nightmares of the PhD.

To my friends from the IQI, Alexander Ziesen, Martin Rymarz and Lisa Otten, I cannot begin to describe how important you have been to me since the beginning. You have made Aachen and the IQI feel like home and for that I am forever grateful. Alex, thank you very much for the unlimited support all these years for acclimatizing to German culture and for helping rid the solar system from various alien invasions. I wish you and Svenja a wonderful journey through life and parenthood. Martin, thank you for educating me into a coffee connoisseur and all the fun discussions about German pop culture. Lisa, you have been a great support during the thesis submitting process and your red velvet cookies are going to haunt me for the rest of my life. I will miss cooking with you.

Thanks to Manuel Rispler, Veit Langrock, Steve Kim and Anton Montag for making the coffee breaks and the the extracurricular activities of IQI more fun.

I want to also thank my parents for their unwavering support all these years, and for reminding me that "the stage is too big for the drama". Mom thank you very much for your continued effort to keep the channels of communication open and taking a great interest in my work. Dad thank you for pushing me to become the best version of myself.

Finally many special thanks to Kostis Revis for all the fun, the deep discussions and his gym brotherhood. Antigone Karavelaki, thank you for making life more exciting and the final stages of the thesis writing feel less painful.

Contents

Preface

The numerical simulation of quantum systems in many-body physics has long posed a significant challenge for classical computers. Due to the exponential scaling of degrees of freedom with system size, computational memory becomes a limiting factor. A potential solution to this problem emerged in 1982 when Feynman introduced the concept of quantum computers, which utilize quantum systems for simulations [1]. Although the groundwork for quantum information was laid with this proposal, numerous technological obstacles had to be overcome before the realization of such a device became feasible. The field experienced a resurgence of interest in 1994 when Shor presented his renowned algorithm [2] for prime factorization with a quantum computer.

In present times, numerous prototype quantum computing devices with several hundred qubits have already been developed [3–5]. Despite these remarkable technological achievements, the realization of large-scale quantum computing continues to face significant challenges due to technological limitations. One of the primary obstacles for scaling up these devices is decoherence, which is the process whereby quantum systems become entangled with their surroundings, leading to the diffusion of quantum information. Once decoherence takes place, the system no longer displays quantum behavior but instead behaves as a classical system in thermal equilibrium described by a thermodynamic ensemble.

However, it is important to note that not all systems undergo thermalization. Specifically, systems that display insulating behavior can evade this fate through the phenomenon of many-body localization. In many-body localization, the correlations between various degrees of freedom diminish exponentially over distance, allowing systems in this phase to preserve their quantum information for extended periods by preventing entanglement with their surrounding environment.

The main objective of this thesis is to investigate the potential of protecting quantum computing devices from decoherence through the implementation of MBL. To conduct a thorough analysis, a specific qubit platform needed to be selected, and in this case, we chose superconducting qubits operated in the trans-

mon regime. Although the findings presented here are focused on the transmon architecture for quantum computing, we believe that similar conclusions can be extrapolated to other architectures as well.

To address our research question, we will approach it in two stages. Firstly, we aim to determine whether transmon qubits exhibit thermalization and, if so, whether a transition to a MBL phase occurs. To draw insights, we can consider the classical analog of an array of interacting transmons, which can be likened to a system of interacting pendulums. As a classical system, it serves as a typical example of a chaotic system. According to the Bohigas-Giannoni-Schmit conjecture [6], the quantized system should demonstrate quantum chaos, which is associated with thermalization. Through our investigation, we will establish that by introducing sufficient disorder, in the form of random fluctuations in the Josephson energies of the transmons, the system can indeed undergo a transition from chaotic to an MBL phase. For this we will use the standard diagnostics of this transition and we will also establish a new one, the Walsh-Hadamard transformation, tailored for the MBL phase of the system.

From an engineering perspective, relying solely on randomness as a mean of protecting our system may not be considered a reliable approach. Therefore, we will also investigate the potential of localizing transmon arrays using quasi-periodic potentials that mimic disorder. To explore this possibility, we will primarily employ the Walsh-Hadamard transform and employ perturbation theory arguments. By adopting a semi-analytical approach, we will be able to calculate the Walsh-Hadamard coefficients of large systems beyond the what is possible by means of exact diagonalization. Our findings reveal that the system can indeed be effectively localized using quasi-periodic potentials, and intriguingly, this approach can achieve even stronger localization than random disorder.

While the approach for studying MBL using transmons [7] we offer a new prospective by taking under consideration MBL effects for the design and reliable operation of transmon qubits. We firmly believe that interaction between the fields of quantum information and MBL physics can prove fruitful for the further development of both. Finally our quasi-periodic potential approach to localization can open new fields of research for designing potentials for optimal operation of transmon qubits, with our novel tool of the Walsh-Hadamard transformation at its core.

The structure of this thesis is as follows: In chapter 1, we will introduce fundamental concepts of quantum information, such as qubits, entanglement, and dephasing (1.1), as well as essential aspects of transmon qubits that will be utilized consistently throughout the thesis (1.2)

In Chapter 2, we will provide a concise overview of thermalization (2.1) by establishing a connection between the eigenstate thermalization hypothesis and the predictions derived from random matrix theory, which describe quantum

chaotic systems. Subsequently, we will outline the pertinent aspects of MBL phenomenology for our study (2.2), as well as the probes we will employ to investigate the transition from chaotic to MBL behavior.

In chapter 3 we introduce the Walsh-Hadamard transformation as a tool to study localization and its connection to the LIOM of MBL (3.1). We will also develop a perturbation theory scheme for the calculation of Walsh-Hadamard coefficients for a specific class of Hamiltonians (3.2).

In chapter 4 we will explore the phase transition of 1D transmon chains with Gaussian disorder from chaotic to MBL(4.1).To ensure better comparability with experimental devices we also apply our diagnostics for modern architectures, including 2D lattice configurations and a new method for tuning Josephson junctions post fabrication to control disorder (4.2).

Finally in chapter 5 we explore the potential of quasi-periodic transmon frequency patterns for localizing the system. Initially we will introduce the details of the model under consideration, based on the Aubry-André model, and its Anderson localization (5.1). We conclude the chapter by comparing the MBL of our system with one using Gaussian disorder and obtain perturbatively the Walsh-Hadamard coefficients for a large transmon array of size comparable to that of experimental devices (5.2).

1

Quantum Information and Transmon Qubits

In this chapter, we will provide an introduction to key concepts in quantum information and explore the utilization of superconducting circuits operating in the transmon regime as quantum memories. We will begin by offering a concise overview of the fundamental resources in quantum information (1.1.1), namely qubits and entanglement. Following that, we will present a simple demonstration of dephasing in quantum systems (1.1.2). Our focus will then shift to superconducting circuits as carriers of quantum information, where we will provide a brief introduction to the basic principles of the charge qubit operated in the transmon regime (1.2.1). Finally, we will introduce an effective model description for an array of N transmons interacting via capacitors (1.2.2).

1.1 Quantum Information Theory

Quantum information theory tries to utilize quantum systems as carriers of information, called qubits. To create a functional quantum computer, it is necessary to have multiple qubits that can interact with one another, thereby generating entanglement. In the subsequent subsection 1.1.1, we will provide a concise introduction to qubits and entanglement as foundational concepts. Once these key notions are established, we will promptly move on to demonstrating the emergence of dephasing phenomena in systems consisting of multiple interacting qubits in subsection 1.1.2.

1.1.1 Qubits and Entanglement

The main idea behind quantum information is to augment the unit of classical information into a quantum system. This unit, called the bit, is a scalar variable that takes two possible values 0 and 1. For quantum system we can represent these two values as two states $|0\rangle$ and $|1\rangle$ in a 2D Hilbert space. However a quantum system can be in any superposition of the two states as well and therefore the basic unit of quantum information, the qubit, will be a vector in the 2D Hilbert space

$$|\psi\rangle = \alpha|0\rangle + \beta|1\rangle \tag{1.1}$$

where α and β are complex values. Their absolute value squared corresponds to the probability of the qubit state $|\psi\rangle$ being measured in state $|0\rangle$ or $|1\rangle$ respectively and therefore they are bound by the normalization condition

$$|\alpha|^2 + |\beta|^2 = 1 \tag{1.2}$$

Another important resource of quantum information is entanglement. This property can emerge only for systems with more than one qubit that are interacting in some manner. The state $|\psi_{\text{tot}}\rangle$ of a non-entangled n-qubit system in turn is described by the tensor product of the states of its subsystems

$$|\psi_{\text{tot}}\rangle = |\psi_1\rangle \otimes |\psi_2\rangle \otimes \cdots \otimes |\psi_n\rangle = |\psi_1, \psi_2, \dots, \psi_n\rangle. \tag{1.3}$$

We use both of these notations interchangeably. States that can be written in this form are called separable. Entangled states on the other hand cannot be written in a product form. Consider for example the 2-qubit state

$$|\Phi_+\rangle = \frac{1}{\sqrt{2}}(|00\rangle + |11\rangle). \tag{1.4}$$

We can try expressing this in the form of a tensor product of two arbitrary qubit states like the one in Eq. (1.1)

$$\frac{1}{\sqrt{2}}(|00\rangle + |11\rangle) = (\alpha_1|0\rangle + \beta_1|1\rangle) \otimes (\alpha_2|0\rangle + \beta_2|1\rangle) \tag{1.5}$$

Simple algebraic arguments can convince one that these equations are not solvable and therefore the state of Eq. (1.4) is not separable.

Since entangled states do not support a vector state representation for their subsystems we can switch to a broader representation for quantum states, the density matrix. For a state $|\psi\rangle$ as the one in Eq. (1.1) which supports a vector

state representation, we say that it is a pure state and the corresponding density matrix is defined simply as

$$\rho = |\psi\rangle\langle\psi| = \begin{pmatrix} |\alpha|^2 & \alpha\beta^* \\ \alpha^*\beta & |\beta|^2 \end{pmatrix}. \tag{1.6}$$

If we go to the eigenbasis of this matrix we can see that the diagonal elements should then correspond to probabilities and therefore they would have to be real, positive and adding up to 1. In other words any density matrix should be Hermitian, positive semi-definite and with trace 1.

However not all matrices that satisfy the above mentioned criteria are of the form of Eq. (1.6). Those that cannot be written in that form correspond to the so called mixed states and these are precisely the states that do not have a vector state representation. We distinguish pure from mixed states by the calculating the square of the density matrix. For a pure state it is trivial to see from Eq. (1.6) that $\rho^2 = \rho$ while for a mixed this will not be true.

In the most general case therefore the density matrix of a qubit is going to be of the form

$$\rho = \frac{1}{2}(1 + \vec{n}\cdot\vec{\sigma}) = \frac{1}{2}\begin{pmatrix} 1-z & x-iy \\ x+iy & 1+z \end{pmatrix}, \tag{1.7}$$

where $\vec{n} = (x, y, z)^T$ is some $\mathbb{R}^3$ vector and $\vec{\sigma} = (X, Y, Z)^T$ is the vector of Pauli matrices. From the form of Eq. (1.7) it is easy to verify that this matrix respects all the previously mentioned conditions to qualify as density matrix, assuming $||\vec{n}|| \leq 1$. Additionally from squaring this expression we obtain

$$\rho^2 = \frac{1}{4}(1 + \vec{n}\cdot\vec{\sigma})(1 + \vec{n}\cdot\vec{\sigma}) = \frac{1}{2}\left(\frac{1 + ||\vec{n}||^2}{2} + \vec{n}\cdot\vec{\sigma}\right) \tag{1.8}$$

so we notice that in general $\rho^2 \neq \rho$ except for the case that the norm of the vector $\vec{n}$ is 1. This naturally leads to the representation of pure single qubit states as vectors on a unit sphere, called Bloch sphere while the mixed states land somewhere inside the sphere. From this we can conclude that the maximally mixed state is the one with $\vec{n}$ being the zero vector, in the sense that it is the furthest away from a pure state.

For separable states we can still define the total state of the system via the tensor product

$$\rho_{\text{tot}} = \rho_1 \otimes \rho_2 \otimes \cdots \otimes \rho_n \tag{1.9}$$

while the entangled states cannot be written in the form once again. However, given the total density matrix of the system we can recover some information about the state of a subsystem using the partial trace. For a 2-qubit state ρ_{12} the

partial trace with respect to subsystem 2 is

$$\rho_1 = \mathrm{Tr}_2(\rho_{12}) = \mathrm{Tr}_2\left(\sum_{i,j,k,\ell=0}^{1} \rho_{12}^{(ijk\ell)} |ij\rangle\langle k\ell|\right) \tag{1.10}$$

$$= \sum_{i,j,k,\ell=0}^{1} \rho_{12}^{(ijk\ell)} |i\rangle\langle k| \sum_{m=0}^{1} \langle m|j\rangle\langle \ell|m\rangle \tag{1.11}$$

$$= \sum_{i,k,m=0}^{1} \rho_{12}^{(imkm)} |i\rangle\langle k|. \tag{1.12}$$

For the case of a separable state this simply reduces to $\mathrm{Tr}_2(\rho_1 \otimes \rho_2) = \rho_1 \mathrm{Tr}(\rho_2) = \rho_1$ while for an entangled state the partial trace has no vector state counterpart and therefore will be a mixed state.

Finally we will quantify the entanglement of a state by the degree to which its subsystems are mixed. The measure we use for that is the normalized von Neumann entropy [8] or entanglement entropy defined as

$$S(\rho_A) = -\mathrm{Tr}(\rho_A \log_2 \rho_A) \tag{1.13}$$

where ρ_A is the partial trace of a system with respect to the complement of A. Assuming that ρ_A is a qubit state we can re-express the von Neumann entropy in terms of the Bloch vector norm by diagonalizing the density matrix of Eq. (1.7)

$$\det(\rho_A - \lambda) = 0 \Rightarrow \lambda = \frac{1}{2}(1 \pm \|\vec{n}\|) \tag{1.14}$$

and therefore

$$S(\rho_1) = -\frac{1+\|\vec{n}\|}{2} \log_2\left(\frac{1+\|\vec{n}\|}{2}\right) - \frac{1-\|\vec{n}\|}{2} \log_2\left(\frac{1-\|\vec{n}\|}{2}\right). \tag{1.15}$$

From this expression it is straightforward to see that for a separable state, and thus pure partial trace with $\|\vec{n}\| = 1$ the von Neumann entropy vanishes while for a maximally entangled state and therefore maximally mixed partial trace with $\|\vec{n}\| = 0$ we have $S(\rho_A) = 1$. For more detail on what was presented here see [B1].

1.1.2 Dephasing

We have covered briefly two key static aspects of quantum information theory: qubits and their entanglement. Here we will discuss some dynamical aspects. Specifically we are interested on how arrays of qubits can be used as quantum

memories. While the classical intuition would be to initialize the system in the desired state that we want to store and then isolate it somewhere undisturbed, reality is not that simple for quantum systems.

Even isolated from their environments, they possess some Hamiltonian H that according to the Schrödinger equation generates dynamics for any arbitrary state $|\psi(t)\rangle$

$$i\partial_t|\psi(t)\rangle = H|\psi(t)\rangle \Rightarrow |\psi(t)\rangle = e^{-iHt}|\psi(0)\rangle \tag{1.16}$$

where we have set $\hbar = 1$ here and throughout the rest of the thesis. An equivalent equation for the density matrix evolution is the von Neumann equation

$$i\partial_t\rho(t) = [H, \rho] \Rightarrow \rho(t) = e^{-iHt}\rho(0)e^{iHt} \tag{1.17}$$

For the case of pure states it is straightforward to see that these two are equivalent by substituting $\rho(t) = |\psi(t)\rangle\langle\psi(t)|$ in Eq. (1.17) and then using the Schrödinger equation to complete the proof. Therefore, unless the system is prepared in an eigenstate of the Hamiltonian, its state will time evolve under its own influence. This characteristic of quantum systems makes the storage of quantum information challenging.

We will demonstrate this here now for a specific choice of system. Consider the 1D spin chain with Hamiltonian

$$H_{ZZ} = \sum_{i=1}^{L} \omega_i Z_i + J \sum_{i=1}^{L-1} Z_i Z_{i+1}, \tag{1.18}$$

where Z_i is the Pauli z matrix acting on site i. Since spin-1/2 particles are 2-level systems they qualify as qubits [9] and therefore the system described by this Hamiltonian is that of a qubit array of length L.

Assuming that $J = 0$ for a moment we can see that the system is no longer interacting and therefore whatever dynamics it has should be trivial. We will prove this right away by making an assumption about the system initialization. We assume that the system is initialized in a product state

$$\rho(0) = \rho_1(0) \otimes \cdots \otimes \rho_L(0) = \bigotimes_{j=1}^{L} \rho_j(0) \tag{1.19}$$

For $J = 0$ the time evolution of the system is separable since every term commutes with every other term and therefore

$$\rho(t) = e^{-iHt} \bigotimes_{j=1}^{L} \rho_j(0) e^{iHt} = \bigotimes_{j=1}^{L} e^{-i\omega_j Z_j t} \rho_j(0) e^{i\omega_j Z_j t}. \tag{1.20}$$

Since each part of the system evolves unitarily they will all remain in a pure state, since we started in a separable state

$$\rho_j(t)^2 = \left(e^{-i\omega_j Z_j t}\rho_j(0)e^{i\omega_j Z_j t}\right)^2 = e^{-i\omega_j Z_j t}\rho_j(0)^2 e^{i\omega_j Z_j t} = \rho_j(t), \tag{1.21}$$

in other words the entanglement entropy remains constantly at zero for any partition of the system.

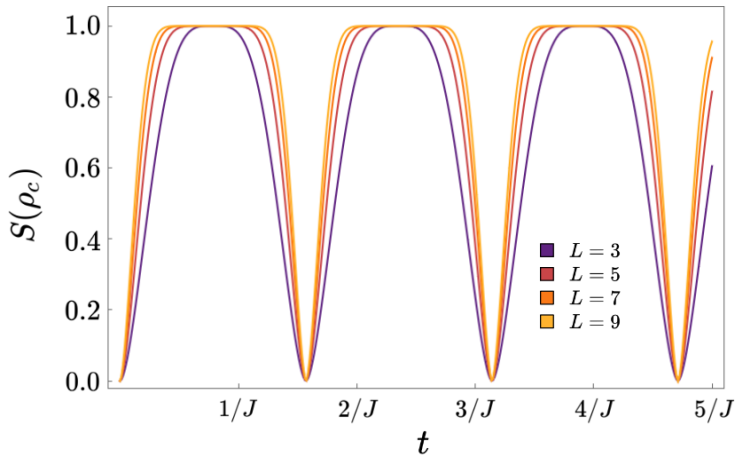

Figure 1.1: Entanglement entropy as a function of time. We present the entanglement entropy of a qubit located at the center of a 1D lattice evolving under the Hamiltonian of Eq. (1.18). We performed this calculation numerically for random ω_i drawn from a Gaussian distribution of mean 5 GHz and standard deviation 0.3GHz for odd chain lengths $L = 3$ through 9. Time is given in units of the inverse of the coupling strength J which was fixed at 1 MHz. The initial state of the system is chosen randomly from the set of product states with each subsystem lying on the equator of the Bloch sphere.

If we now turn the coupling J back on and starting again with the assumption of a separable initial state the dynamics are no longer trivial. The time evolution is no longer separable and we cannot make a simple analytic argument about the entanglement entropy of the system. We can however calculate the dynamics numerically for finite size systems. We performed this numerical analysis and the results are reported in Fig. 1.1. Since there is some randomness involved in our initialization of the system we needed to make sure that the system is initialized far from an eigenstate. The eigenstates of the Hamiltonian in Eq. (1.18) are obviously product states of the eigenstates of the Z matrix therefore we chose to initialize the system in product states of the form

$$\rho(0) = \frac{1}{2^L}\bigotimes_{j=1}^{L}\begin{pmatrix} 1 & e^{-i\phi_j} \\ e^{i\phi_j} & 1 \end{pmatrix} \tag{1.22}$$

In other words we chose the initial state of each qubit to be the furthest away possible from a Z eigenstate which corresponds to the states with 0 z-component for the Bloch vector. The ϕ_j angles are chosen randomly.

We immediately notice that the situation is drastically different with $J \neq 0$. Even thought the system as a whole evolves unitarily with the global state remaining pure, the qubits become maximally entangled. As a result, the partial trace of the system evolves from a pure state to a completely mixed state, something which is not possible for unitary dynamics as we have seen. Therefore the quantum information of a single qubit at the center of the lattice spreads out completely to the rest of the system. This is reminiscent to the mechanism of dephasing.

In dephasing, a density matrix undergoes non-unitary evolution and transitions into a mixed state by gradually erasing its off-diagonal elements. In the case of a qubit state, this corresponds to the shrinking of its Bloch vector and its alignment with the z-axis. Dephasing is part of a broader category of processes known as decoherence, wherein quantum systems exhibit classical behavior. Decoherence typically occurs in open systems that interact with an external reservoir. However, in the present case, the role of the reservoir is played by the system itself, which acts on one of its qubits.

The situation becomes progressively more dire as we increase the length of the chain, by reaching maximum entropy faster and remaining there for longer times. We do also recover the initial state of the system periodically in time and for brief intervals which become smaller and smaller as we increase L. This is the well know phenomenon of quantum revivals [10].

The reason we did not compare the time evolution of the two cases directly is because the time evolution of the states is frame dependent. For example we can always go to the Heisenberg frame and then states do not evolve for any system. However entanglement entropy as it was defined in Eq. (1.13) is frame independent because of the trace. Therefore it makes a stronger statement about why for $J = 0$ the system has no dynamics and is thus an ideal quantum memory while for $J \neq 0$ it has dynamics and local information of the system becomes scrambled.

Maintaining control over the type of dephasing we have demonstrated here is of utmost importance for a system designed to function as a quantum memory. The conventional approach to achieve this control is by minimizing the coupling as much as possible. However, this presents a challenge as it leads to longer gate operation times required for qubit manipulation. We will show later on, that an alternative solution to address this issue is to increase the spread of qubit frequencies, denoted as ω_i, using the phenomenon of many-body localization.

1.2 The Transmon as a Qubit Platform

In recent years, one of the most promising platforms for quantum computation has been superconducting qubits, particularly when operated in the transmon regime [3, 4]. Here we outline briefly the main idea behind charge qubits and the crucial role of anharmonicity for their manipulation in subsection 1.2.1. Once the charge qubit has been introduced, we derive an effective description of the system of capacitively coupled transmons as a Bose-Hubbard model in subsection 1.2.2.

1.2.1 The Role of Anharmonicity

As we have mentioned earlier any quantum system with two discrete energy levels can be a qubit. But most quantum systems have more energy levels. This is not a problem as long as we can guarantee that our system will remain confined in the Hilbert space defined by two energy levels, typically the ground state $|0\rangle$ and the first excited state $|1\rangle$. One of the first ideas that come to mind for the implementation of a qubit is the harmonic oscillator

$$H_{\mathrm{HO}} = \frac{p^2}{2m} + \frac{1}{2}m\omega^2 x^2 \tag{1.23}$$

with x and p the position and momentum operator of the oscillator respectively and their commutation relation

$$[x, p] = i \tag{1.24}$$

Upon closer examination, it becomes apparent that the chosen realization of a qubit using a harmonic oscillator poses a fundamental problem. The energy levels in this system are equally spaced, indicating that the frequency driving the transition between $|0\rangle$ and $|1\rangle$ is the same as the frequency for the transition between $|1\rangle$ and $|2\rangle$, and so on. Consequently, during the necessary manipulations for quantum computation, our system can evolve outside the designated qubit sector of the Hilbert space. This phenomenon is commonly referred to as leakage.

We can avoid this issue if we introduce some anharmonicity in the system. For example we can consider the system of a pendulum in a gravitational field

$$H_{\mathrm{P}} = \frac{p^2}{2m} + mg\ell(1 - \cos(x)). \tag{1.25}$$

For the quantized Hamiltonian the constant term $mg\ell$ contributes only a global phase for the eigenstates and a constant shift for all energy levels therefore it can

be ignored

$$H_{\mathrm{P}} = \frac{p^2}{2m} - mg\ell\cos(x). \tag{1.26}$$

Manufacturing such a quantum system is preposterous, the mass of the oscillator would have to be so small that gravitational effects could no longer be relevant. What we can use instead is the electric circuit analogue of the system. For the harmonic oscillator the corresponding circuit is the well know LC circuit

$$H_{\mathrm{LC}} = \frac{Q^2}{2C} + \frac{\Phi^2}{2L} \tag{1.27}$$

where Q is the charge of the capacitor with capacitance C and Φ is the flux through the inductor of inductance L defined as

$$\frac{d\Phi}{dt} = V(t). \tag{1.28}$$

Since the charge and the voltage are related via the known relation

$$Q = CV \Rightarrow \frac{d\Phi}{dt} = \frac{Q}{C}, \tag{1.29}$$

therefore the role of momentum is carried by the charge while the role of position is carried by the flux and the mass of the system corresponds to the capacitance.

From this we can already make an ansatz for the Hamiltonian of the circuit analogue of the pendulum

$$H_{\mathrm{PA}} = \frac{Q^2}{2C} - E_{\mathrm{J}}\cos(2\pi\Phi/\Phi_0). \tag{1.30}$$

The kinetic term of this Hamiltonian is equivalent to the one in Eq. (1.27) therefore it should also describe a capacitor. The second term however describes a superconducting non-linear element called Josephson junction. The constant $\Phi_0 = h/(2e)$ is called the flux quantum with h being Planck's constant and e the electron charge. E_{J} is the Josephson energy related to the critical current I_{c} of the junction via the relation $E_{\mathrm{J}} = \Phi_0 I_{\mathrm{c}}/(2\pi)$. We will take a phenomenological approach here and we will not go through the details of superconductivity. For more details on superconductivity see [B2] and for a more detailed derivation of the Hamiltonian Eq. (1.30) see [11].

For convenience we define two dimensionless variables, the quantized superconducting phase $\varphi = 2\pi\Phi/\Phi_0$ and the quantized charge $n = Q/(2e)$. The charge is quantized in multiples of $2e$ since the superconducting current consists of Cooper pairs. With these new definitions we rewrite the Hamiltonian of the charge qubit as

$$H_{\mathrm{CQ}} = 4E_{\mathrm{C}}(n - n_{\mathrm{g}})^2 - E_{\mathrm{J}}\cos\varphi \tag{1.31}$$

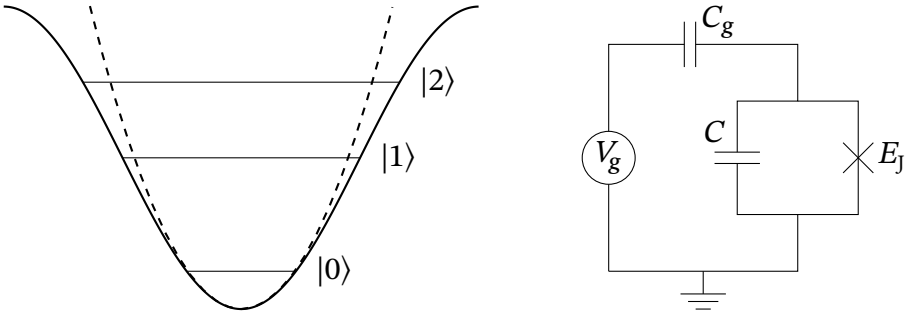

Figure 1.2: Charge Qubit. On the left panel we present a qualitative sketch of the first three energy levels of the charge qubit also comparing the potential to that of the harmonic oscillator. On the right we present the circuit analogue of a pendulum. In the circuit we have a voltage source denoted V_g which is connected via the capacitor C_g to a Josephson junction (denoted by and x) shunted by the capacitance C. The circuit is called a charge qubit or Cooper pair box.

where we have also included an offset charge n_g and also define the capacitive energy unit $E_C = e^2/(2C_{tot})$ with $C_{tot} = C + C_g$ the total capacitance of the system (see Fig. 1.2). Drawing again from the correspondence to position and momentum operators our new variables will have the commutation relation

$$[\varphi, n] = i \tag{1.32}$$

If we write the eigenvalue problem for the Hamiltonian of Eq. (1.31) in the phase basis we obtain the differential eigenvalue problem

$$\left[4E_C\left(i\partial_\varphi + n_g\right)^2 - (E_n + E_J\cos\varphi)\right]\psi_n(x) = 0 \tag{1.33}$$

with the boundary condition $\psi_n(\varphi) = \psi_n(\varphi+2\pi)$. After the substitution $g_n(x) = e^{-2in_g x}\psi_n(2x)$ Eq. (1.33) yields

$$\left[\partial_x^2 + \left(\frac{E_n}{E_C} + \frac{E_J}{E_C}\cos(2x)\right)\right]g_n(x) = 0 \tag{1.34}$$

with the accompanying boundary condition $g(x) = e^{i2\pi n_g}g(x+\pi)$. Eq. (1.34) is called the Mathieu differential equation with exact eigenvalues and eigenfunctions given by the Mathieu functions [B3]. Using these function we plot the spectrum of the system for the first three energy levels in Fig. (1.3). There we have plotted the spectrum as a function of the gate charge for 4 different values of the ratio E_J/E_C. Our first observation is that the energy levels are not equidistant as in the case of the harmonic oscillator. However the spectrum fluctuates strongly with the offset charge n_g when this ratio E_J/E_C is close to one. By increasing the

ratio however the fluctuations are diminishing and eventually in the regime of $E_J/E_C \gg 1$ the states are virtually independent of the gate charge. This is called the transmon regime [12, B4] and we will from now on always assume that our system is operating in this region and that $n_g = 0$.

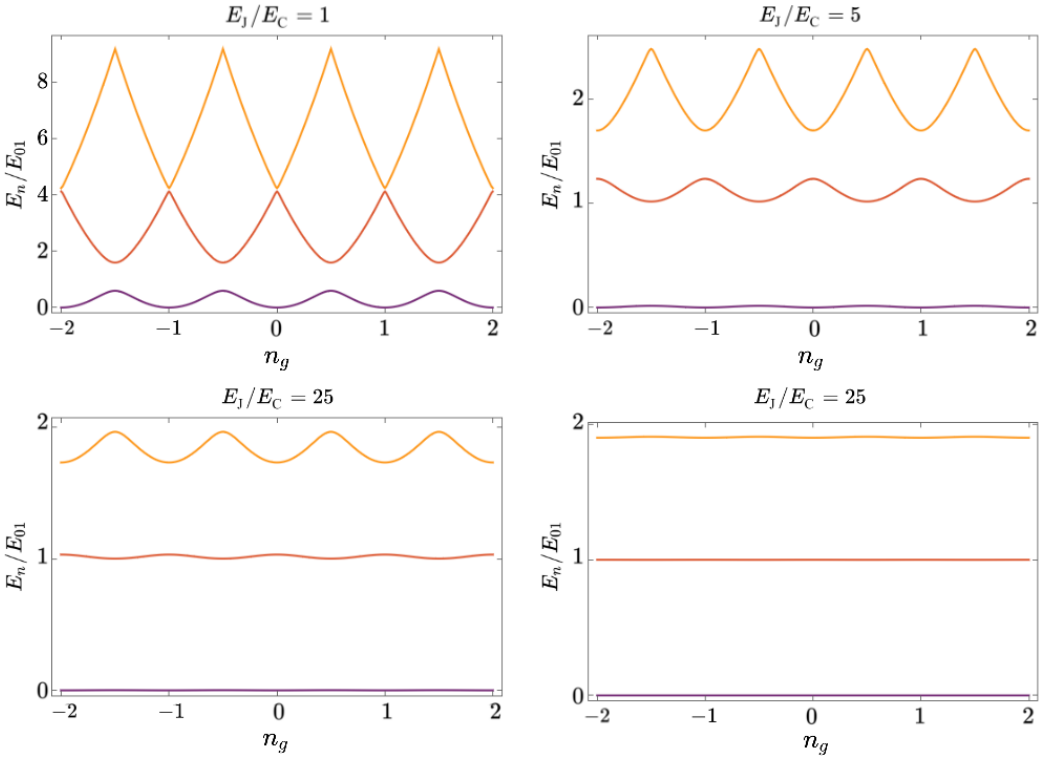

Figure 1.3: Gate charge dependence of the energy levels of the Cooper pair box We present the first 3 energy levels of the Cooper pair box as a function of the gate charge n_g. The energy levels are give in units of the transition energy from ground state to first excited E_{01} at $n_g = 1/2$. We plot these energy levels for progressively higher E_J/E_C approaching the transmon limit.

1.2.2 Bose-Hubbard Approximation

We will now move on to transmon arrays coupled via capacitors. The Hamiltonian describing such a system is

$$H_{\mathrm{CCT}} = 4E_C \sum_{i=1}^{N} n_i^2 - \sum_{i=1}^{N} E_{J_i} \cos\varphi_i + \lambda \sum_{\langle i,j \rangle} n_i n_j \tag{1.35}$$

where the coupling parameter λ is related to the capacitance that connects two nearest neighbor transmons on a lattice, and we have assumed that its value is

uniform. The same holds true for the capacitive energy E_C while we allow for the Josephson junctions to have varying Josephson characteristics.

We will now derive an approximate expression for this Hamiltonian which yields a more intuitive interpretation and is more useful for numerical calculations. We start by expanding the cosine to fourth order

$$H_{CCT} = 4E_C \sum_{i=1}^{N} n_i^2 + \sum_{i=1}^{N} E_{J_i} \left(\frac{\varphi_i^2}{2} - \frac{\varphi_i^4}{24} \right) + \lambda \sum_{\langle i,j \rangle} n_i n_{i+1}. \tag{1.36}$$

We have also dropped the constant term since it does not contribute anything to the phenomenology of the system. In fact we will also drop any constant terms that appear for the rest of the derivation as well.

Our next step is to switch to a second quantization description of the system by performing the canonical transformation

$$n_i = \frac{i}{2} \sqrt[4]{\frac{E_{J_i}}{2E_C}} (a_i^\dagger - a_i) \quad \text{and} \quad \varphi_i = \sqrt[4]{\frac{2E_C}{E_{J_i}}} (a_i^\dagger + a_i) \tag{1.37}$$

where $a_i^\dagger$ and a_i are the bosonic creation and annihilation operators acting on transmon i with the algebra $[a_i, a_j^\dagger] = \delta_{ij}$. The Hamiltonian then assumes the form

$$H_{CCT} = \sum_{i=1}^{N} \Omega_i a_i^\dagger a_i - \frac{E_C}{12} \sum_{i=1}^{N} (a_i^\dagger + a_i)^4 - \sum_{\langle i,j \rangle} J_{ij} (a_i^\dagger - a_i)(a_j^\dagger - a_j), \tag{1.38}$$

where we used the definitions

$$\Omega_i = \sqrt{8E_{J_i} E_C} \quad \text{and} \quad J_{ij} = \frac{\lambda}{4} \frac{\sqrt[4]{E_{J_i} E_{J_j}}}{\sqrt{2E_C}}. \tag{1.39}$$

Finally we will employ a rotating wave approximation (RWA) [13] to discard terms that oscillate rapidly (with a frequency much higher than the energy amplitude of the oscillating term) in the rotating frame given by the transformation

$$U_{rot}(t) = \exp\left(it \sum_{i=1}^{N} \Omega_i a_i^\dagger a_i \right). \tag{1.40}$$

According to the Lemma 3 of appendix A each ladder operator will rotate with the onsite frequency Ω_i but creation and annihilation operators rotate in the opposite direction. Therefore terms that have an equal number of creation and annihilation operators will not oscillate at all.

The only terms that are oscillating in the rotating frame are therefore in the second and third term of the Hamiltonian Eq. (1.40). The terms with an unequal number of creation and annihilation operators from the second sum are oscillating with a frequency that is going to be an integer multiple of the on site frequency Ω_i. Since in the transmon regime $E_C/\Omega_i \ll 1$ we can drop these terms and thus from the remaining, after normal ordering, we obtain

$$\frac{E_C}{12}\sum_{i=1}^{N}(a_i^\dagger + a_i)^4 \overset{\text{RWA}}{\simeq} \frac{E_C}{2}\sum_{i=1}^{N} a_i^\dagger a_i^\dagger a_i a_i + E_C\sum_{i=1}^{N} a_i^\dagger a_i. \tag{1.41}$$

With a similar argument for the last term we will have

$$\sum_{\langle i,j\rangle} J_{ij}(a_i^\dagger - a_i)(a_j^\dagger - a_j) \overset{\text{RWA}}{\simeq} -\sum_{\langle i,j\rangle} J_{ij}(a_i^\dagger a_j + a_i a_j^\dagger) \tag{1.42}$$

assuming that

$$\frac{J_{ij}}{\Omega_i + \Omega_j} \simeq \frac{J_{ii}}{2\Omega_i} = \frac{\lambda}{32E_C} \ll 1. \tag{1.43}$$

This is typically true for experimental setups with the coupling λ being approximately 2 orders of magnitude smaller than E_C.

Recombining everything back in Eq. (1.40) we obtain the Bose-Hubbard approximation of the transmon array Hamiltonian

$$H_{\text{BHA}} = \sum_{i=1}^{N}\omega_i\, a_i^\dagger a_i - \frac{E_C}{2}\sum_{i=1}^{N} a_i^\dagger a_i^\dagger a_i a_i + \sum_{\langle i,j\rangle} J_{ij}(a_i a_j^\dagger + a_i^\dagger a_j) \tag{1.44}$$

where we defined $\omega_i \equiv \sqrt{8E_{J_i}E_C} - E_C$ and we can also re-express the coupling with respect to the new frequency definition

$$J_{ij} = \frac{\lambda}{16}\sqrt{\left(1 + \frac{\omega_i}{E_C}\right)\left(1 + \frac{\omega_j}{E_C}\right)}. \tag{1.45}$$

Upon examining the on-site Hamiltonian, it becomes evident that as E_C tends towards zero, the system behaves as a harmonic oscillator. However, when E_C is finite, the energy levels are no longer evenly spaced. Specifically, the energy difference between E_{01}, the excitation energy for the transition $|0\rangle \to |1\rangle$, and E_{12}, the excitation energy for the transition $|1\rangle \to |2\rangle$, is equal to E_C. This signifies the restoration of anharmonicity in the system, with the anharmonicity magnitude being equal to E_C.

Before concluding this section, it is crucial to note that the Hamiltonian described in Equation (1.44) is unbounded from below, which can lead to unphysical

predictions. It is essential to recognize that this expression serves as an approximation within a limited energy range. While it is possible to derive an exact second quantization form for the complete Hamiltonian (refer to Appendix B), it remains uncertain whether this formalism is suitable for numerical calculations. Therefore, we will only employ Eq. (1.44) as an approximation when dealing with the Hamiltonian, acknowledging its limitations and the need for careful interpretation of the results obtained.

2

Many Body Localization and Quantum Chaos

In this chapter, we will explore fundamental concepts of quantum chaos and localization theory. We will commence by introducing some basic aspects of random matrix theory (2.1.1) and establish its connection to thermalization and the eigenstate thermalization hypothesis (2.1.2). Moving forward, we will delve into Anderson localization as the starting point for our basic illustration of localization theory (2.2.1), followed by an introduction to the phenomenology of the more intricate case of many-body localization (2.2.2). Once both of these dynamic phases of matter have been introduced, we will present the tools utilized for studying the transition between them, namely level spacing statistics (2.3.1) and the inverse participation ratio (2.3.2).

2.1 Chaotic Phase

A significant theoretical challenge lies in understanding the emergence of classical chaotic behavior from quantum systems. While classical chaos requires some non-linearity in the dynamics of the system, in quantum mechanics time evolution is determined from the Schrödinger equation which is linear. Bridging the gap between these seemingly disparate behaviors involves the utilization of random matrix theory. RMT deals with Hamiltonians that belong to ensembles of random matrices, leading to the interpretation of the eigenstates of these matrices as independent and random. Initially, this notion may appear counter-

intuitive since one would expect that small perturbations in the parameters of a Hamiltonian, would only cause slight changes in its eigenstates. Consequently, the new eigenstates, still belonging to the same ensemble, could not be independent from the previous eigenstates. Yet this is exactly what happens for a particular class of systems which are called quantum chaotic due to the drastic mixing of eigenstates under slight alteration of parameters. In this section, we provide a concise introduction to RMT and establish its connection to the thermalization of quantum systems through the eigenstate thermalization hypothesis.

2.1.1 Random Matrix Theory

We primarily study disordered systems in this thesis and here we present various generic properties exhibited by such systems. Disorder manifests in physical systems through random fluctuations in the system parameters. The description of a quantum system starts by writing down its Hamiltonian which will depend on these parameters. For disordered systems with a finite Hilbert space the Hamiltonian assumes the form of a random matrix. We impose no additional constraints on the Hamiltonian, apart from it being a real symmetric matrix. Although the concepts discussed in this chapter can be extended to the broader realm of Hermitian matrices, the systems under consideration here possess real symmetric Hamiltonians. Hence, for the sake of simplicity, we confine our discussion to this particular case.

In the case of a real symmetric matrix, the eigenvectors are also real and constitute an orthonormal basis. Since our matrices are random, the eigenvectors exhibit a corresponding random nature. The distribution that characterizes these vectors should correspond to a uniform coverage the unit hypersphere S^{d-1}, where d denotes the dimension of the Hilbert space. Therefore it is straightforward to write down the distribution of these eigenvectors with components $\psi_1, \psi_2, \dots, \psi_d$ in some arbitrary basis [14]

$$\rho(\psi_1, \psi_2, \dots, \psi_d) = C_d \delta\left(\sum_{i=1}^{d} \psi_i^2 - 1\right) \tag{2.1}$$

and the normalization coefficient can be easily determined by switching to spherical coordinates and integrating the distribution

$$\int dV_d \rho(\psi_1, \psi_2, \dots, \psi_d) = C_d \int_0^1 dr \frac{2\pi^{d/2}}{\Gamma(d/2)} r^{d-1} \delta(r^2 - 1) = C_d \frac{\pi^{d/2}}{\Gamma(d/2)}. \tag{2.2}$$

Therefore our normalized distribution will be

$$\rho(\psi_1, \psi_2, \dots, \psi_d) = \frac{\Gamma(d/2)}{\pi^{d/2}} \delta\left(\sum_{i=1}^{d} \psi_i^2 - 1\right) \tag{2.3}$$

For our calculations later on we will find it beneficial to have the distribution of the individual components of the eigenvectors rather than the the distribution for the full eigenvector that we obtained here in Eq. (2.3). In order to do that we can simply integrate the last $d-1$ variables of the distribution by switching to spherical coordinates, as we did for the normalization, to obtain

$$\rho(\psi) = \int d\psi_2 \dots d\psi_d \rho(\psi, \psi_2, \dots, \psi_d) = \frac{\Gamma\left(\frac{d}{2}\right)}{\sqrt{\pi}\Gamma\left(\frac{d-1}{2}\right)} (1-\psi^2)^{\frac{d-3}{2}}. \tag{2.4}$$

The moments of this distribution can be readily obtain by simple integration. The odd moments are trivially vanishing since the distribution is even and thus we only have even moments of the form

$$\overline{\psi^{2\kappa}} = \frac{(2\kappa-1)!!}{2^\kappa} \frac{\Gamma\left(\frac{d}{2}\right)}{\Gamma\left(\frac{d}{2}+\kappa\right)} \simeq \frac{(2\kappa-1)!!}{d^\kappa} + O(d^{-(\kappa+1)}). \tag{2.5}$$

Note that the averaging here is done with respect to some fictitious ensemble of Hamiltonians, called the Gaussian orthogonal ensemble (GOE) in our case, and we will reserve the overline notation for this kind of averaging. Later on we will refer to this as disorder averaging. One might immediately recognize the leading term of these moments as the moments of the Gaussian distribution with mean zero and standard deviation $1/d$. Therefore we can conclude that in the limit of large Hilbert spaces $d \to \infty$ the rescaled variable $d^{1/2}\psi$ behaves as a random variable given by a Gaussian distribution of mean zero and standard deviation 1.

We could now proceed to the distribution of energy levels but we will return to this in subsection 2.3.1. Now we will consider the implications of random matrix theory for the observables of such a Hamiltonian. We assume some observable with spectral decomposition

$$\mathcal{O} = \sum_{i=1}^{d} O_i |i\rangle\langle i|. \tag{2.6}$$

Using the completeness relation of the eigenstates of the Hamiltonian, which we denote with Greek indices and reserve Latin indices for the eigenbasis of $\mathcal{O}$, we

can express the observable in the eigenbasis of the Hamiltonian as

$$\mathcal{O} = \sum_{\mu,\nu=1}^{d} \langle\mu|\mathcal{O}|\nu\rangle|\mu\rangle\langle\nu| = \sum_{i,\mu,\nu=1}^{d} O_i \psi_i^\mu \psi_i^\nu |\mu\rangle\langle\nu|. \tag{2.7}$$

with $\psi_i^\mu = \langle\mu|i\rangle$ the amplitude of eigenstate $|\mu\rangle$ of the Hamiltonian on eigenstate $|i\rangle$ of the observable and similarly for ψ_i^ν.

The ensemble average of the diagonal elements of the observable exhibit different behavior from the off-diagonal elements

$$\overline{\mathcal{O}_{\mu\mu}} = \sum_{i=1}^{d} O_i \overline{\left(\psi_i^\mu\right)^2} \simeq \frac{1}{d}\sum_{i=1}^{d} O_i = \overline{O} \tag{2.8}$$

$$\overline{\mathcal{O}_{\mu\nu}} = \sum_{i=1}^{d} O_i \overline{\psi_i^\mu \psi_i^\nu} = \frac{1}{d}\sum_{i=1}^{d} O_i \overline{\Psi_i^\mu \Psi_i^\nu} \simeq 0 \tag{2.9}$$

In the first line we made use of Eq. (2.5) and in the second line we used the observation that the rescaled variables $\Psi_i^\mu = d^{1/2}\psi_i^\mu$ and $\Psi_i^\nu = d^{1/2}\psi_i^\nu$ behave approximately as independent random variables drawn from the same Gaussian distribution for the reasons explained after Eq. (2.5). For the average of the off-diagonal elements we have also invoked Lemma 5 in appendix C. Similarly for the variance of the elements of $\mathcal{O}$ we obtain

$$\overline{\mathcal{O}_{\mu\mu}^2} - \overline{\mathcal{O}_{\mu\mu}}^2 = \frac{1}{d^2}\sum_{i,j=1}^{d} O_i O_j \overline{\left(\Psi_i^\mu\right)^2 \left(\Psi_j^\mu\right)^2} - \overline{O}^2 \simeq \frac{2}{d}\overline{O^2} \tag{2.10}$$

$$\overline{\mathcal{O}_{\mu\nu}^2} - \overline{\mathcal{O}_{\mu\nu}}^2 = \frac{1}{d^2}\sum_{i,j=1}^{d} O_i O_j \overline{\Psi_i^\mu \Psi_i^\nu \Psi_j^\mu \Psi_j^\nu} \simeq \frac{1}{d}\overline{O^2} \tag{2.11}$$

where we used again the Gaussian approximation for the rescaled variables and Lemmas 6 and 8 in appendix C.

We can summarise all these results in the following ansatz for the elements of the observable $\mathcal{O}$

$$\mathcal{O}_{mn} \simeq \overline{O}\delta_{mn} + \sqrt{\frac{\overline{O^2}}{d}} R_{mn} \tag{2.12}$$

where R_{mn} is a random matrix with moments

$$\overline{R_{mn}} = 0 \quad , \quad \overline{R_{mn}^2} = 1 + \delta_{mn}. \tag{2.13}$$

It is very straightforward to confirm that this ansatz reproduces the first two moments of the elements of any observable $\mathcal{O}$ for a random matrix Hamiltonian.

Since the fluctuations of the elements of $\mathcal{O}$ around the mean are vanishing for large enough systems with $d \to \infty$, assuming that $\overline{O^2}$ itself does not scale with d, the ansatz Eq. (2.12) should be approximately valid for any single Hamiltonian.

2.1.2 Eigenstate Thermalization Hypothesis

The RMT ansatz, as presented in Eq. (2.12), serves as an initial framework for understanding the thermalization of quantum systems. Thermalization refers to the phenomenon where a system gradually approaches thermal equilibrium over an extended period of self-interaction or interaction with a reservoir. Once thermalization is achieved, the statistical behavior of the system's observables aligns with the predictions of one of the thermodynamic ensembles. At first glance, this definition appears contradictory to quantum mechanics, given that the dynamics of any closed system are inherently unitary

$$|\psi(t)\rangle = e^{-iHt}|\psi(0)\rangle = \sum_{n=1}^{d} c_\mu e^{-iE_\mu t}|\mu\rangle, \tag{2.14}$$

where $c_\mu = \langle\mu|\psi(0)\rangle$. Correspondingly the time evolution of an observable is

$$O(t) = \langle\psi(t)|\mathcal{O}|\psi(t)\rangle = \sum_{\mu,\nu=1}^{d} c_\mu^* c_\nu e^{i(E_\mu - E_\nu)t}\langle\mu|\mathcal{O}|\nu\rangle \tag{2.15}$$

and after a long time

$$\langle O(t)\rangle_\infty = \lim_{T\to\infty}\frac{1}{T}\int_0^T dt\; O(t) = \sum_{\mu=1}^{d}|c_\mu|^2\langle\mu|\mathcal{O}|\mu\rangle \tag{2.16}$$

assuming that there are no degeneracies or that they are extremely rare. According to the ergodic hypothesis this average should be equivalent to the ensemble average of the system. Yet the time average of Eq. (2.16) is clearly dependent on the initialization of the system $|\psi(0)\rangle$ via the coefficients $c_\mu = \langle\mu|\psi(0)\rangle$ and therefore it cannot be compatible with the definition of thermalization.

If however the system has a Hamiltonian which aligns with the assumptions of RMT then the long time average of the observable yields

$$\langle O(t)\rangle_\infty \simeq \overline{O}\sum_{\mu=1}^{d}|c_\mu|^2 = \overline{O} \tag{2.17}$$

and therefore if $\overline{O}$ is the average predicted by a thermodynamic ensemble thermalization can be reconciled with quantum mechanics. The first one to note the

connection between RMT and thermalization of quantum systems was Deutch in 1991 [15].

It is now advantageous to provide a more qualitative explanation for the mechanism through which quantum systems undergo thermalization and connect it to quantum information. While globally the system evolves under unitary evolution, for the case of a closed system, locally the system can evolve into mixed states, by erasing the off-diagonal elements of the partial trace of the system, via the known mechanism of dephasing (see subsection 1.1.2). Consequently, the system effectively acts as a bath for its own degrees of freedom, scrambling the quantum information of its state. The term "locally" here refers to a subset of the entire system under consideration, encompassing only a limited number of degrees of freedom, significantly fewer than the total degrees of freedom of the entire system. Notably, these local observables are the ones accessible in experimental settings, as opposed to global observables. However, one issue remains unresolved: the long-term average predicted by RMT is independent of energy, a characteristic that holds true only in the limit of infinite temperature for the ensembles.

The resolution of this issue was given by Srednicki [16] in the form of the eigenstate thermalization hypothesis which can be stated in the form of the following ansatz for the matrix elements of an observable

$$\mathcal{O}_{\mu\nu} = O\left(\overline{E}\right)\delta_{\mu\nu} + e^{-S\left(\overline{E}\right)/2} f\left(\overline{E}, \omega\right) R_{\mu\nu} \tag{2.18}$$

where the variables $\overline{E} = (E_\mu + E_\nu)/2$ and $\omega = E_\nu - E_\mu$ have been introduced, $R_{\mu\nu}$ is a symmetric random matrix with element mean 0 and variance 1 and $S\left(\overline{E}\right)$ is the thermodynamic entropy of the system and $O\left(\overline{E}\right)$ and $f\left(\overline{E}, \omega\right)$ are smooth functions of their arguments.

It is worth noting that the ETH ansatz, given in Eq. (2.18), bears a remarkably similar structure to the RMT ansatz defined in Equation (2.12). The key distinction lies in the inclusion of energy dependent factors for the elements of the observable within the ETH ansatz. In fact, within a small energy window, the spectral function $f\left(\overline{E}, \omega\right)$ approximately remains constant. Consequently, the two equations become practically indistinguishable. Hence, in a sense, RMT can be viewed as a zeroth-order approximation of the ETH. This convergence between the two approaches accounts for the interchangeable use of terms such as RMT, thermalizing, and quantum chaotic within the literature.

2.2 Localized Phase

In the previous section, we discussed how systems that adhere to the ETH are destined to exhibit thermal behavior. A fundamental aspect of thermalization in quantum systems is their ability to act as reservoirs for their subsystems, by allowing for the exchange of energy and particles between different parts of the system. Therefore, for a system to avoid thermalization, it must prevent transport and exhibit insulating behavior. This is precisely the case for systems that undergo Anderson localization or many-body localization. In this section, we will explore some essential characteristics of these two phenomena.

2.2.1 Anderson Localization

In the beginning of the previous section we hinted towards the connection of RMT Hamiltonians with Hamiltonians of classical systems that exhibit chaotic behavior. A natural question we can ask now is what happens for systems that are classically integrable. For example consider N uncoupled harmonic oscillators. This system is trivially integrable and its quantum counterpart has energy levels given by

$$E_n = \sum_{i=1}^{N} n_i \omega_i \tag{2.19}$$

where we assumed that each oscillator has a different characteristic frequency ω_i and n is a list of integer values n_i. Clearly these energy levels are uncorrelated. This fact becomes apparent when we examine nearby energy levels within the high-energy sector of this system. Although these levels may be closely spaced, they originate from distinct sets of coefficients n_i. This stands in stark contrast to the scenario observed in GOE Hamiltonians, as we shall explore in subsection 2.3.1.

However, the example provided earlier was rather simplistic, and it is necessary to explore the potential for avoiding thermalization in a more realistic system. Let us consider a one-dimensional spin 1/2 chain described by the Hamiltonian:

$$H_0 = \frac{1}{2}\sum_{i=1}^{N} \epsilon_i Z_i + \frac{J}{2}\sum_{\langle i,j\rangle} (X_i X_j + Y_i Y_j) \tag{2.20}$$

In this expression, X_i, Y_i and Z_i are the Pauli operators acting on site i of the lattice. The values ϵ_i are randomly selected from a uniform distribution within the range $[-W/2, W/2]$, where W represents the strength of the disorder. The term J corresponds to the hopping strength, while $\langle i, j\rangle$ indicates ordered nearest

neighbor pairs. The ground state of the system is the all spins down configuration. Qualitatively this system can be thought of as a disordered spin lattice where spin excitations are hopping around the lattice like particles without interacting with any of the other excitations. This in combination with the fact that the total spin-z operator

$$Z = \sum_{i=1}^{N} Z_i \tag{2.21}$$

commutes with the Hamiltonian, means that our analysis can be confined to the single-excitation sector.

In order to understand the behavior of this system we can consider the two extreme limits of no disorder ($W = 0$) and infinite disorder ($J/W = 0$). In the first case periodicity is restored in the lattice and therefore the eigenstates will be plane waves

$$\psi_k(x) = \langle x|\psi_k\rangle = \frac{1}{\sqrt{N}} e^{ikx} \tag{2.22}$$

where $k = 2\pi m/N$ with $m \in \{0, 1, \dots, N-1\}$, and the energy levels are given by

$$E_k = 2J\cos(k). \tag{2.23}$$

For a state $|x\rangle$ with one spin up at position x of the lattice at time $t = 0$, after it is allowed to evolve under the periodic Hamiltonian of Eq. (2.20) the return probability will be

$$|\langle x|e^{-iH_0 t}|x\rangle|^2 = \left|\sum_k e^{-iE_k t}\langle x|\psi_k\rangle\langle\psi_k|x\rangle\right|^2 = \frac{2}{N^2}\sum_{p>k}\cos\left[(E_p - E_k)t\right]. \tag{2.24}$$

Therefore the probability of returning to the initial state is quasi-periodic in time and we have infinite revivals. However the situation is different if we consider the thermodynamic limit of $N \to \infty$

$$|\langle x|e^{-iH_0 t}|x\rangle|^2 = \frac{1}{2\pi^2}\int_0^{2\pi} dp \int_0^{p} dk\ \cos\left[(E_p - E_k)t\right] = J_0(2Jt)^2. \tag{2.25}$$

where $J_0(x)$ is the Bessel function of the first kind [B3]. For long times this function behaves approximately as $1/t$ and therefore the return probability is vanishing and the system behaves diffusively.

The infinite disorder case is far more trivial. Essentially the spins decouple and therefore we simply have eigenstates of the form

$$\psi_m(x) = \langle x|\psi_m\rangle = \delta_{x,m} \tag{2.26}$$

where δ indicates the Kronecker delta and m is the site at which the eigenstate is localized. For the energy levels we simply have $E_m = \epsilon_m$ and the return probably is calculated as

$$|\langle x|e^{-iH_{\text{TB}}t}|x\rangle|^2 = \left|\sum_m e^{-iE_m t}\langle x|\psi_m\rangle\langle\psi_m|x\rangle\right|^2 = 1. \tag{2.27}$$

Therefore the excitation initialized at site x remains there indefinitely regardless of whether we go to the thermodynamic limit or not.

In the realm of intermediate cases between diffusion and extreme localization, one might anticipate a diffusive behavior that is hindered by the scattering of excitations with the disorder potential. However, this expectation is refuted by Anderson's groundbreaking work [17], which demonstrates that the system remains localized for any finite strength of disorder. This remarkable result holds true even for two-dimensional lattices, although in three dimensions, a transition to a delocalized phase occurs, as established by renormalization group arguments [18]. Within the intermediate localized phase, the eigenstates adopt a specific form:

$$\psi_m(x) = \langle x|\psi_m\rangle = A_m(x)e^{-|x-x_m|/\xi_E} \tag{2.28}$$

Here, x_m denotes the position in real space around which the eigenstate $|\psi_m\rangle$ localizes, and ξ_E represents the localization length, which generally depends on the energy. The function $A_m(x)$ is a bounded function which cannot be determined with analytic considerations. Since systems in this regime maintain their initial states over extended periods of time, they exhibit a lack of transport and thus evade thermalization.

2.2.2 Many Body Localization

We have seen that systems can evade thermalization by the mechanism of Anderson localization. However Anderson localized systems are non-interacting and therefore are not particularly relevant for practical applications, like quantum computing for instance. A natural question after this consideration, and in fact one that Anderson himself contemplated, is whether Anderson localization survives if we introduce many body interactions. As it turns out such a mechanism exists, called many body localization and we will go through its main features here.

Most of the Anderson localization properties transfer as well for the case of MBL: uncorrelated spectra, localized eigenstates (though not in the same sense as Anderson localization, see subsection 2.3.2) and insulating behavior. However MBL is a less robust phase, as it exhibits a transition to a chaotic phase even in

1D. This transition is driven by the interplay between the disorder strength and the coupling strength of the system.

One of the most remarkable properties of MBL is the fact that the eigenstates exhibit an area law. To understand this we consider a system which is MBL and divide it into two parts, A and its compliment B. Assume that initially the two subsystems are decoupled. The state of the system will then be a tensor product of the states of the two subsystems $|\alpha\rangle \otimes |\beta\rangle$. At $t = 0$ we turn on the coupling and by interacting the two subsystems will become entangled, meaning that the full state of the system can no longer be written as a product state. However due to the localization of the system, only degrees of freedom within a localization length ξ_1 from the boundary can interact while correlations away from the boundary decay exponentially. Therefore the entanglement entropy should depend on the surface of the boundary. In other words the system remains close to a product state, in the sense that its Schmidt decomposition will have one coefficient close to 1 and all other coefficients will be exponentially smaller.

As a consequence of the area law entanglement in MBL eigenstates, the transformation that diagonalizes the Hamiltonian exhibits quasi-locality. To illustrate this concept, we consider a specific system. We will augment the previously mentioned Hamiltonian of Eq. (2.20) with an additional term to introduce many-body interactions, characterized by a coupling strength V

$$H_{\mathrm{XXZ}} = \frac{1}{2}\sum_{i=1}^{N} \epsilon_i Z_i + \frac{J}{2}\sum_{\langle i,j\rangle}(X_iX_j + Y_iY_j) + \frac{V}{4}\sum_{\langle i,j\rangle} Z_iZ_j. \tag{2.29}$$

This is the Heisenberg XXZ Hamiltonian and the added term describes a repulsion between excitations. Initially we consider what happens for $J = 0$. While this is still a many body interacting Hamiltonian it is clearly diagonal and the local particle spin operators Z_i are integrals of motion since they commute with the Hamiltonian. Furthermore the eigenstates are separable.

Upon reintroducing the hopping term, the new eigenstates become connected to the old eigenstates through a transformation U. This transformation also relates the previous integrals of motion to new ones, given by

$$\tau_i^z = UZ_iU^\dagger \tag{2.30}$$

while the Hamiltonian transforms into

$$\widetilde{H} = UH_{\mathrm{XXZ}}U^\dagger = \sum_i h_i\tau_i^z + \sum_{i<j} J_{ij}\tau_i^z\tau_j^z + \sum_{i<j<k} K_{ijk}\tau_i^z\tau_j^z\tau_k^z + \ldots \tag{2.31}$$

This transformation, however, is not unique to MBL and can also be applied to chaotic systems. What sets MBL apart is the quasi-local nature of the transformation U [19–21]. Quasi-locality means that the transformation U can be

decomposed into a product of operations acting on two sites $U_i^{(2)}$, three sites $U_i^{(3)}$, and so on (as shown in Fig. 2.1) with each layer of operations approaching the identity exponentially fast with an increasing range $||1 - U_i^{(m)}||^2 < e^{-m/\xi_1}$, where $||\cdot||$ represents the operator Frobenius norm. Due to the quasi-locality of U, the operators τ_i^z are commonly referred to as quasi-local integrals of motion (LIOM).

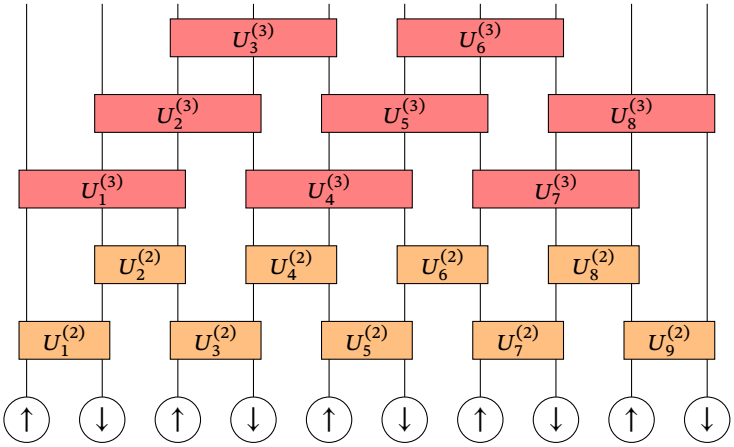

Figure 2.1: Quasi-local transformation. Graphical representation of how a quasi-local transformation acts on a spin chain state. Here, the index i in $U_i^{(m)}$ denotes the leftmost site number, ranging from 1 to $N - m - 1$ and m corresponds to the number of sites acted upon by the operator

To capture the significance of the Hamiltonian in the LIOM decomposition, we present it in a more concise form that is independent of the specific Heisenberg chain example:

$$H_{\text{LIOM}} = \sum_{\vec{a}} w_{\vec{a}} (\tau_1^z)^{a_1} \dots (\tau_N^z)^{a_N}. \tag{2.32}$$

According to the phenomenology of MBL the coefficients $w_{\vec{a}} \propto e^{-\ell/\xi_2}$ decay exponentially with correlation range ℓ, defined here as the maximum distance between 2 non zero elements of $\vec{a}$.

If the system is fermionic then $\vec{a}$ are vectors where all elements are 0 or 1. This follows from the observation that each of the LIOM squares to the identity

$$(\tau_i^z)^2 = UZ_iU^\dagger UZ_iU^\dagger = 1 \tag{2.33}$$

and therefore including products with higher exponents does not add new terms to the Hamiltonian. The situation is less trivial for the bosonic case. In general, the squares of the LIOM can be different LIOM themselves and therefore

we surmise that in that case the most general expression should contain higher exponents as well. Regardless, there has been experimental evidence [22] and theoretical studies [23–25] that confirm the existence of a bosonic MBL phase.

The astute reader might have noticed that we have written down two different localization lengths ξ_1 for the quasi-local transformation norm and ξ_2 for the coefficients of Eq. (2.32). At present, it remains unclear whether these two parameters are distinct or identical, and further investigation is required to determine their relationship.

Before we conclude this section we will connect the phenomenology of MBL to the example of dephasing that we presented in the subsection 1.1.2. The LIOM Hamiltonian of Eq. (2.31) actually contains the Hamiltonian of Eq. (1.18) up to the unitary transformation U. It contains additionally longer range two-body interactions, three body interactions and so on. However the dephasing mechanism remains qualitatively similar, and we anticipate the dephasing time to be proportional to $1/J_{ij}$ (see Fig. 1.1). The benefit of having the system in the MBL phase however is that J_{ij} is exponentially suppressed as $\sim e^{-(j-i)/\xi_2}$ and therefore the dephasing time increases exponentially with localization length. Therefore by ensuring that our system is deep in the MBL regime we can enable it to function as a reliable quantum memory for an extended period of time.

2.3 Probes of the Transition

In the preceding sections, we introduced the concept of the chaotic phase and the localized phase. Both of these phases require a certain level of randomness on the system under consideration. It is natural to question whether there exist systems that can manifest both of these two dynamical phases under suitable parameter settings. In reality, numerous disordered systems undergo a phase transition between the chaotic and localized phases. Although delving into the intricacies of this transition extends beyond the scope of this thesis and remains an open problem, quantifying this transition is relatively more straightforward. This section focuses on presenting two commonly employed diagnostics for studying this transition: level spacing statistics and the inverse participation ratio.

2.3.1 Level Spacing Statistics

Here we will present the level spacing statistics for both integrable and chaotic systems. We will point out the differences between the two distributions and summarise how they can be used to diagnose whether a system is in the localized or the chaotic regime.

We begin with the simpler case, the integrable systems. As we have mentioned in the previous section, these systems have uncorrelated eigenstates. Therefore the distribution of the energy levels and by extension (see Lemma 4 in appendix C) the distribution of the adjacent level spacings $s_n = E_{n+1} - E_n$ will be Poissonian

$$\rho_{\mathrm{P}}(s_n) = e^{-s_n}. \tag{2.34}$$

In order to avoid the unpleasant procedure of performing a spectral unfolding of this distribution however we can switch our variable of level spacings s for the adjacent level spacing ratio defined as

$$r = \min\left(\frac{s_n}{s_{n+1}}, \frac{s_{n+1}}{s_n}\right). \tag{2.35}$$

Furthermore this quantity is more easily comparable to what is actually measured in an experiment and therefore we re-express the distribution in terms of this variable using Lemma 4 of appendix C

$$\begin{aligned}
\rho_{\mathrm{P}}(r) &= \int\int ds_n ds_{n+1} \rho_{\mathrm{P}}(s_n)\rho_{\mathrm{P}}(s_{n+1})\delta\left(r - \min\left(\frac{s_n}{s_{n+1}}, \frac{s_{n+1}}{s_n}\right)\right) \\
&= \int ds_n\, s_n \rho_{\mathrm{P}}(s_n)\rho_{\mathrm{P}}(rs_n) + \int ds_{n+1}\, s_{n+1}\rho_{\mathrm{P}}(rs_{n+1})\rho_{\mathrm{P}}(s_{n+1}) \\
&= 2\int dx\, x\rho_{\mathrm{P}}(x)\rho_{\mathrm{P}}(rx) = \frac{2}{(1+r)^2}
\end{aligned} \tag{2.36}$$

For the GOE the situation is more complicated and we will only sketch the derivation of the level spacing distribution here, for more information see [B5]. We begin with the distribution of the Hamiltonians. The distribution that we write down here will depend in general in the $d(d+1)/2$ independent elements that are Gaussian random variables. Furthermore the probability should not be different between matrices within the ensemble related via an orthogonal transformation and therefore the only natural choice for the distribution is

$$\rho_{\mathrm{GOE}}(H) \propto e^{-\frac{1}{2\sigma^2}\mathrm{Tr}(H^2)}. \tag{2.37}$$

with σ an arbitrary real parameter. In order to derive the distribution of the energy levels we move to the eigenbasis of the Hamiltonian via the transformation

$$H = UEU^T, \tag{2.38}$$

where U is the orthogonal transformation that diagonalizes the symmetric Hamiltonian and E is a diagonal matrix with elements the energy levels of the system. In

the new basis our distribution will be in general a function of the d energy levels and the $d(d-1)$ independent elements of U and we will have

$$dH\rho_{\mathrm{GOE}}(H) \propto |\Delta_d| U dU^T dE_1 \dots dE_d \, e^{-\frac{1}{2\sigma^2}\sum_{k=1}^{d} E_k^2} \tag{2.39}$$

where Δ_d is the Vandermond determinant

$$\Delta_d = \prod_{i>j=1}^{d} (E_i - E_j) \tag{2.40}$$

and it appears as the Jacobian of the transformation of the differential. We can now integrate the U dependence away trivially, since the probability density does not depend on in due to the trace and obtain the probability distribution for the energy levels

$$\rho_{\mathrm{GOE}}(E_1, \dots, E_d) \propto \prod_{i>j=1}^{d} (E_i - E_j) e^{-\frac{1}{2\sigma^2}\sum_{k=1}^{d} E_k^2} \tag{2.41}$$

where without loss of generality have assumed ordered energy levels to get rid of the absolute value. Note here that if any two levels become degenerate the probability density is vanishing. This behavior is an essential property of quantum chaotic systems and it is called level repulsion in the literature.

From Eq. (2.41) we could integrate all but one energy levels to obtain the probability distribution of an individual energy level, from that the adjacent level spacing distribution and then the adjacent level spacing ratio distribution as we did for the Poisson distribution. Unfortunately these integrations cannot be carried out analytically and one has to resort into semi-analytic methods to derive the following result [26]

$$\rho_{\mathrm{GOE}}(r) = \frac{27}{8} \frac{r + r^2}{(1 + r + r^2)^{5/2}} \tag{2.42}$$

This is the distribution we will use when comparing the level spacing statistics with GOE for the rest of the thesis.

However if we relax our requirements for precision an approximate analytic expression can be derived for the level spacings distribution

$$\rho_{\mathrm{W}}(s) = \frac{\pi s}{2} e^{-\pi s^2/4}. \tag{2.43}$$

This is known in the literature as the Wigner surmise, originally derived by Wigner to describe the spectra of heavy nuclei in 1956. Using the same procedure as we did for the Poisson distribution we can express this in terms of the

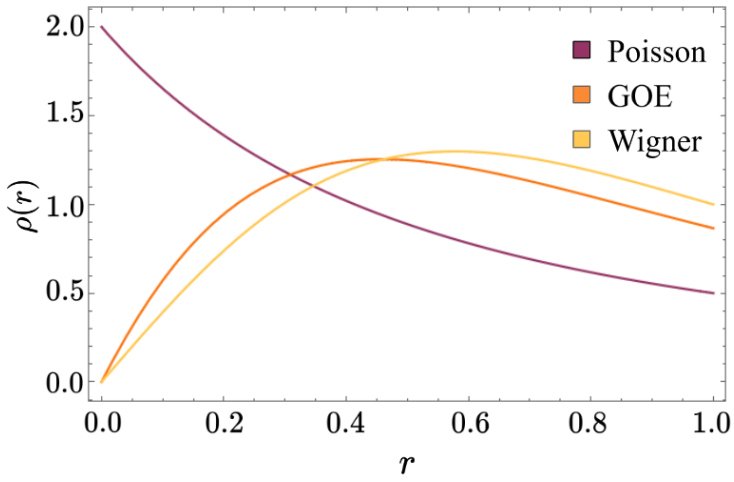

Figure 2.2: Adjacent level spacing ratio distributions. We present the probability distributions of the three discussed distributions in this section, plotted as a function of the adjacent level spacing ratio given by Eq. (2.35). Upon examining the plot, it becomes evident that the Wigner surmise, while slightly less accurate, effectively captures all the fundamental characteristics of the GOE distribution. Additionally, we observe a significant disparity between the localization statistics and the chaotic statistics when the adjacent level spacing ratio r approaches zero.

r ration of Eq. (2.35)

$$\rho_{\mathrm{W}}(r) = 2\int dx\, x\rho_{\mathrm{W}}(x)\rho_{\mathrm{W}}(rx) = \frac{4r}{(1+r^2)^2}. \tag{2.44}$$

All of the distributions we presented here are ploted in Fig. 2.2 for comparison.

2.3.2 Inverse Participation Ratio

In the preceding section, we explored the level spacing statistics as a tool for analyzing chaotic and localized systems. However, to fully equip ourselves for studying the transition between these two phases, we require a measure that directly characterizes the eigenstates. Consequently, we need to examine the distinctions between the eigenstates of the two phases.

To develop a better understanding of the diagnostic tool we are about to introduce, it is helpful to compare the eigenstates of Anderson localized systems with those of Gaussian Orthogonal Ensemble (GOE) systems. In Anderson localized states, the wavefunction $\psi(x) = \langle x|\psi\rangle$ decays exponentially as we move away from a specific position in real space. For the sake of convenience and to align with the systems we are interested in, we will consider a lattice system with

discretised coordinates. In this scenario, for a large system size or a small localization length ξ, the wavefunction can be approximated as a Kronecker delta, such that $\psi(x) \propto e^{-|x-x_0|/\xi} \simeq \delta_{x,x_0}$, where x_0 represents the chosen position.

In contrast, for eigenstates of a GOE Hamiltonian, we recall that the individual components of the eigenstates can be treated as independent random variables drawn from a Gaussian distribution. Consequently, we expect most of these components to cluster around the mean value, resulting in a relatively uniform overall eigenstate wavefunction. In other words, due to normalization, we anticipate $\psi(x) \simeq 1/\sqrt{N}$, where N represents the number of lattice sites in the system. The inverse participation ration is defined as

$$\mathrm{IPR}(|\psi\rangle) = \sum_{x=1}^{N} |\langle x|\psi\rangle|^4 \tag{2.45}$$

Clearly this quantity is very different for the two cases we just mentioned. For localized eigenstates this yields a value close to 1 while for the delocalized states of a GOE Hamiltonian it goes to $1/N$ or zero in the limit of large system size $N \to \infty$.

This definition however for the IPR is problematic for the case of MBL. Namely, in real space many body eigenstates are unlikely to be localized and in fact this is usually not the case even for MBL states. Instead, in the case of MBL, localization of a state happens within a region of Fock space. Therefore in this case it would be more reasonable to define IPR as

$$\mathrm{IPR}(|\psi\rangle) = \sum_{n=1}^{d} |\langle n|\psi\rangle|^4 \tag{2.46}$$

with n a basis state of the d-dimensional Fock space. Of course Fock space is infinite and therefore for practical application d refers to the dimensionality of the truncated Fock space.

It is remarkable that calculating the IPR of a GOE state in the Fock space, rather than in real space, does not alter its predicted value. In fact, the choice of basis for calculating the IPR of a chaotic state should not have any significant impact. An intuitive way to understand this is as follows:

Assume that we have a specific Hamiltonian of the GOE for which we engineer a basis in such a way that the eigenstates appear localized. For example, this could be the eigenbasis itself. However, in order to apply the results from RMT, we need to consider the ensemble of eigenstates from various different Hamiltonians. Consequently, we would also need to calculate the eigenstates of many other Hamiltonians from the ensemble in the same chosen basis. Since the eigenstates of these Hamiltonians are uncorrelated, for roughly every other member

of the ensemble, the eigenstates would appear completely random in that basis. As a result, delocalization is restored as the average behavior of the ensemble eigenstates.

There is however an even more rigorous diagnostic that helps us get rid of the IPR basis dependence, especially the ambiguity in the localized regime, namely the Walsh-Hadamard transform which will be introduced in the following chapter.

3

Walsh-Hadamard Coefficients

Here we introduce the concept of Walsh-Hadamard coefficients as a diagnostic for MBL and a tool to recover the coefficients of the local integrals of motion decomposition of a qubit Hamiltonian (3.1.1). We will also present the main hurdle in obtaining the Walsh Hadamard coefficients, namely tracking the identity of the computational eigenstates as we vary the system parameters, especially across an avoided crossing, using the state fidelity (3.1.2). Next we derive an analytic approximation for the Walsh-Hadamard coefficients. We do this here for a generalised second quantization model featuring only two body-interactions using Rayleigh-Schrodinger perturbation theory (3.2.1,3.2.2). The perturbation parameter is the strength of the two body interactions and we obtain the energy levels to second order. From the expressions for the energy levels we will then immediately obtain the Walsh-Hadamard coefficients (3.2.3) from a direct application of the definition. We develop this perturbation scheme in order to downsize the computational costs of the Walsh-Hadamard coefficients from diagonalizing fully a bosonic system to obtaining the energy levels of a fermionic system of the same size.

3.1 Walsh-Hadamard Transformation

In subsection 2.2.2 we introduced the concept of the Local Integrals of Motion (LIOM) and highlighted their significance in the description of the MBL phase. Yet despite their key role in the phenomenology of MBL, obtaining them for a practical application remains an elusive goal despite the immense effort [19, 20],

even more so for bosonic systems like the ones that we are interested in here. However, recovering the coefficients of the LIOM decomposition of the qubut Hamiltonian is a much more manageable goal, and it is one that we set out to accomplish here, at least for the effective Hamiltonian of the qubit sector of our system.

3.1.1 Qubit Sector LIOM Decomposition

The entire scheme of quantum computation with transmons relies on our capability of setting up the system parameters such that the Hamiltonian of the system is effectively confined within the qubit subspace. In this sector of the Fock space, populated with states that have at most one excitation per site, the Hamiltonian written in the eigenbasis takes the form of Eq.(2.32) for $\tau_i^z = Z_i$ and the summation running over the set $\mathbb{B}^N$, of all bit-strings of length N

$$H = \sum_{b\in\mathbb{B}^N} w_b Z_1^{b_1} \dots Z_N^{b_N}. \tag{3.1}$$

This last equation in turn can be interpreted as a system of linear equations that we need to solve with respect to the coefficients w_b. To do this we first rewrite Eq. (3.1) as an element-wise equation and since both sides are diagonal we will have for some qubit state $|q\rangle$

$$E_q = \sum_{b\in\mathbb{B}^N} w_b \langle q|Z_1^{b_1} \dots Z_N^{b_N}|q\rangle \tag{3.2}$$

$$= \sum_{b\in\mathbb{B}^N} w_b \langle q_1|Z_1^{b_1}|q_1\rangle \dots \langle q_N|Z_N^{b_N}|q_N\rangle \tag{3.3}$$

where $E_q = \langle q|H|q\rangle$ is the energy of eigenstate $|q\rangle$. In the usual convention of quantum information the Pauli z matrix is expressed in the $\{|0\rangle, |1\rangle\}$ basis where the 0 state is not identified as the physical ground state. We do not adapt this convention here and instead we have

$$Z = \sum_{i=0}^{1} (-1)^{\bar{i}} |i\rangle\langle i| \tag{3.4}$$

where $\bar{i}$ denotes the flipped bit i. Substituting back into Eq. (3.3) we obtain

$$E_q = \sum_{b\in\mathbb{B}^N} w_b (-1)^{b\cdot\bar{q}}, \tag{3.5}$$

which can be readily identified as the N-dimensional discrete Fourier transform of size $2 \times 2 \times \cdots \times 2$ and immediately inverted to yield

$$w_b = \frac{1}{2^N} \sum_{q \in \mathbb{B}^N} (-1)^{b \cdot \bar{q}} E_q. \tag{3.6}$$

This is the Walsh-Hadamard transform [B6] of the eigenenergies of the system Hamiltonian H with LIOM decomposition given by Eq. (3.1).

3.1.2 State Identity Tracking

Despite the apparent simplicity of Eq. (3.6), in order to obtain the Walsh-Hadamard coefficients for practical applications we need to actually be able to separate the qubit eigenstates from any other non-computational states of the full spectrum, and also assign a unique bit-string identifier to every single one of them. Isolating the qubit states is trivial for fermionic systems since every eigenstate is a qubit state, for bosonic systems however, such as our transmon arrays, this is a much more complicated task. Not only is the number of non-computational states infinite, the qubit energy levels are also not well separated from the leakage states, in fact, even under small perturbations these can become strongly correlated to each other.

For quantum information systems in idle mode we usually have Hamiltonians which can be broken down to two parts, a part describing the individual degrees of freedom of the system i, the qubits, and another one that determines the coupling between two such degrees of freedom i and j

$$H = \sum_{i=1}^{N} h_i + \lambda \sum_{\substack{i,j=1 \\ i<j}}^{N} V_{ij}. \tag{3.7}$$

The form of h_i determines the type of qubit platform under consideration while V_{ij} determines the type of coupling we have between qubits and λ is the parameter that determines the strength of the coupling.

For this type of systems we can always think of a particular limit were all degrees of freedom are decoupled, for the Hamiltonian in Eq. (3.7) that would be $\lambda \to 0$, and then the total spectrum of the system becomes a superposition of the spectra of the individual qubits. In this limit, labeling a state by a bit-string can be done unambiguously by simply identifying which qubits are in the ground state $|0\rangle$ and which are on the first excited state $|1\rangle$. Once this is done then we only need a convention that maps positions on the bit-string to our qubit positions.

As soon as there is some finite coupling however, the eigenstates of the system, slowly but surely will start mixing into superpositions of the decoupled

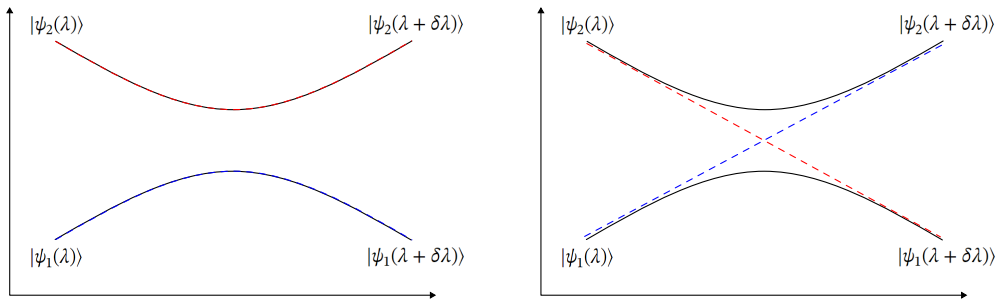

Figure 3.1: Avoided Crossings. In these plots we present an avoided crossings between two energy levels as a functions of some arbitrary parameter λ. The colored dashed lines indicate the identities of the corresponding states. On the the left plot we have an adiabatic avoided crossing with the implication that $\langle\psi_1(\lambda)|\psi_2(\lambda+\delta\lambda)\rangle \simeq \langle\psi_2(\lambda)|\psi_1(\lambda+\delta\lambda)\rangle \simeq 0$ while on the right plot we have a diabatic crossing with $\langle\psi_1(\lambda)|\psi_2(\lambda+\delta\lambda)\rangle \simeq \langle\psi_2(\lambda)|\psi_1(\lambda+\delta\lambda)\rangle \simeq 1$.

eigenstates. Inevitably, far away from the decoupled limit the eigenstates will become nearly uniform superpositions of the decoupled eigenstates, especially so for chaotic systems, thus rendering any kind of labeling with a bit-string devoid of all meaning. For weak coupling, for instance $\delta\lambda \ll 1$, the parameter dependent eigenvector $|\psi_n(\lambda)\rangle$ of the n-th energy level at coupling strength λ should not mix strongly with other states and therefore we should have approximately

$$|\langle\psi_n(\delta\lambda)|\psi_m(0)\rangle|^2 \simeq \delta_{nm} \tag{3.8}$$

This means that we can associate the weak coupling eigenstates uniquely to the decoupled qubit states. In fact we can repeat this process recursively for small $\delta\lambda$ steps and keep track of the qubit energy levels.

This procedure works as long as Eq. (3.8) is valid which is not the case if our spectrum reaches an avoided crossing. The involved states close to the avoided crossing will become strongly correlated and have a non vanishing overlap with both of the perturbed states. Tracking the identity of the states across the avoided crossing can only be done reliably if we know the character of the avoided crossings (see Fig. 3.1).

Assuming the character of the avoided crossing is known we only need to have a way to determine when and where do the avoided crossings occur which we can do with the fidelity susceptibility [27–29]

$$\chi_n(\lambda) = -\lim_{\delta\lambda\to 0} \frac{\ln F_n(\lambda)}{\delta\lambda^2}, \tag{3.9}$$

where $F_n(\lambda)$ is the fidelity of state n as it is usually defined in the context of quantum information $F_n(\lambda) = |\langle\psi_n(\lambda)|\psi_n(\lambda+\delta\lambda)\rangle|^2$. For sufficiently small steps

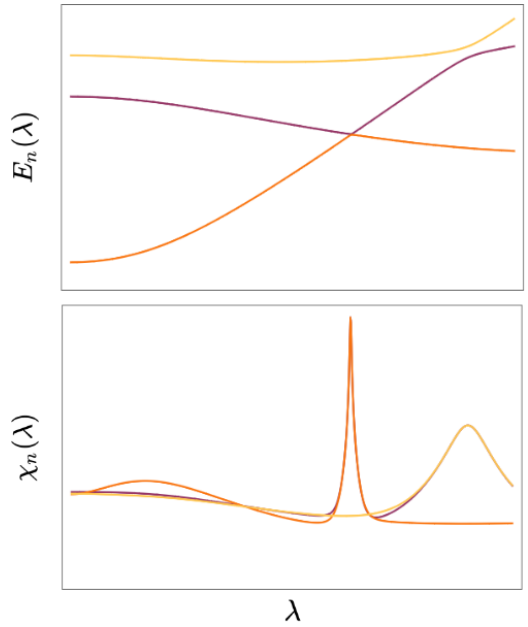

Figure 3.2: Fidelity Susceptibility. Plots of 3 energy levels energy(top panel) for an arbitrary Hamiltonian of the form Eq. (3.7) as function of the coupling parameter λ in arbitrary units. Within this parameter range we detect 2 avoided crossings, in order of appearance from left to right: between 1 and 2, between 2 and 3. The first crossing is of diabatic nature while the second one is adiabatic. The crossings are detected as the peaks of the eigenstate fidelity as a function of the coupling parameter. The character of the anticrossings is reflected on the sharpness of the peaks, the first two crossings correspond to sharp delta-like peaks while the last one corresponds to a lower and broader peak.

$\delta\lambda$ near an avoided crossing the fidelity should be vanishing and therefore the susceptibility will be clearly divergent. For finite $\delta\lambda$ this divergence should manifest as sharp peaks of the fidelity susceptibility which can be used as detection events for avoided crossings. On the contrary, near a regular region of the parameter space with no avoided crossings the fidelity should be close to 1 and the susceptibility is indeterminate. In practice, we will use a simplified version of the fidelity susceptibility by expanding $|\psi_n(\lambda + \delta\lambda)\rangle$ to second order in $\delta\lambda$ and obtaining

$$\chi_n(\lambda) = \sum_{m \neq n} \frac{|\langle\psi_m(\lambda)|V|\psi_n(\lambda)\rangle|^2}{(E_n(\lambda) - E_m(\lambda))^2}, \tag{3.10}$$

with $V = \sum_{i<j} V_{ij}$ standing for the interaction potential of Eq. (3.7). This behavior is demonstrated in Fig. 3.2

3.2 Walsh-Hadamard Perturbation Theory

We begin with a second quantization Hamiltonian of a lattice model of arbitrary dimensions and N sites in total

$$H = H_0 + gV_{\alpha\beta\mu\nu}c^\dagger_\alpha c^\dagger_\beta c_\mu c_\nu, \tag{3.11}$$

where c_μ and $c^\dagger_\mu$ are bosonic annihilation and creation operators respectively, acting on site μ of the lattice. We have also used the following summation convention and we will keep using it though out the chapter

Convention 1. *Any indices that do not appear on both sides of an equation are to be summed over the range* $[1, N]$

For the tensor $V_{\alpha\beta\mu\nu}$ we assume that it is real and we impose no further restrictions, however there are two symmetries that will simplify our calculation significantly without loss of generality. The first one is the fact that

$$\sum_{\alpha,\beta,\mu,\nu} V_{\alpha\beta\mu\nu}c^\dagger_\alpha c^\dagger_\beta c_\mu c_\nu = \sum_{\alpha,\beta,\mu,\nu} V_{\alpha\beta\mu\nu}c^\dagger_\beta c^\dagger_\alpha c_\mu c_\nu = \sum_{\alpha,\beta,\mu,\nu} V_{\beta\alpha\mu\nu}c^\dagger_\alpha c^\dagger_\beta c_\mu c_\nu, \tag{3.12}$$

where in the first step we used the commutativity of the bosonic operators and in the second step we performed a summation index relabeling. Even though this property does not guarantee that $V_{\alpha\beta\mu\nu} = V_{\beta\alpha\mu\nu}$, it does suggest that if $V_{\alpha\beta\mu\nu}$ has an antisymmetric component with respect to the first two indices then that component yields no contribution to the sum. Since we can always decompose $V_{\alpha\beta\mu\nu}$ to a symmetric and an antisymetric component it means we can assume without loss of generality that $V_{\alpha\beta\mu\nu}$ can always be symmetrized with respect to the first two indices without changing the Hamiltonian of the system. The exact same argument can be made for the last two indices. The second argument follows along similar lines

$$\sum_{\alpha,\beta,\mu,\nu} V_{\alpha\beta\mu\nu}c^\dagger_\alpha c^\dagger_\beta c_\mu c_\nu = \sum_{\alpha,\beta,\mu,\nu} V_{\alpha\beta\mu\nu}c^\dagger_\nu c^\dagger_\mu c_\beta c_\alpha = \sum_{\alpha,\beta,\mu,\nu} V_{\mu\nu\alpha\beta}c^\dagger_\alpha c^\dagger_\beta c_\mu c_\nu, \tag{3.13}$$

where in the first step we used the Hermiticity of the sum and in the second step we performed a summation index relabeling. Once again, this does not imply $V_{\alpha\beta\mu\nu} = V_{\mu\nu\beta\alpha}$, however any component antihermitian with respect to the index pair exchange would have vanishing contribution to the sum and hence $V_{\alpha\beta\mu\nu}$ can be thought as symmetric with respect to the index pair exchange without loss of generality. In summary our symmetries for the tensor are

$$V_{\alpha\beta\mu\nu} = V_{\beta\alpha\mu\nu} = V_{\alpha\beta\nu\mu} = V_{\mu\nu\alpha\beta} \tag{3.14}$$

For the dimensionless parameter we assume $g \ll 1$ and obtain the eigenvalues of H perturbatively from the known eigenvalues of H_0

$$H_0 = E_\mu c_\mu^\dagger c_\mu. \tag{3.15}$$

Since the ladder operators are bosonic the system has an infinite number of eigenstates. However, for the Walsh-Hadamard coefficients, we are only interested in the finite subspace of qubit states

$$|b\rangle = \prod_{\mu=1}^{N} (c_\mu^\dagger)^{b_\mu} |0\rangle \tag{3.16}$$

where b is a bit-string and b_μ is the μ-th digit of b. For this family of states the unperturbed energy levels take the form

$$E_b^{(0)} = \langle b|H_0|b\rangle = E_\mu b_\mu \tag{3.17}$$

while for the full interacting system of Eq. (3.11) we have approximately up to second order in g

$$E_b \simeq E_b^{(0)} + gE_b^{(1)} + g^2 E_b^{(2)} \tag{3.18}$$

with $E_b^{(1)}$ and $E_b^{(2)}$ being the usual Rayleigh-Schrödinger perturbation theory first and second order corrections respectively.

3.2.1 First Order Energy Correction

We now proceed with the calculation of the first order correction. By definition

$$E_b^{(1)} = V_{\alpha\beta\mu\nu} \langle b|c_\alpha^\dagger c_\beta^\dagger c_\mu c_\nu|b\rangle. \tag{3.19}$$

If we substitute the state of Eq. (3.16) in this definition, the calculation of the first order correction boils down to a single vacuum expectation value, which in turn can be evaluated by means of Wick contractions. Since this is a vacuum expectation value only the fully contracted terms of Wick's theorem are non vanishing. An additional layer of complexity for this calculation is due to the fact that the ladder operators that appear from substitution of Eq. (3.16) in Eq. (3.19) come with an ambiguous exponent that can be either 0 or 1. We will refer to these operators as *external* while the ladder operators that originate from the perturbing potential we will refer to as *internal*.

Since the internal operators are already normal ordered, we cannot have internal-internal contractions according to the standard Wick contraction rules

$$\overbracket{c_\mu c_\nu^\dagger} = \delta_{\mu\nu} \quad \text{and} \quad \overbracket{c_\mu^\dagger c_\nu} = \overbracket{c_\mu c_\nu} = \overbracket{c_\mu^\dagger c_\nu^\dagger} = 0, \tag{3.20}$$

therefore internal operators have to be contracted with external ones. As already stated however the external operators appear with an ambiguous exponent and therefore we have to consider different contraction rules. For contractions involving only one external operator we can distinguish the two cases

$$\overbrace{c_\mu(c_\nu^\dagger)^{b_\nu}} = \begin{cases} c_\mu 1 - \mathcal{N}(c_\mu 1) = 0, & b_\nu = 0 \\ c_\mu c_\nu^\dagger - \mathcal{N}(c_\mu c_\nu^\dagger) = \delta_{\mu\nu}, & b_\nu = 1. \end{cases} \tag{3.21}$$

where $\mathcal{N}(\cdot)$ is denoting normal ordering. The situation for ambiguous exponent on the annihilation operator instead is completely equivalent. This expression can be neatly summarised by

$$\overbrace{c_\mu(c_\nu^\dagger)^{b_\nu}} = \overbrace{(c_\mu)^{b_\mu}c_\nu^\dagger} = b_\mu \delta_{\mu\nu}. \tag{3.22}$$

Finally we have to consider contractions between external operators. Since these are only possible between operators acting on the same lattice site this condition automatically forces the exponents to be equal. If they are both 1 then we simply have the first case in Eq. (3.20). If they are both 0, direct application of the definition of Wick contractions would yield 0, however if they are both zero it means we are attempting to contract two identity operators which makes no sense, therefore we do not need to contract them in that case and instead we get a factor of 1 again, therefore

$$\overbrace{(c_\mu)^{b_\mu}(c_\nu^\dagger)^{b_\nu}} = \delta_{\mu\nu}. \tag{3.23}$$

All of the above can be summarised in the following contraction rules

$$\overbrace{(c_\mu)^{b_\alpha}(c_\nu^\dagger)^{b_\beta}} = \delta_{\mu\nu}\delta_{b_\alpha,b_\beta} \tag{3.24}$$

and all other contractions are vanishing. It is completely straightforward to verify that this expression encompasses all of the previous cases by considering that $\delta_{b_\mu,1} = b_\mu$.

Equipped with the Wick contraction rules we can now return to the calculation of the amplitude of Eq. (3.19). In order to do this we need to fully contract the operators. We will do this using the permanent method described in [30], which consists of calculating the permanent of the matrix whose elements corresponding to all possible Wick contractions between an annihilation operator, corresponding to a row, and a creation operator, corresponding to a column. Using the basis $\{c_\mu, c_\nu, c_1^{b_1}, \dots, c_N^{b_N}\}$ for the rows and $\{c_\alpha^\dagger, c_\beta^\dagger, (c_1^\dagger)^{b_1}, \dots, (c_N^\dagger)^{b_N}\}$ for

the columns we can write Eq. (3.24) in matrix form

$$\mathcal{C}_{\alpha\beta\mu\nu}(b) = \begin{pmatrix} 0 & 0 & b_1\delta_{\mu,1} & \dots & b_N\delta_{\mu,N} \\ 0 & 0 & b_1\delta_{\nu,1} & \dots & b_N\delta_{\nu,N} \\ b_1\delta_{\alpha,1} & b_1\delta_{\beta,1} & 1 & \dots & 0 \\ \vdots & \vdots & \vdots & \ddots & \vdots \\ b_N\delta_{\alpha,N} & b_N\delta_{\beta,N} & 0 & \dots & 1 \end{pmatrix}. \tag{3.25}$$

For the first order correction we will have from Eq. (3.19)

$$E_b^{(1)} = V_{\alpha\beta\mu\nu}\,\mathrm{perm}\left(\mathcal{C}_{\alpha\beta\mu\nu}(b)\right). \tag{3.26}$$

By definition, the permanent of a $d\times d$ matrix is the sum over all possible products consisted of d elements of the matrix with no two of them sharing a row or column. From the first two rows, only elements past column 2 have a non vanishing contribution to the product therefore, for example, if we select elements $2+\rho$ and $2+\sigma$ from the first and second row respectively, we will have a factor of $b_\rho b_\sigma \delta_{\mu\rho}\delta_{\nu\sigma}$ with the restriction that $\rho \neq \sigma$ which can be enforced by multiplying this expression with $|\varepsilon_{\rho\sigma}|$ with ε denoting the fully antisymetric tensor. Having selected an element from columns $2+\rho$ and $2+\sigma$ means that we have effectively removed these entire columns and therefore at the corresponding rows the only possible choices that lead to a non vanishing contribution are from columns 1 and 2 yielding either $b_\rho b_\sigma \delta_{\alpha\rho}\delta_{\beta\sigma}$ or $b_\rho b_\sigma \delta_{\alpha\sigma}\delta_{\beta\rho}$. With the first two rows and columns of the matrix removed means we can only choose elements from the identity matrix at the bottom right of the contraction matrix. The permanent for our two-body case yields

$$E_b^{(1)} = V_{\alpha\beta\mu\nu} b_\rho b_\sigma |\varepsilon_{\rho\sigma}| \delta_{\mu\rho}\delta_{\nu\sigma}(\delta_{\alpha\rho}\delta_{\beta\sigma} + \delta_{\alpha\sigma}\delta_{\beta\rho}). \tag{3.27}$$

Performing the summation with respect to ρ, σ, α and β and using the symmetries of the interaction potential Eq. (3.14) we obtain

$$E_b^{(1)} = \mathcal{E}^{\mu\nu} b_\mu b_\nu. \tag{3.28}$$

where we used the tensor definition

$$\mathcal{E}_{\mu\nu} = 2V_{\mu\nu\mu\nu}. \tag{3.29}$$

as well as the following index raising convention

Convention 2. *An element for which any two of the $n \leq m$ raised indices of an m-dimensional tensor $\mathcal{M}$ take the same value is vanishing*

$$\mathcal{M}^{i_1\dots i_n}_{i_{n+1}\dots i_m} = |\varepsilon_{i_1\dots i_n}| \mathcal{M}_{i_1\dots i_m}.$$

Note that according to the symmetries of $V_{\alpha\beta\mu\nu}$ given in Eq. (3.14) the tensor $\mathcal{E}$ should be symmetric

$$\mathcal{E}_{\mu\nu} = \mathcal{E}_{\nu\mu} \tag{3.30}$$

3.2.2 Second Order Energy Correction

We now proceed with the second order correction given by

$$E_b^{(2)} = V_{\alpha_1\beta_1\mu_1\nu_1} V_{\alpha_2\beta_2\mu_2\nu_2} \sum_{m\neq b} \frac{\langle b|c^\dagger_{\alpha_1} c^\dagger_{\beta_1} c_{\mu_1} c_{\nu_1}|m\rangle\langle m|c^\dagger_{\alpha_2} c^\dagger_{\beta_2} c_{\mu_2} c_{\nu_2}|b\rangle}{E_b - E_m}. \tag{3.31}$$

We have a new complication here, since the eigenstates $|m\rangle$ of the free Hamiltonian are not necessarily qubit states anymore and as a result Wick contraction rules for arbitrary exponents become significantly more complicated. However we can circumvent this using the following argument. The state resulting from the application of $c^\dagger_{\alpha_2} c^\dagger_{\beta_2} c_{\mu_2} c_{\nu_2}$ on the qubit state $|b\rangle$ is still an eigenstate $|n_2\rangle$ of the free Hamiltonian although it might not be normalised anymore

$$c^\dagger_{\alpha_2} c^\dagger_{\beta_2} c_{\mu_2} c_{\nu_2}|b\rangle = \lambda_2|n_2\rangle. \tag{3.32}$$

A similar argument follows for the bracket

$$\langle b|c^\dagger_{\alpha_1} c^\dagger_{\beta_1} c_{\mu_1} c_{\nu_1} = \lambda_1\langle n_1|. \tag{3.33}$$

and therefore we can write using Eq. (3.31)

$$E_b^{(2)} = \lambda_1\lambda_2 V_{\alpha_1\beta_1\mu_1\nu_1} V_{\alpha_2\beta_2\mu_2\nu_2} \sum_{m\neq b} \frac{\langle n_1|m\rangle\langle m|n_2\rangle}{E_b - E_m} \tag{3.34}$$

$$= \lambda_1\lambda_2 V_{\alpha_1\beta_1\mu_1\nu_1} V_{\alpha_2\beta_2\mu_2\nu_2} \sum_{m\neq b} \frac{\delta_{n_1,m}\delta_{n_2,m}}{E_b - E_m} \tag{3.35}$$

$$= \lambda_1\lambda_2 V_{\alpha_1\beta_1\mu_1\nu_1} V_{\alpha_2\beta_2\mu_2\nu_2} \left.\frac{\delta_{n_1,n_2}}{E_b - E_{n_2}}\right|_{n_2\neq b} \tag{3.36}$$

$$= V_{\alpha_1\beta_1\mu_1\nu_1} V_{\alpha_2\beta_2\mu_2\nu_2} \left.\frac{\lambda_1\lambda_2\langle n_1|n_2\rangle}{E_b - E_{n_2}}\right|_{n_2\neq b}. \tag{3.37}$$

Finally since by definition the state $|n_2\rangle$ is obtained from $|b\rangle$ by extracting two excitations from sites μ_2 and ν_2 and adding two at sites α_2 and β_2 we will have

$$E_{n_2} = E_b - E_{\mu_2} - E_{\nu_2} + E_{\alpha_2} + E_{\beta_2} \tag{3.38}$$

and in total

$$E_b^{(2)} = V_{\alpha_1\beta_1\mu_1\nu_1} V_{\alpha_2\beta_2\mu_2\nu_2} \left.\frac{\langle b|c^\dagger_{\alpha_1} c^\dagger_{\beta_1} c_{\mu_1} c_{\nu_1} c^\dagger_{\alpha_2} c^\dagger_{\beta_2} c_{\mu_2} c_{\nu_2}|b\rangle}{E_{\mu_2} + E_{\nu_2} - E_{\alpha_2} - E_{\beta_2}}\right|_{\{\alpha_2,\beta_2\}\neq\{\mu_2,\nu_2\}}, \tag{3.39}$$

where $\{\alpha_2, \beta_2\} \neq \{\mu_2, \nu_2\}$ is meant in the sense of set inequality. Once again we have an amplitude involving only a single qubit state and therefore we can use the Wick rules from the first order calculation leading directly to the contraction matrix

$$\begin{pmatrix} 0 & 0 & \delta_{\mu_1\alpha_2} & \delta_{\mu_1\beta_2} & b_1\delta_{\mu_1,1} & \dots & b_N\delta_{\mu_1,N} \\ 0 & 0 & \delta_{\nu_1\alpha_2} & \delta_{\nu_1\beta_2} & b_1\delta_{\nu_1,1} & \dots & b_N\delta_{\nu_1,N} \\ 0 & 0 & 0 & 0 & b_1\delta_{\mu_2,1} & \dots & b_N\delta_{\mu_2,N} \\ 0 & 0 & 0 & 0 & b_1\delta_{\nu_2,1} & \dots & b_N\delta_{\nu_2,N} \\ b_1\delta_{\alpha_1,1} & b_1\delta_{\beta_1,1} & b_1\delta_{\alpha_2,1} & b_1\delta_{\beta_2,1} & 1 & \dots & 0 \\ \vdots & \vdots & \vdots & \vdots & \vdots & \ddots & \vdots \\ b_N\delta_{\alpha_1,N} & b_N\delta_{\beta_1,N} & b_N\delta_{\alpha_2,N} & b_N\delta_{\beta_2,N} & 0 & \dots & 1 \end{pmatrix}. \tag{3.40}$$

For this case, since the effective four-body interaction is not normal ordered already, we also have internal-internal contractions. There are multiple ways to deal with this, namely normal ordering the interaction term using the bosonic algebra, the method of reduced permanents or considering cases as we did before for the first order correction. The results are summarised in the following expression

$$E_b^{(2)} = \mathcal{D}_{\mu\nu}^{\alpha\beta} b_\alpha b_\beta + 8(\mathcal{D}_\nu^{\alpha\beta\mu} + \mathcal{S}_\nu^{\alpha\beta\mu}) b_\alpha b_\beta b_\mu, \tag{3.41}$$

where conventions 1 and 2 still hold and we have also introduced the tensor definitions

$$\mathcal{S}_{\alpha\beta\mu\nu} = \begin{cases} 2\dfrac{V_{\alpha\mu\alpha\nu}V_{\beta\mu\beta\nu}}{E_\mu - E_\nu}, & \mu \neq \nu \\ 0, & \mu = \nu \end{cases} \tag{3.42}$$

$$\mathcal{D}_{\alpha\beta\mu\nu} = \begin{cases} \dfrac{|V_{\alpha\beta\mu\nu}|^2}{E_\alpha + E_\beta - E_\mu - E_\nu}, & \{\alpha, \beta\} \neq \{\mu, \nu\} \\ 0, & \{\alpha, \beta\} = \{\mu, \nu\}. \end{cases} \tag{3.43}$$

Note that in the element-wise definitions of Eqs. (3.42) and (3.43) there are no implied summations and in conjunction with Eq. (3.14) we can conclude the following symmetries

$$\mathcal{S}_{\alpha\beta\mu\nu} = \mathcal{S}_{\beta\alpha\mu\nu} = -\mathcal{S}_{\alpha\beta\nu\mu}, \tag{3.44}$$

$$\mathcal{D}_{\alpha\beta\mu\nu} = \mathcal{D}_{\beta\alpha\mu\nu} = \mathcal{D}_{\alpha\beta\nu\mu} = -\mathcal{D}_{\mu\nu\alpha\beta}. \tag{3.45}$$

The antisymmetric property of the tensors $\mathcal{S}$ and $\mathcal{D}$ is the reason why in the second order correction of Eq. (3.41) we have no four-bit terms. Indeed, Eq. (3.41) is the result of the summation over all possible full contractions of the amplitude in Eq. (3.39). The two-bit terms $\mathcal{D}_{\mu\nu}^{\alpha\beta} b_\alpha b_\beta$ are the result of the full amplitude

contractions that include two internal-internal contractions, the three-bit terms $(\mathcal{D}_\nu^{\alpha\beta\mu} + \mathcal{S}_\nu^{\alpha\beta\mu})b_\alpha b_\beta b_\mu$ are those with only one internal-internal contraction and finally one would expect four-bit terms since there also full amplitude contractions without any internal-internal contractions. These four-bit terms however are of the form $(\mathcal{D}^{\alpha\beta\mu\nu} + \mathcal{S}^{\alpha\beta\mu\nu})b_\alpha b_\beta b_\mu b_\nu$, meaning we have a sum over an anitsymmetric product which is trivially vanishing.

3.2.3 Second Order Walsh-Hadamard Coefficients

With the Rayleigh-Schrödinger perturbation theory results of Eqs. (3.28) and (3.41) for the qubit state energy levels we are now able to derive the Walsh-Hadamard coefficients via direct application of the definition in Eq. (3.6). Furthermore, since the transformation is linear we can perform it term by term

$$w_b^{(n)} = \frac{1}{2^N} \sum_{q \in \mathbb{B}^N} (-1)^{b\cdot\bar{q}} E_q^{(n)}, \; n \in \{0, 1, 2\}. \tag{3.46}$$

We start with the zeroth order term of Eq. (3.17)

$$w_b^{(0)} = \frac{1}{2^N} \sum_{q \in \mathbb{B}^N} (-1)^{b\cdot\bar{q}} E_\mu q_\mu. \tag{3.47}$$

In order to carry out the Boolean summation we split the bit-string summation over a product of bit-digit summations and use the properties

$$\sum_{q=0}^{1} (-1)^{b\bar{q}} = 2\bar{b} \quad \text{and} \quad \sum_{q=0}^{1} (-1)^{b\bar{q}} q = 1. \tag{3.48}$$

As an example we present the summation explicitly for zeroth order case

$$w_b^{(0)} = \frac{E_\mu}{2^N} \sum_{q \in \mathbb{B}^N} (-1)^{b\cdot\bar{q}} q_\mu \tag{3.49}$$

$$= \frac{E_\mu}{2^N} \left(\prod_{\substack{\rho=1 \\ \rho\neq\mu}}^{N} \sum_{q_\rho=0}^{1} (-1)^{b_\rho \cdot \bar{q}_\rho} \right) \left(\sum_{q_\mu=0}^{1} (-1)^{b_\mu \cdot \bar{q}_\mu} q_\mu \right) \tag{3.50}$$

$$= \frac{E_\mu}{2} \prod_{\substack{\rho=1 \\ \rho\neq\mu}}^{N} \bar{b}_\rho, \tag{3.51}$$

and for the first and second order terms it follows similarly that

$$w_b^{(1)} = \frac{\mathcal{E}^{\alpha\beta}}{4} \prod_{\substack{\rho=1 \\ \rho\neq\alpha,\beta}}^{N} \bar{b}_\rho \tag{3.52}$$

$$w_b^{(2)} = \frac{1}{4}\mathcal{D}_{\mu\nu}^{\alpha\beta} \prod_{\substack{\rho=1 \\ i\neq\alpha,\beta}}^{N} \bar{b}_\rho + (\mathcal{D}_\nu^{\alpha\beta\mu} + \mathcal{S}_\nu^{\alpha\beta\mu}) \prod_{\substack{\rho=1 \\ \rho\neq\alpha,\beta,\mu}}^{N} \bar{b}_\rho. \tag{3.53}$$

The products of the flipped bit digits pose a sharp cutoff for the weight of Walsh-Hadamard coefficients we can estimate at a finite order of perturbation theory. Namely for a bit-string $b^{(m)}$ of weight m, the product of all flipped bit digits excluding k, with $m > k$, will be vanishing for any set of excluded flipped digits since at least one of them will be zero. Therefore, to second order in perturbation theory, we can only obtain corrections for the Walsh-Hadamard coefficients of weight up to 3. For the non vanishing cases with $m \leq k$, assuming that the non zero digits of the bit-string are located at positions ℓ_1 through ℓ_m in ascending order, the product will yield one if $\{\ell_1, \dots, \ell_m\}$ is a subset of the excluded digits. The above can be summarised in the following expression

$$\prod_{\rho\neq\mu_1,\dots,\mu_k} \bar{b}_\rho^{(m)} = \theta(k-m) \sum_{s\in[\mu_1,\dots,\mu_k]^m} \prod_{j=1}^{m} \delta_{\ell_j,s(j)}, \tag{3.54}$$

with θ denoting the Heaviside step function with the convention $\theta(0) = 1$ and $[\mu_1, \dots, \mu_k]^m$ denotes the set of all oriented subsets of length m of the set $\{\mu_1, \dots, \mu_n\}$. As an example the flipped digit product for a bit-string of weight $m = 2$ with $k = 3$ excluded digits yields

$$\prod_{\rho\neq\mu_1,\mu_2,\mu_3} \bar{b}_\rho^{(2)} = \delta_{\ell_1}^{\mu_1}\delta_{\ell_2}^{\mu_2} + \delta_{\ell_1}^{\mu_2}\delta_{\ell_2}^{\mu_1} + \delta_{\ell_1}^{\mu_1}\delta_{\ell_2}^{\mu_3} + \delta_{\ell_1}^{\mu_3}\delta_{\ell_2}^{\mu_1} + \delta_{\ell_1}^{\mu_2}\delta_{\ell_2}^{\mu_3} + \delta_{\ell_1}^{\mu_3}\delta_{\ell_2}^{\mu_2}. \tag{3.55}$$

We used upper indices here only for presentation purposes and no additional context. We summarise the results for the Walsh-Hadamard coefficients Eqs. (3.51), (3.52) and (3.53) using the expression for the flipped digit products in Eq. (3.54) for all possible combinations of bit-string weight m and number of excluded digits k in appendix D.

4

Chaotic Fluctuations of Transmons

In this chapter we will explore the localizing effects of disorder for transmon arrays. We begin by establishing that the system is subject to an MBL to chaotic phase transition using the spectral statistics measures (4.1.1). We will demonstrate that quantum computation is safe only deep in the MBL regime using the Walsh-Hadamard coefficients (4.1.2). Finally we close this chapter with a brief overview of our results for cutting edge transmon array architectures (4.2) including 2D lattice configurations (4.2.1) and the intricate case of frequency patterns designed with the LASIQ technique (4.2.2). We find that the results for these cases do not differ at a qualitative level from the random disorder 1D cases and whatever minor deviations appear are still compliant with expectation of MBL theory. This reinforces the message that ensuring a sufficient degree of disorder is present in quantum computation systems will be crucial for future architecture designs.

As a general disclaimer for this chapter only: This chapter is based on our joint paper [A1] with our colleagues from Cologne, C. Berke, S. Trebst and A. Altland. All calculations reported here involving Kullback-Leibler divergence and inverse participation ratios have been carried out by C. Berke while the Walsh-Hadamard calculations have been carried by the author of this thesis, E. Varvelis.

4.1 Disordered Transmon Chain

The classical analogue of an array of capacitively coupled transmons is an array of pendulums which are interacting via inerters [31], with Hamiltonian given by

Eq. (1.35) after relabeling the parameters and substituting the variables φ_i and n_i with position and momentum respectively. Such a system is prone to chaotic behavior and thus according to the BGS conjecture [6, 32], we expect a quantum chaotic phase for transmon arrays.

For actual realisations of the quantum system we will unavoidably have some parameter variation from transmon to transmon. There are three parameters in our Hamiltonian of Eq. (1.35) through which we can introduce disorder in our model. The first possibility is the capacitive energy E_C of each transmon. However this parameter is related to the capacitance of a transmon which can actually be fixed accurately to a very high percentage. Since we consider capacitively coupled transmons, the same argument can be made for the coupling strength parameter λ with the additional technical constraint that it cannot be larger than E_C. The only remaining choice is the Josephson energy E_J. Until recently this parameter had significant statistical fluctuations of the order of a few percent and thus it is a natural candidate for being the carrier of disorder.

For our calculations we fixed the capacitive energy to a typical value of $E_C \simeq 250$ MHz and coupling strength varied in the range of $\lambda \simeq 0 - 50$ MHz. Josephson energies are the carrier of our disorder and they will be treated as random variables drawn from a Gaussian distribution with average value E_J and standard deviation δE_J, called the disorder strength in MBL literature, and they were both allowed to vary. In order to have our results directly comparable to the available experimental data we will also some times refer to the qubit frequency standard deviation $\delta\omega$ as our disorder strength. The two disorder strengths can be used interchangeably since they can be related directly via the relation

$$\delta\omega = \sqrt{\frac{2E_C}{E_J}}\delta E_J \tag{4.1}$$

In order for such an array of transmons to be considered a quantum computing device we need to be able to perform logical operations on them, or gates, and thus they need to be able to communicate. The coupling of such non-linear oscillators in conjunction with the existence of disorder lay the groundwork for a possible MBL phase and therefore we expect and MBL-chaotic phase transition.

For a quantum computing system it is imperative to be deep within the localized regime as we will establish here. The reason for this is two-fold. First of all, it is crucial to be able to identify qubit eigenstates accurately. Since the transmon is only effectively a qubit system, while in reality it is a bosonic system, we need to be able to distinguish the computational states among the ocean of leakage states (see Fig. 4.1). As we will see later on, this cannot be done reliably in the chaotic regime. The second reason is that we need our quantum devices to have as long a coherence time as possible. Coherence time is related to the so called

ZZ coupling strength [33], which is the strength of nearest neighbor coupling in the eigenbasis of the Hamiltonian. In other words these are the coefficients of the LIOM decomposition of the Hamiltonian corresponding to nearest neighbor two-body terms in Eq. (2.31). These are exponentially weak only deep within the MBL phase.

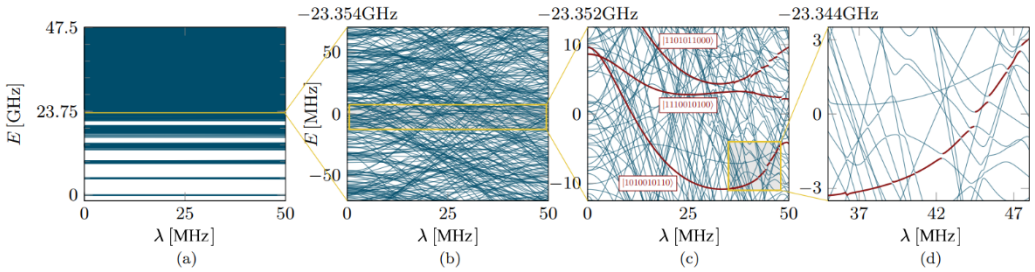

Figure 4.1: Transmon array spectrum. Energy spectrum of a length 10, 1D capacitively coupled transmon array as a function of coupling strength, on varying energy scales. Panel (a) illustrates the global structure of the spectrum, separated into energy bundles corresponding to the total number of bosonic excitations. In panel (b) we zoom into the 5-excitation band, which demonstrates level repulsions that become more clear by zooming in furhter in panel (c). In panel (c) we also track the bit-label identity of the only three computational states in this energy window, marked in red, using the state identification protocol 4.1.2. In the last panel we single out only one of these states which changes identity through several avoided level crossings.

4.1.1 Kullback-Leibler Divergence and Inverse Participation Ratio

We begin our effort of identifying an MBL-chaotic transition for the transmon array described by Eq. (1.35) by looking at the spectral statistics both in the form of level spacing statistics as well as the inverse participation ratios of the eigenstate wavefunctions. As we have discussed before in chapter 2, if the system is in the chaotic regime, we expect Wigner-Dyson statistics for the energy level spacings and Poisson statistics for the MBL regime.

The standard method for determining if the system is in the chaotic or the MBL phase in level spacing statistics studies, is by looking at the behavior of the distribution near zero spacing. The two competing distributions have distinctively different behaviors around this region, Wigner-Dyson is vanishing while Poisson is maximal. However since the level spacing distribution does not change instantly at the transition from MBL to chaotic, but rather it continuously deforms from one to the other, near the transition the distribution will be neither

Poisson nor Wigner-Dyson. Therefore in order to study the transition we need a method of quantifying the distance of two distributions and the measure we employed here is the Kullback-Leibler divergence defined in the following equation

$$D_{\mathrm{KL}}(P|Q) = \sum_i p_i \log\left(\frac{p_i}{q_i}\right). \tag{4.2}$$

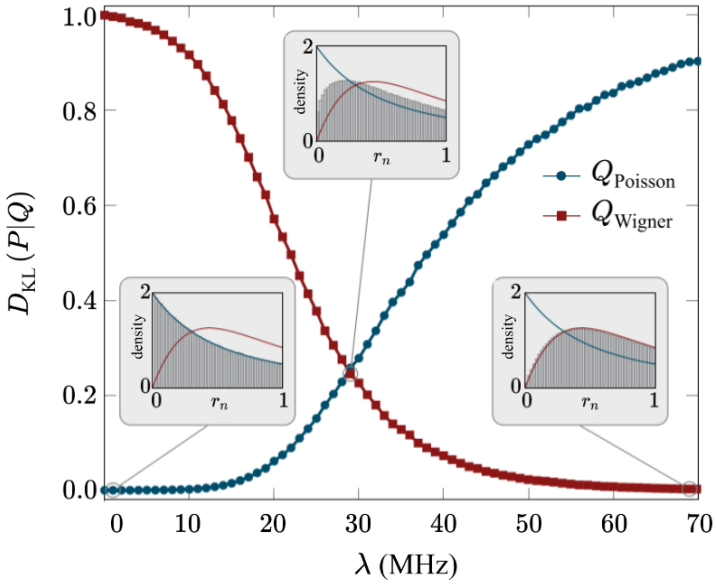

Figure 4.2: Demonstration of KL divergence. KL Data for a chain of $N = 10$ transmons versus the coupling parameter λ. The average Josephson energy is fixed to $E_{\mathrm{J}} = 44$ GHz and $\delta E_{\mathrm{J}} = 1.17$ GHz. KL divergences D_{KL} are calculated for the distribution of ratios of consecutive level spacings r_n in the energy spectrum, such as the ones illustrated in the insets for three characteristic couplings. The KL divergences are normalized such that $D_{\mathrm{KL}}(P_{\mathrm{Wigner}}|Q_{\mathrm{Poisson}}) = 1$ and vice versa. We probe an energy bundle of excited states, which are generated by a total of $N/2 = 5$ excitations. For the $N = 10$ transmon chain at hand, this manifold contains a total of 2002 different states. All results are averaged over at least 2500 disorder realizations

In case that the two distributions under comparison, P and Q, are identical then clearly the KL divergence is vanishing since $p_i = q_i, \forall i$. If they are different then it is strictly positive and its exact value is dependent on the distributions under comparison as well as the order of comparison, *i.e.* $D_{\mathrm{KL}}(P|Q) \neq D_{\mathrm{KL}}(Q|P)$ in general. This behavior is demonstrated in Fig. 4.2 where we compare the level spacing distribution of a specific disorder realisation for a 1D transmon array to both the Poisson and Wigner-Dyson distributions as we vary the coupling strength. In the intermediate coupling region of this plot we observe that

the level spacing distribution is neither Poisson nor Wigner-Dyson and thus it would be complicated to identify a transition solely by looking at the distribution. KL divergence however gives us naturally a transition point, the point where our distribution is equidistant from both possible distributions. In Fig. 4.3 we present the resulting phase diagram from calculating the KL divergence for varying coupling strength and average Josephson energy.

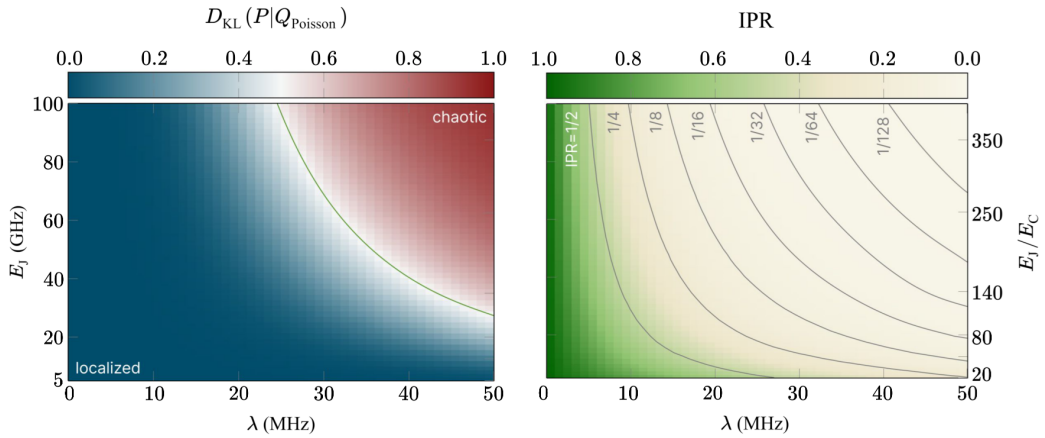

Figure 4.3: Phase diagrams. KL divergence D_{KL} with respect to the Poisson distribution in the plane spanned by the Josephson energy E_{J} and the transmon coupling λ (left panel) for weak disorder ($\delta\omega \simeq 0.12$ GHz). The KL divergence is color coded so that the MBL regime is denoted with blue (Poisson distribution) and the quantum chaotic regime is denoted with red (Wigner-Dyson distribution). Wave function statistics for the same parameters are presented in the right panel and are color-coded by the mean IPR value showing a fast drop to values below 1/2 already for moderate coupling strength. The grey lines indicate contour lines of constant IPR. All results are averaged over at least 2000 disorder realizations. The spread of the Josephson energies varies from $\delta E_{\mathrm{J}} \simeq 0.4$ GHz for $E_{\mathrm{J}} = 5$ GHz to $\delta E_{\mathrm{J}} \simeq 1.7$ GHz for $E_{\mathrm{J}} = 100$ GHz.

In order to complete our statistical analysis of the transition we need to do wavefunction statistics which we did here using the inverse participation ratio. Since for zero coupling the eigenbasis are the Fock states, it is natural to express our eigenvectors in the the Fock space and calculate the IPR in this representation. In order to get an overview of the system behavior we will use the averaged IPR over all relevant eigenstates. The resulting phase diagram by calculating the average IPR for varying coupling strength and average Josephson energy is reported in Fig. 4.3. Notice that the IPR $= 1/2$ critical line is reached much earlier than the equidistant distribution line of KL divergence, as we vary coupling strength. This is an artefact of finite size effects since we are considering relatively small system sizes of 10 transmons or less. However even for such small systems the number of states is exponentially large by any numerical standard. Furthermore,

the exact position of the critical line within this region between the IPR = 1/2 line and the $D_{\mathrm{KL}}(P|Q_{\mathrm{Poisson}}) = D_{\mathrm{KL}}(P|Q_{\mathrm{WD}})$ line, which we called the "twilight zone", is irrelevant for us and might be related to an intermediate phase between MBL and chaos [34]. We are interested in locating where quantum computation is safe and for that we need a new diagnostic which we present in the following section.

4.1.2 Walsh-Hadamard and Avoided Crossings

As we have seen in the previous section transmon arrays do exhibit an MBL-chaotic phase transition with an ambiguous border between the two phases. Here we want to consider the consequences of MBL and chaos from a quantum information prospective. For that we look back at the LIOM Hamiltonian Eq. (2.32). The adjacent site two body terms and their effects on quantum information processing systems have been studied copiously in the literature of quantum information [33, 35–37], where they are usually referred to as ZZ couplings with Z denoting to the Pauli z since these are the LIOM for a quantum memory. These ZZ couplings are closely related to the dephasing time of qubits and they are also an inhibitor for precise two-qubit operations.

For static always-on coupling, which is the case we are concerned with here, these terms cannot be completely eliminated. We will ignore for the moment longer range and higher weight terms thus bringing our Hamiltonian to the form

$$H_{ZZ} = \sum_{i=1}^{N} \omega_i Z_i + \sum_{\langle i,j \rangle} J_{ij} Z_i Z_j. \tag{4.3}$$

This is similar to the Hamiltonian of Eq. (1.18) but with bond dependent coupling strength J_{ij}. As we have seen in subsection 1.1.2, this is not a true quantum memory and we will repeat a sketch of that argument here. If we only had the first term in Eq. (4.3) then we could measure in the rotating frame and therefore completely eliminate any dynamics for our system. As soon as there is any finite ZZ coupling in our system however dynamics are restored and general states will time evolve under this Hamiltonian.

From the above it should be now evident why we need to keep quantum memories deep into the many body localized regime. Since ZZ, and worse, longer range or higher weight correlations are inevitable we need to keep them under control. MBL does that effectively by forcing an exponential hierarchy to these couplings but only deep within the localization regime. On the extreme opposite of quantum chaos all the many body terms converge towards the same order of magnitude, in an "everyone talks to everyone" situation, rendering quantum

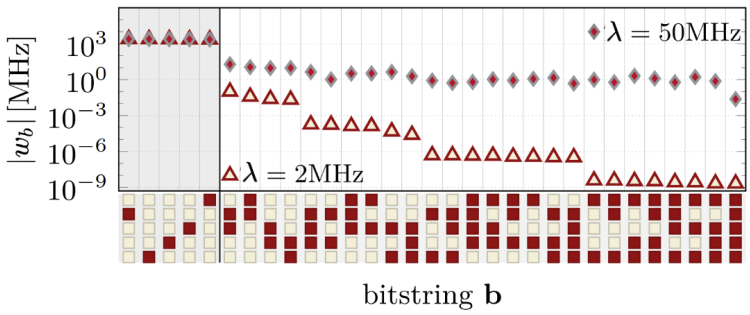

Figure 4.4: Walsh coefficients exponential hierarchy. Comparison of the Walsh coefficients for a 5-qubit chain with weak disorder, for two values of the coupling λ. Along the x-axis are all the possible values of the bit-string b of length 5, except of the all-zero case. We use a graphical depiction of each bitstring, as a vertical column of five boxes, εmpty boxes correspond to zero and filled boxes to a one, read from top to bottom, so that the first bitstring from the left is 01000, the second 00001 and so on. With this convention it is immediately evident which of the five qubits are involved in the given LIOM Hamiltonian coefficient. The coefficients are sorted in descending order for the $\lambda = 2$ MHz data. Correlation range in this context corresponds to the maximal distance between two 1's in the bitstring

computation completely unreliable. We confirm that our system behavior complies with this description in Fig. 4.4.

Here we quantified these many body correlations via the Walsh-Hadamard coefficients. As we have seen in chapter 3 the Walsh-Hadamard transformation allows us to recover the effective LIOM Hamiltonian of the qubit sector. The main hurdle we needed to overcome for the determination of the Walsh-Hadamard coefficients was tracking the bit-label identity of each qubit state as we varied coupling strength λ. We overcame this using the identification procedure presented in subsection 3.1.2 We repeat the protocol here more formally and precisely:

State Identity Tracking Protocol.

1. *Calculate the energy levels and fidelity susceptibility of Eq.* (3.10) *for varying coupling strength.*

2. *Initially identify the qubit states simply using the ordering of the decoupled eigenstates*

3. *Repeat for all qubit states:*

    - *Repeat until all avoided crossings along the path of the qubit state have been dealt with:*

(a) *Locate the first avoided crossing involving a specific qubit state, from the peaks of the fidelity susceptibility.*

(b) *Recognise the partner state for the avoided crossing by looking for the closest matching fidelity susceptibility peak, in height, width and location along the λ axis among the two adjacent levels to the qubit state.*

(c) *Exchange the identities of the two states after the crossing.*

This protocol however is not full-proof and in fact it is guaranteed to fail eventually deep in the chaotic regime. In this region we have avoided crossings of ambiguous character, such as soft level repulsions with small curvature or level repulsions between non adjacent levels, across which the state identity cannot be tracked reliably. Yet quantum computing with transmons relies on the ability to identify exactly these states amongst the non-computational states.

For our calculation, we can diagnose protocol failure by looking at the Walsh-Hadamard coefficients. If they exhibit discontinuities, in the form of jumps, then any value beyond the first jump is unreliable. However, even if the protocol is successful the Walsh-Hadamard coefficients may still exhibit two types of irregularities in the form of sharp cusps. Downwards pointing cusps are attributed to the Walsh-Hadamard coefficients crossing zero. Since we are presenting the absolute value of the coefficients in logarithmic scale these downward cusps are expected and they are completely benign. Upwards pointing cusps on the other hand are more delicate and they are related to the diabatic change of identity a qubit state across an avoided crossing. Qualitatively this behavior can be explained as follows. When the identity of an eigenstate changes diabaticaly across an avoided crossing the corresponding energy level will look locally like a step function. Since the Walsh-Hadamard transform is a special case of the discrete Fourier transform we can expect that the result for the coefficients will look like a Dirac delta locally. All of the above behaviours of the Walsh-Hadamard coefficients as a function of the coupling strength are reported in Fig. 4.5. Since averaging is washing out the intricate structure of the Walsh-Hadamard coefficients we also show for comparison the absolute value of the Walsh coefficient for the specific bitstring $b = 01101$.

Note that the non averaged Walsh-Hadamard coefficient becomes progressively more distorted as we approach the chaotic regime by increasing strong coupling. Yet trouble for quantum computation starts before that. Note that the highest Walsh-Hadamard averaged family, which corresponds to the typical ZZ coupling, crosses the threshold of manageable ZZ terms according to modern techniques ($\sim$ 100 kHz, see [35]) at a coupling strength of about $\sim$ 4 MHz far away from the chaotic region. This reinforces the message of the IPR in a basis independent way.

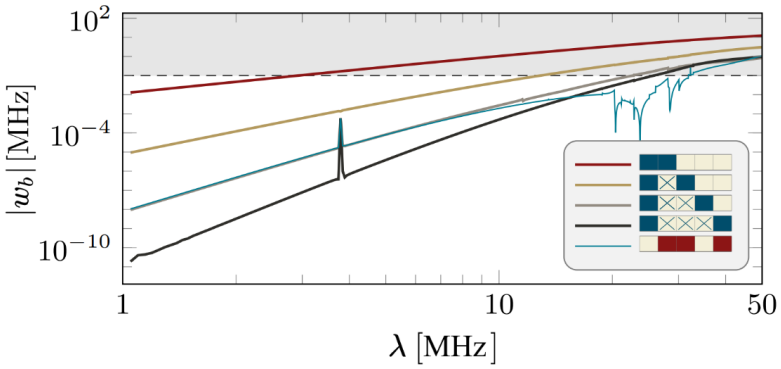

Figure 4.5: Walsh coefficients as a function of coupling strength. Absolute value of averaged Walsh coefficients for a 5-qubit chain with weak disorder as a function of the coupling strength λ. Here we have averaging with respect to two indices, one is disorder averaging across different realizations and the other is within Walsh-Hadamard coefficients of the same correlation range (as defined in Fig. 4.4) depicted graphically in the inset. Note that the correlation range 2 group, denoted by two filled boxes separated by one empty box, contains next-nearest two-body terms (there are 3 of these in the 5-qubit 1D chain) but also closely packed three-body terms (also 3 of these in the 5-qubit 1D chain). The dashed line and the shading above marks the "danger zone" $|w_b| \geq 100$ kHz indicated by recent experimental studies on ZZ coupling [35].

4.2 Advanced Architectures

We have established by means of three different diagnostics that 1D transmon arrays with random Gaussian disorder exhibit an MBL to chaotic phase transition. While the main message of our work has significant implications for the future of quantum computation with transmons our employed model may seem disconnected from modern architectures. Here we will discuss two main extensions to our model and their implications for the MBL-chaos transition. Employing the tools we have already used for the 1D random Gaussian disorder model we will study 2D lattices and a different disorder scheme relying on a laser annealing technique for the tuning of Josephson junctions post fabrication, developed by IBM [38]. We found that the main message of our results so far does not change drastically but only up to some minor nuanced effects.

4.2.1 2D Arrays

While we have only discussed 1D transmon chains so far, modern quantum processing devices have moved towards 2D configurations [3, 5, 39, 40]. There are several advantages associated with using 2D structures, such as faster qubit ma-

nipulation, effective error correcting with surface codes [41, 42] and higher qubit density which allows for easier scaling. Here we present briefly the effects of 2D architectures on the MBL-chaos transition of our system.

According to the MBL literature, the expectation is that the MBL phase becomes increasingly more unstable as we increase the dimensions d of our system. Already at $d = 3$, even the existence of an MBL phase at all is questionable [43]. The intuition behind this expectation is that in $d = 1$ rare instances of unusually strong disorder in some site may block effectively communication between distant sites resulting in stronger localization. If lattice sites have higher coordination number however such rare occasions of strong on-site disorder can be circumvented more easily and transport may be restored in the system resulting in more delocalized states.

We confirm this expectation of localization theory for our system by demonstrating the phase diagrams of KL divergence and IPR as we did for the 1D case. We do not employ the Walsh-Hadamard diagnostic here since its computation is prohibitively costly for the system sizes required here. Considering that the only difference between chain 7 and surface 7 is the inclusion of only two additional bonds, the shifts in both the KL divergence critical line and the IPR critical line are drastic.

4.2.2 LASIQ: Towards Frequency Pattern Engineering

As we have mentioned before, Josephson junctions were the primary source of fluctuations for transmon qubit frequencies. Recently, with the development of a new technique by IBM, called LASIQ [38] (Laser Annealing of Stochastically Impaired Qubits), it became possible to tune the Josephson energy post fabrication to a higher degree of accuracy.

IBM has employed this technique in an attempt to enhance the fidelity of the CR-gate by fixing the detuning of neighboring transmons within a specific range in order to avoid signal crosstalk. A minimal working example of this is presented in Fig. 4.7 in the form of a 2D lattice of transmons in a staggered frequency pattern consisted of two frequencies A and B. In this configuration and assuming perfect reproducibility of transmon frequencies we would only have one value for detuning between adjacent sites.

However, in a realistic setup there is going to be some residual disorder on top of the post fabrication tuning procedure. From our perspective the smallness of the residual disorder leaves the door open for quantum chaotic behavior. While a staggered pattern like the one in Fig. 4.7 may suppress ZZ crosstalk, we argue that next-nearest neighbor terms of the LIOM Hamiltonian Eq. 2.31 may become more relevant unless disorder strength is sufficient to localize the system.

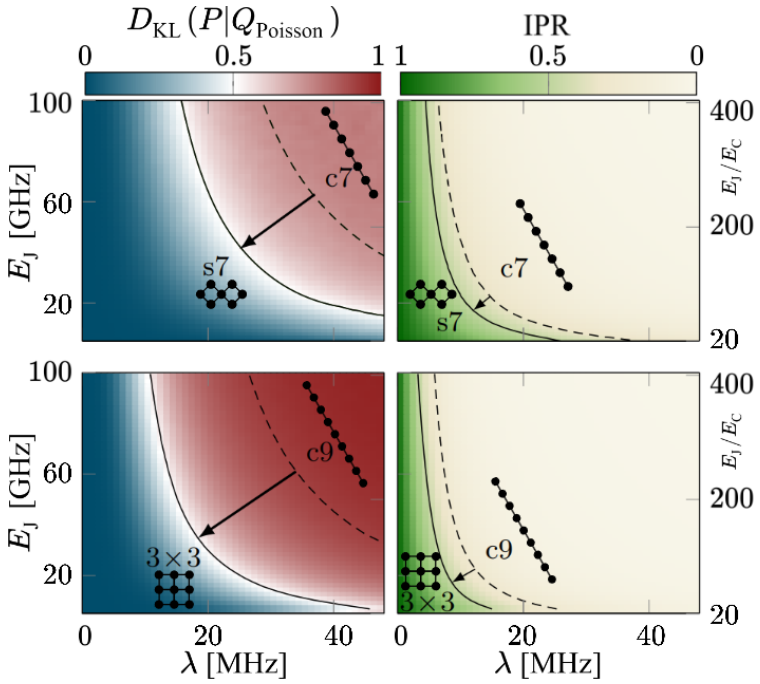

Figure 4.6: 2D transmon arrays - Phase diagrams. . In all of the phase diagrams we highlight the critical line (which corresponds to a value of 0.5 for both the KL divergence and the IPR) with a solid line and the corresponding critical line for a 1D lattice with the same number of transmons with a dashed line. In the top two panels we present the phase diagram of seven coupled transmons, arranged in a surface 7 (s7) geometry (indicated in the inset of each plot). All results are averaged over at least 1500 disorder realizations. In the bottom two panels we have the same phase diagrams for a 3×3 lattice. All results are averaged over at least 2500 disorder realizations. For both geometries, the on-site disorder is drawn from the same Gaussian distribution as in Fig. 4.3.

In order to investigate this possible complication we will incorporate disorder in our model again via the Josephson energies of the transmons. We will treat them as random variables drawn from a Gaussian distribution, but this time we will have two distributions corresponding to the two different types of sites, sites of type A with mean Josephson energy $E_{\mathrm{J,A}}$ and sites of type B with mean Josephson energy $E_{\mathrm{J,B}}$. The standard deviation will be δE_{J} for both types of sites.

We begin by presenting our result for the mean IPR as a function of the disorder strength in Fig. 4.7. On the top left we present the lattice configuration and the frequency pattern while on the top right we present the corresponding frequency distributions for lattice sites of type A (gray) and of type B (red) for two different values of the disorder strength δE_{J}. The first distribution corresponds to energetically well separated transmons with some residual disorder within each

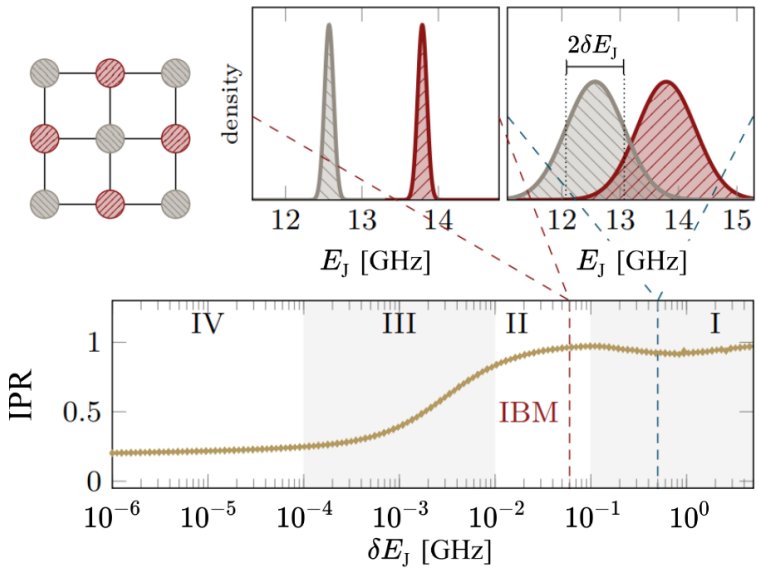

Figure 4.7: Frequency staggering and IPR. We present the average IPR of the 5-excitation bundle eigenstates of a 3×3 transmon array with a staggered frequency pattern calculated for varying disorder strength δE_J (bottom plot). The corresponding averages for the two distributions are fixed at the values of $E_{J,A} = 12.58$ GHz and $E_{J,B} = 13.80$ GHz according to [38] and we vary only their standard deviation. Since disorder strength varies we fix the coupling strength at the typical low value of $\lambda = 3$ MHz. Results are averaged over at least 8000 disorder realizations.

subgroup and yield a local maximum of the IPR in region II. This is where IBM typical system parameters have landed. The second distribution corresponds to the scenario where the disorder strength is roughly equal to half the distance between the two averages, yielding a local minimum in the IPR. Increasing the disorder further in region I, effectively yields a single Gaussian distribution and therefore it matches our previous results.

In region III of the plot in Fig. 4.7 we have a drop of the IPR indicating that the system is entering the delocalized regime. We confirm this by looking at the KL divergence in Fig. 4.8. In this plot we see indeed that the KL divergence is vanishing for the Wigner distribution here and we also note the corresponding lever repulsions on the top panel, typical for quantum chaotic behavior. Peculiarly, for vanishing disorder in region IV, none of the two distributions describe the spectrum of the system even though the IPR suggests delocalized eigenstates. If we examine this regime more carefully however this behavior is expected. In the idealised case of reaching zero disorder our system becomes periodic and therefore we expect to have delocalized Bloch states. This however does not mean that the systems is chaotic and this is reflected in the level spacings not

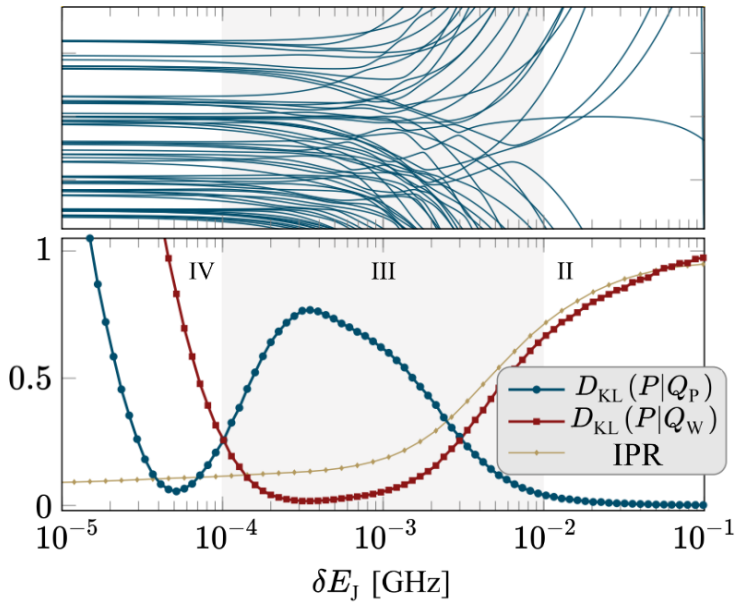

Figure 4.8: Permutation multiplets and KL. We present a zoom in of the 5-excitation bundle energy levels of a 3×3 transmon array with a staggered frequency pattern calculated for varying disorder strength δE_{J} (top plot). The part of the spectrum presented here corresponds to a particular multiplet of the 5-excitation bundle that contains all permutations of states that include 3 A and 2 B transmons in the first excited state and everything else in the ground state. On the bottom we present the IPR and KL divergence with respect to both of the two candidate distributions (Poisson, Wigner-Dyson). The parameters and number of realizations used are the same as in Fig. 4.7

following the Wigner distribution.

From the above it is clear that while the staggering of qubit frequencies is a useful tool for localizing our system as well as enhancing gate fidelity one should not go too far with removing the disorder. Arguably it is not clear whether turning disorder off completely is problematic for quantum computation, yet realistically we expect that there will always be some residual disorder in the manufacturing of these devices, and in that case we should make sure to have enough of it to localize our system. Finally, one may envision that using more complicated qubit frequency patterns could lead to localizing transmon arrays, not with random disorder but by a quasi-periodic or fractal pattern of qubit frequencies. This is an intriguing possibility and it is one that we will explore in the following chapter.

5

Quasiperiodic Potential Localization

In chapter 4, we have presented findings indicating a transition between a many-body localized and a quantum chaotic phase in transmon qubit architectures. Maintaining the system within the localized regime is crucial for quantum computation, typically achieved through disorder in Josephson junction parameters. We propose an alternative approach utilizing quasiperiodic patterning of parameters as a substitute for random fluctuations. Initially, we demonstrate the localization of our employed model, a two-dimensional extension of the Aubry-André model 5.1.1, in subsection 5.1.2. Following the introduction of our model and its Anderson localization, we employ the Walsh-Hadamard diagnostic in subsection 5.2.1 to establish the higher efficacy of quasiperiodicity in achieving many-body localization. To investigate the localizing properties of our novel Hamiltonian for large, experimentally relevant system sizes, we develop a many-body perturbation theory with a computational cost that scales similarly to that of the corresponding non-interacting system 5.2.2.

5.1 Anderson Localization with Quasiperiodic Potential

Despite immense advances in quantum computing using the superconducting qubit platform [3–5], two-qubit gate fidelity remains a thorn in the side of further progress with these devices. One prominent source of these errors is quantum cross talk in the form of qubit ZZ couplings [44], with Z denoting the Pauli z

operator. This cross talk is the result of always-on coupling of qubits, even in idle mode. There are two primary strategies for dealing with these residual couplings, tunable coupling [45] and static coupling between opposite anharmonicity qubits [35, 46]. Each of these coming with disadvantages: additional hardware overlay of couplers for the former and lower coherence time of capacitively shunted flux qubits for the latter.

In real devices the presence of inherent random disorder is unavoidable and most notably observed in the critical current of Josephson junctions. Although modern devices allow for tuning of Josephson junctions even after fabrication using laser annealing techniques [38], some degree of residual disorder persists, as discussed in the previous chapter, and can be sufficient to localize the system. Nevertheless, relying on the happenstance of random disorder to protect our system from quantum chaos is an inefficient approach from an engineering perspective. Thus, we will explore the possibility of localizing our system using quasiperiodic frequency patterns. Before delving into the potential for a MBL phase, we will first consider the simpler case of Anderson localization in our model.

Our chosen model is a modified version of the Aubry-André model. We will begin by introducing the one-dimensional Aubry-André model and elucidate its well-established Anderson localized-delocalized phase transition. Subsequently, we will introduce the Metallic-Aubry-André model, an extension of the one-dimensional Aubry-André model capable of accommodating two-dimensional lattices. We will conclude by demonstrating that this variant also exhibits an Anderson localized phase.

5.1.1 1D Aubry-André Model

Here we will present some generic properties of the Aubry-André model, but in order to keep the discussion closely related to our topic, we will do this in the context of transmon arrays. Starting from the capacitively coupled transmon array Hamiltonian of Eq. (1.35) and recasting it in second quantization form, expanding the cosine term only up to second order and employing a rotating wave approximation (see 1.2.2) we obtain

$$H_0 = \sum_{i=1}^{N} \omega_i a_i^\dagger a_i + J \sum_{\langle i,j \rangle} a_i^\dagger a_j. \tag{5.1}$$

This Hamiltonian is the usual tight binding model that is used in Anderson-localization studies [17, 47] and also in Eq. (2.20). Note that the ladder operators are bosonic — we are not restricted to the single-excitation manifold of the

Fock space. Strictly speaking, the dressed coupling strength J would be bond-dependent according to Eq. (1.45). Here we have omitted this bond dependence in order to simplify the calculations and we will instead substitute the transmon frequencies with their mean value, yielding the relation

$$J = \frac{\lambda}{16}\left(1 + \frac{\langle\omega\rangle}{E_C}\right). \tag{5.2}$$

We find that this does not substantially alter our results.

The case of a transmon chain with frequencies that have a spatial distribution given by

$$\omega_i = \langle\omega\rangle + A\cos(2\pi\beta x_i + \phi) \tag{5.3}$$

with free parameters $\langle\omega\rangle$, A, β and ϕ and x_i the spatial coordinate of lattice site i, corresponds to the Aubry-André model [48–52]. For a 1D geometry we can have the simple map $x_i = i$, by setting the lattice constant to 1. Here we will focus only on irrational values for β for reasons that will be more clear in the following subsection 5.1.2. What we discuss here can be extended to rational values for β but this discussion is more nuanced and not relevant for our topic.

The Hamiltonian in Eq. (5.1) is invariant under a transformation that maps localized states to delocalized states and vice versa with a suitable exchange of the parameters J and A. This property is called the Aubry-André duality [53]. When $A = 2J$ the Hamiltonian is self dual and this is when the transition between localized and delocalized eigenstates occurs. We present this behavior by tracking the mean IPR across all eigenstates of the Hamiltonian for varying coupling strength in Fig. 5.1 . Specifically we plot IPR vs the ratio of the dressed coupling strength J over the disorder strength Δ defined by the normalization

$$\Delta = \lim_{N\to\infty}\sqrt{\frac{1}{N}\sum_{i=1}^{N}(\omega_i - \langle\omega\rangle)^2} = \frac{A}{\sqrt{2}}. \tag{5.4}$$

Substituting from Eq. (5.4) we find the Aubry-André transition at $J/\Delta = \sqrt{2}/2$, but since we are going to set $\Delta = 2E_C$ in all our calculations we will use the ratio of the dressed coupling over the anharmonicity E_C instead and therefore the transition will be at $J/E_C = \sqrt{2}$. This expectation is confirmed in Fig. 5.1.

5.1.2 Metallic-Aubry-André Model

For our application of designing a frequency pattern for our transmon arrays, which should serve as a localizing disorder potential, the essential feature is to make it non repeating in order to avoid resonances. Using integer-valued real

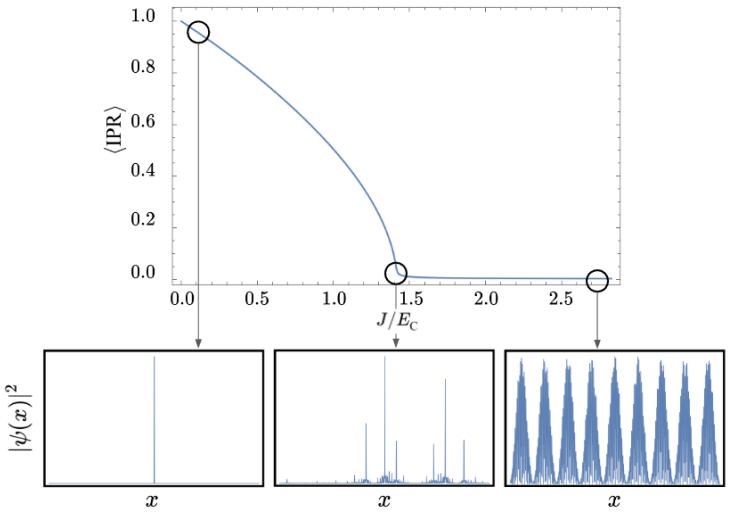

Figure 5.1: Aubry-André Phase Transition: We plot the average eigenstate IPR versus the ratio of the dressed coupling J of Eq. (1.45) over the anharmonicity E_C for the tight binding approximation of a transmon chain of length 1000. Underneath this plot we also present eigenstate probability distributions corresponding to three values of J/E_C, one for high average IPR one at the transition and one at low IPR. The chosen eigenstates are selected by requiring an eigenstate with IPR close to average and maximum probability closest to the center of the chain. The average frequency was set to $\langle\omega\rangle = 5.5$ GHz and the capacitive energy at $E_C = 0.33$ GHz

space coordinate x_i for site i, we could use the Aubry-André model with a periodicity that is incommensurate to the lattice periodicity by making β irrational, for instance we can set β equal to the golden ratio

$$\omega_i = \langle\omega\rangle + \Delta\sqrt{2}\sin\left[\pi\left(1+\sqrt{5}\right)x_i\right]. \tag{5.5}$$

Here we have set the arbitrary phase ϕ of Eq. (5.3) to $\pi/2$ without loss of generality and the amplitude of the trigonometric function equal to the disorder strength Δ times a normalization factor of $\sqrt{2}$.

We wish to generalise this frequency pattern however by allowing it to accommodate 2D lattice geometries. One possible choice for this is envisioning the generalised model as a series of Aubry-André chains that are laterally connected. In order to avoid resonances across different chains we need to use different periodicity and furthermore these periodicities need to be again incommensurate to each other. We achieved that here by making β a function of the y coordinate and the function of choice is the generating function of the family of irrational numbers called the metallic ratios [54]

$$\omega_i = \langle\omega\rangle + \Delta\sqrt{2}\sin\left[\pi\left(y_i+\sqrt{y_i^2+4}\right)x_i\right]. \tag{5.6}$$

Note that for $y_i = 1$ we recover the frequency pattern of Eq. (5.5). Furthermore as the y_i coordinate tends to infinity, the ratio of the periods of adjacent chains tends to 1 and therefore this is not a suitable model for square lattice geometries since it will eventually become approximately periodic along the y axis. However here we focus on a quasi-1D square lattice with dimensions $2\times L$ as the one depicted in Fig. 5.3. Such a lattice geometry is already in use for actual quantum computing devices [55] and may also become even more relevant for future designs.

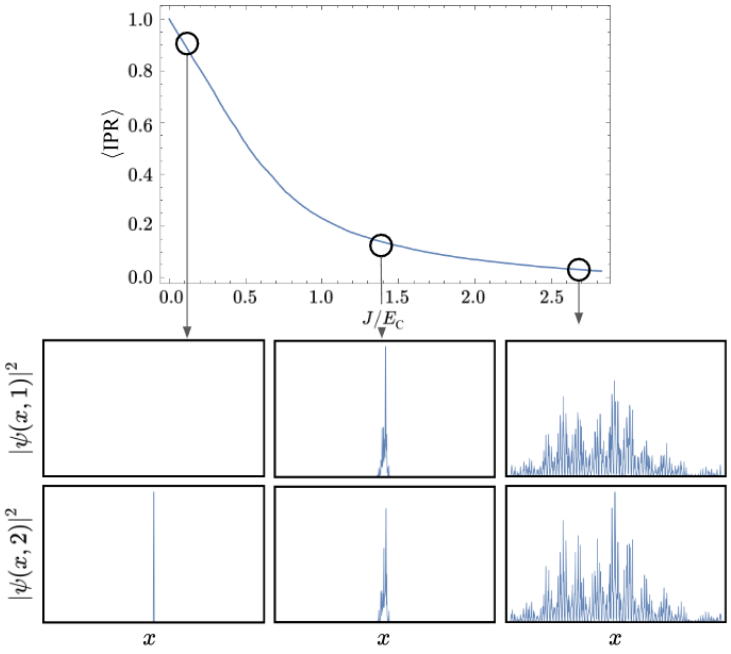

Figure 5.2: Metallic-Aubry-André Phase Transition: We plot the average eigenstate IPR versus the ratio of the dressed coupling J of Eq. (1.45) over the anharmonicity E_C for the tight binding approximation of a quasi-1D transmon lattice of dimensions 2×500. Underneath this plot we also present eigenstate probability distributions corresponding to three values of J/E_C, one for high average IPR one at the transition (of the 1D model) and one at low IPR. The top row of panels corresponds to probability distributions as a function of the x coordinate with the y coordinate fixed at $y = 1$ while the bottom row of panels corresponds to coordinate y fixed at $y = 2$. The chosen eigenstates are selected by requiring an eigenstate with IPR close to average and maximum probability closest to the center of the lattice. The average frequency was set to $\langle\omega\rangle = 5.5$ GHz and the capacitive energy at $E_C = 0.33$ GHz.

We performed the same average IPR analysis that we did for the 1D Aubry-André and the results for this transition are shown in Fig. 5.2. We remark that the phase transition from localized to delocalized is qualitatively different from the one for the 1D Aubry-André. This is due to the fact that our frequency pat-

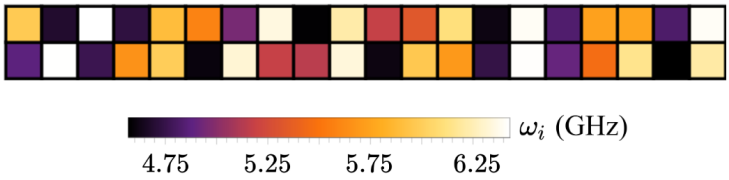

Figure 5.3: Metallic-Aubry-André frequency pattern: Transmon frequency frequency pattern ω_i (Eq. (5.6)) for a quasi-1D lattice of dimensions 2×20. We use mean frequency $\langle\omega\rangle = 5.5$ GHz and disorder strength is set at $\Delta = 2E_C$ and the capacitive energy is fixed at $E_C = 0.33$ GHz. The on-site frequencies are color-coded according to the given color bar and the values are given in GHz. The bottom row of the lattice corresponds to $y = 1$ and the top to $y = 2$. The leftmost sites of the lattice have $x = 1$ and the rightmost $x = 20$.

tern breaks the Aubry-André duality. While it is possible to employ different 2D extensions of the Aubry-André model that preserve this symmetry [51] we find that they are not as efficient in localizing the eigenstates. Notice particularly how different the eigenstates look for the same system parameters from Fig. 5.1 to Fig. 5.2. Even deep in the delocalized regime the eigenstates of the Metallic-Aubry-André still attain some form of weak localization (maximum probability somewhere near the center of the lattice that decays sub-exponentially away from it). In contrast the eigenstates of the 1D Aubry-André are already nearly periodic in the same parameter range and are thus not localized by any sense.

5.2 Many Body Localization with Quasiperiodic Potential

The many body system formed by a network of N Josephson qubits, with random disorder and fixed coupling, is a prime candidate for quantum chaos. In the last chapter we have established that there is in fact a phase transition between quantum chaotic and many body localization for transmon arrays [A1] of this type. The phenomenology of this transition can be summarised by considering the diagonalized Hamiltonian of such a multi-qubit system in Eq. (3.1). The coefficients w_b with a bit-string b consisting of only two 1s in adjacent sites correspond, by definition, to the ZZ-couplings. Longer range ZZ couplings or higher weight terms have generally been neglected, a treatment which is consistent in the MBL phase where we have an exponential hierarchy of these terms with respect to correlation range [19, 20]. This is in stark contrast with the chaotic regime however, where all of these terms are of the same order of magnitude.

In the following subsections, we will expand upon the free Hamiltonian presen-

ted in Eq.(5.1) by incorporating a many-body interaction term. Additionally, we will employ the Metallic-Aubry-André frequency pattern described in Eq.(5.6). The Anderson localization of the free Hamiltonian, observed for sufficiently weak coupling or strong disorder, suggests the potential existence of a many-body localized (MBL) phase in the interacting Hamiltonian. Our findings confirm the presence of such a phase in our model and demonstrate its enhanced ability to localize the system compared to random Gaussian disorder, as evidenced by exact diagonalization techniques. The identification of an MBL phase opens up the possibility of performing a perturbative analysis within the strongly localized regime. To this end, we combine our Walsh-Hadamard perturbation theory (refer to section 3.2) with a bosonic adaptation of the Møller-Plesset perturbation theory. This hybrid perturbation scheme enables us to determine the ZZ coefficients for significantly larger system sizes that are otherwise unattainable through numerical computations.

5.2.1 Many Body Metallic-Aubry-André vs Gaussian Disorder

So far we have been restricted to system sizes that are admittedly small compared to the already available quantum computing devices. The main restriction has been the exponential scaling of computational memory for numerical calculations. We wish to circumvent that here by employing some analytic method for the analysis of our model using perturbation theory. However such a treatment of the full model Eq. (1.35) seems impractical. To address this, we turn to the framework of second quantization, which offers a more intuitive approach. While a second quantized form of the Hamiltonian, as presented in appendix B, is available, it remains a complex undertaking. Nevertheless, we have discovered that by employing the Bose-Hubbard approximation described by Eq.(1.44), we can already capture significant aspects of the model, yielding meaningful results.

We need to include many-body contributions in our model, which means anharmonicity effects. Thus, we must further expand the cosine of Eq. (1.35) at least to fourth order, at which point we end up (after further rotating-wave approximations) with the Bose-Hubbard Hamiltonian

$$H_{\mathrm{BH}} = H_0 - \frac{E_{\mathrm{C}}}{2} \sum_{i=1}^{N} a_i^\dagger a_i^\dagger a_i a_i, \tag{5.7}$$

where H_0 is the free Hamiltonian of Eq. (5.1).

Our aim was to assess the effectiveness of the Metallic-Aubry-André model in localizing our system compared to random disorder. To conduct this analysis,

we focused on a smaller system of size 2×3 for which exact diagonalization was feasible. The results, depicted in Fig. 5.4, validate that our model outperforms random disorder of the same strength. Specifically, the ZZ coefficients associated with the two localizing potentials consistently differ by approximately one order of magnitude within the plotted range, indicating weaker ZZ correlations in the Metallic-Aubry-André model. It is noteworthy that the adoption of a double logarithmic scale, combined with the linearity observed for typical ZZ values, suggests a power-law relationship: $\langle |ZZ| \rangle \propto (J/E_C)^2$. However, determining origin of this behavior lies beyond the scope of our current work. Finally, the IPR plot reveals that both cases exhibit localization, yet Gaussian disorder exhibits a more rapid departure from localization.

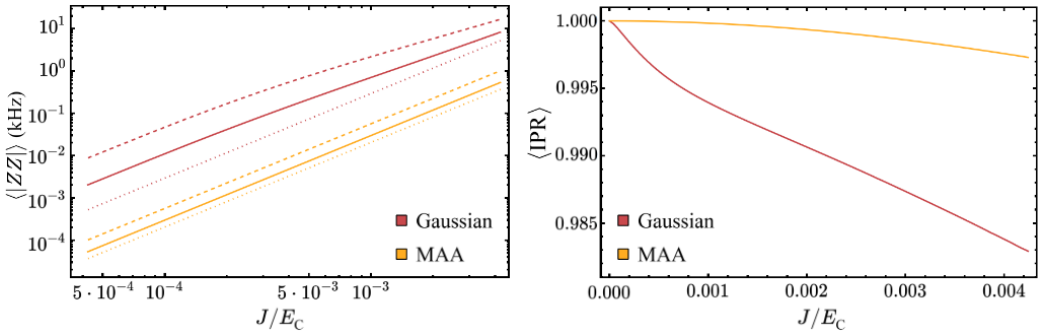

Figure 5.4: Random Gaussian disorder vs Metallic-Aubry-André: Exact diagonalization results depicting the averaged absolute values of ZZ coefficients (left panel) and the averaged inverse participation ratio (right panel) as a function of the ratio between the dressed coupling of Eq. (1.45) and the anharmonicity E_C, considering Metallic-Aubry-André disorder and random Gaussian disorder with matching disorder strength $\Delta = 2E_C$. The averaging is performed over the absolute values of Walsh-Hadamard coefficients with weight 2 and a correlation range $\ell = 1$ (nearest neighbor, ZZ), while for the IPR, averaging is done over all eigenstates. In the case of Gaussian random disorder, an additional averaging is conducted over 100 different realizations. Additionally on the left panel we have besides the averaged absolute value of ZZ the maximal coefficient (dashed line) and the minimal coefficient (dotted line). Their color matches the solid line that they correspond to. The parameter values utilized are $E_C = 0.33$ GHz, $\langle \omega \rangle = 5.5$ GHz, and the coupling J is varied within the range of 0 to 1.4 MHz. The chosen range for J avoids the initial avoided crossings, which emerge as early as $J \simeq 1.5$ MHz. The system size for both cases is 2×3.

Given the established presence of many-body localization (MBL) in our system, which exhibits higher effectiveness compared to the random disorder model, we can now employ an analytic approach. We will utilize the Hamiltonian described by Eq. (5.7) as an effective description of our system. In the subsequent subsection, we will determine the Walsh-Hadamard coefficients perturbatively

in the anharmonicity. Although the capacitive energy E_C may not be the smallest energy scale in our system, the application of perturbation theory is justified within the transmon regime $E_C/\omega_i \sim \sqrt{E_C/E_{J_i}} \ll 1$.

5.2.2 Møller-Plesset Analysis of the Many Body Metallic-Aubry-André Model

We develop a new bosonic variant of Møller-Plesset perturbation theory [56] to treat the localized regime, obtaining the energy levels of the qubit sector of the system. This perturbation theory directly determines the coefficients w_b of Eq. (3.1) via the Walsh-Hadamard transform Eq. (3.6). Here we will justify why our system Hamiltonian is of the form of Eq. (3.11) using an argument similar to the Hartree-Fock approximation and then directly draw conclusions by substituting in the results of section 3.2.

For the Walsh-Hadamard coefficients we only need to obtain the perturbed energy levels that correspond to qubit states $|b\rangle$ with b standing for a bit-string of length equal to the number of lattice sites N. Therefore, before we proceed with any calculation it is crucial to address the issue of how to identify the qubit states $|b\rangle$ and distinguish them from non-computational states.

Labeling a state with a bit-string might misleadingly imply that it is an eigenstate of the local particle number operator $a_i^\dagger a_i$ of the bare basis in Eq. (5.7). But $|b\rangle$ is rather an eigenstate of the non-interacting Hamiltonian H_0 (Eq. (5.1)). Therefore $|b\rangle$ is an eigenstate of the local particle number operator in the *dressed* basis

$$|b\rangle = \prod_{\mu=1}^{N} (c_\mu^\dagger)^{b_\mu} |0\rangle, \tag{5.8}$$

where b_μ is the μ-th digit of bit-string b and $c_\mu^\dagger$ is the creation operator of single-excitation eigenstate μ of H_0

$$H_0 = \sum_{\mu=1}^{N} E_\mu c_\mu^\dagger c_\mu. \tag{5.9}$$

For sufficiently weak transmon coupling J our system should be localised and the dressed basis should be nearly identical to the bare basis $c_\mu^\dagger \simeq a_\mu^\dagger$. By definition

$$c_\mu^\dagger |0\rangle \stackrel{!}{=} \left(\sum_{i=1}^{N} \psi_\mu(x_i, y_i) a_i^\dagger \right) |0\rangle, \tag{5.10}$$

meaning that $c_\mu^\dagger$ generates a single-excitation eigenstate $|\psi_\mu\rangle$ of H_0, which is exponentially localised around lattice site μ with coordinates (x_μ, y_μ). To avoid any possible confusion we will reserve Latin indices for the bare basis and Greek indices for the dressed basis.

Starting from Eq. (5.10) it is straightforward to find the inverse transformation, as demonstrated here

$$\sum_{i=1}^{N} \psi_\mu(x_i, y_i) a_i^\dagger = c_\mu^\dagger \Rightarrow \sum_{\mu=1}^{N}\sum_{i=1}^{N} \psi_\mu(x_i, y_i)\psi_\mu^*(x_j, y_j) a_i^\dagger = \sum_{\mu=1}^{N} \psi_\mu^*(x_j, y_j) c_\mu^\dagger \tag{5.11}$$

$$\Rightarrow a_j^\dagger = \sum_{\mu=1}^{L} \psi_\mu^*(x_j, y_j) c_\mu^\dagger \tag{5.12}$$

and express every term of the perturbative expansion in the dressed basis. In the second step we have used the unitarity of the transformation. Using this relation we can express the Hamiltonian in the dressed basis

$$H_{\mathrm{BH}} = E_\mu c_\mu^\dagger c_\mu - \frac{E_{\mathrm{C}}}{2}\langle \psi_\alpha \psi_\beta \psi_\mu \psi_\nu \rangle c_\alpha^\dagger c_\beta^\dagger c_\mu c_\nu \tag{5.13}$$

where we have used again the summation convention 1 and we introduced the notation for the 4 point function

$$\langle \psi_\alpha \psi_\beta \psi_\mu \psi_\nu \rangle = \sum_{i=1}^{N} \psi_\alpha(x_i, y_i)\psi_\beta(x_i, y_i)\psi_\mu(x_i, y_i)\psi_\nu(x_i, y_i). \tag{5.14}$$

Note that the Hamiltonian of Eq. (5.13) is identical to the one in Eq. (3.11) and therefore we can use the results of Eqs. (3.51),(3.52) and (3.53) of section 3.2 immediately by identifying the factor $-E_{\mathrm{C}}\langle \psi_\alpha \psi_\beta \psi_\mu \psi_\nu \rangle/2$ as $V_{\alpha\beta\mu\nu}$ with corresponding tensors

$$\mathcal{E}_{\mu\nu} = -E_{\mathrm{C}}\langle \psi_\mu^2 \psi_\nu^2 \rangle \tag{5.15}$$

$$\mathcal{S}_{\alpha\beta\mu\nu} = \begin{cases} \dfrac{E_{\mathrm{C}}^2}{2} \dfrac{\langle \psi_\alpha^2 \psi_\mu \psi_\nu \rangle \langle \psi_\beta^2 \psi_\mu \psi_\nu \rangle}{E_\mu - E_\nu}, & \mu \neq \nu \\ 0, & \mu = \nu \end{cases} \tag{5.16}$$

$$\mathcal{D}_{\alpha\beta\mu\nu} = \begin{cases} \dfrac{E_{\mathrm{C}}^2}{4} \dfrac{\langle \psi_\alpha \psi_\beta \psi_\mu \psi_\nu \rangle^2}{E_\alpha + E_\beta - E_\mu - E_\nu}, & \{\alpha, \beta\} \neq \{\mu, \nu\} \\ 0, & \{\alpha, \beta\} = \{\mu, \nu\}. \end{cases} \tag{5.17}$$

In order to carry out this calculation we therefore only need to obtain the single-particle sector eigenenergies E_μ and eigenstates $|\psi_\mu\rangle$. Since we are only

interested in the localised regime of the system, we could obtain those perturbatively as well in the coupling J. However this adds one additional layer of complexity for our final expressions without leading into any particular new insights. Therefore we choose to obtain the single-particle sector spectrum numerically and use these results as input to our derived analytic expressions from second order perturbation theory in the anharmonicity E_C.

The energy denominators of perturbation theory are notoriously known to cause issues with accuracy, particularly when the involved basis states are resonant (i.e. when denominators are vanishing). Even though these denominators involve energy levels of the dressed basis, in the localised regime these are essentially indistinguishable from the bare basis energy levels $E_\mu \simeq \omega_\mu$. Therefore we can straightforwardly associate spatial coordinates (x_i, y_i) on our lattice to them. From the form of the perturbing potential in the dressed basis, it is clear that only states which are two hops apart can have a non vanishing amplitude. Thus the energy denominator can involve between 2, 3, or 4 different sites. The terms involving only 2 sites can be thought of as effectively single hops and are all included in $\mathcal{S}$. These resonances we will refer to as *site* resonances or simply resonances. The terms involving 3 or 4 sites can only be described as double hoping terms and are all included in $\mathcal{D}$. These resonances we will refer to as *mode* resonances.

With the introduction of the Metallic-Aubry-André scheme, our motivation has been to set up a quasi-random disorder potential without resonances and with well separated near-resonant sites. However a direct implication of Eq. (5.17) is that this consideration is not sufficient to successfully localize the system. Granted that having such a denominator vanishing or being much smaller than E_C does not necessarily mean that our system is chaotic but it does suggest strong hybridization between certain modes which is certainly not desirable for quantum computation. While the denominator of $\mathcal{D}_{\alpha\beta\mu\nu}$ creates these dangers for perturbation theory, its numerators have a counteracting effect. They are proportional to the square of the 4 point function $\langle\psi_\mu\psi_\nu\psi_\alpha\psi_\beta\rangle$ of the single particle wavefunctions involving the same states as the ones in the denominator. Anderson localization theory shows that these correlations decay exponentially with range.

Our next goal is to obtain Walsh-Hadamard coefficients for a much larger system of dimensions 2×20. Before doing that however we need to know the accuracy of our perturbation theory by comparing it with exact diagonalization results. For this comparison, still restricted to the 2×3 system size, see Fig. 5.5. It is evident that the agreement of the two results is restricted to a rather small parameter range and that range is strongly dependent on the disorder strength. Even though the second order perturbation theory is very accurate for the energy levels, with an error of $\sim 10^{-1}$ kHz for eigenenergies spanning a few tens of GHz,

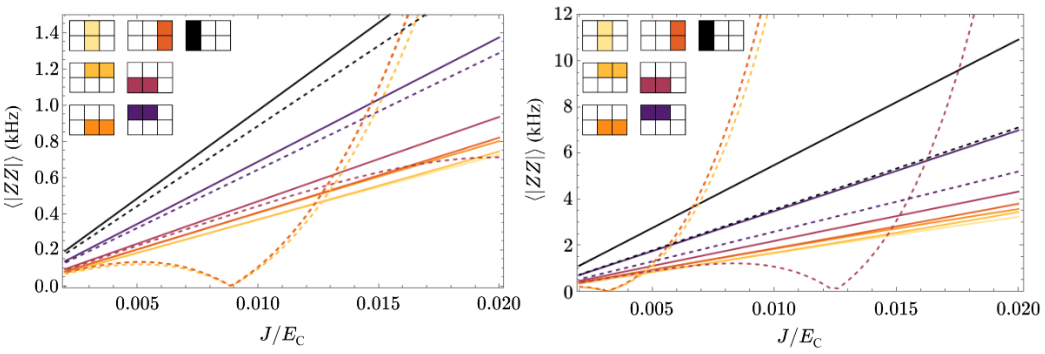

Figure 5.5: Exact diagonalization vs perturbation theory: Plots of all the Walsh-Hadamard coefficients of weight 2 and correlation range $\ell = 1$ (ZZ coefficients) as a function of ratio of the dressed coupling of Eq. (1.45) over the anharmonicity E_C using exact diagonalization (solid) and perturbation theory (dashed). For the left panel we have set disorder strength at $\Delta = 2E_C$ while for the right panel we have set $\Delta = E_C$. For both plots we used $\langle\omega\rangle = 5.5$ GHz, $J = 1$ MHz and E_C is varying in the range of 0.05 to 0.5GHz. Coefficients are color-coded to match the lattice representation of the ZZ-correlated sites in the legend. System size is 2×3.

the error is of the same order of magnitude as the Walsh-Hadamard coefficients of weight 2, and is about 2 orders of magnitude larger that coefficients of weight 3. This is why we only report the weight 2 coefficients here. Unfortunately the accuracy of the energy levels is not found to be improved by introducing higher order terms [57]; our perturbation theory is equivalent to that of the φ^4 theory, which is known to have a vanishing radius of convergence. Already at third order of perturbation theory the disagreement with the exact diagonalization results starts to increase.

Despite these difficulties, meaningful results about the Walsh-Hadamard coefficients can be obtained deep in the localized regime and the order of magnitude is correct within the specified parameter range in Fig. 5.5. Therefore we deem it informative to obtain the weight 2 coefficients using perturbation theory for the much larger 2×20 system, far beyond the size that is accessible by exact diagonalization. The results for this calculation are reported in Fig. 5.6. They confirm the expectation that these Walsh-Hadamard coefficients exhibit a hierarchy of values, decreasing exponentially with range; this is as expected within many body localization theory (see [A1]).

We have demonstrated that it is possible to localize a many body quantum computing system without the use of random disorder but rather with a deterministically designed, quasi-periodic potential. We believe that the disorder potential we studied here is not yet optimal and that meticulous frequency pattern engineering should play a crucial role in the design of future quantum computing

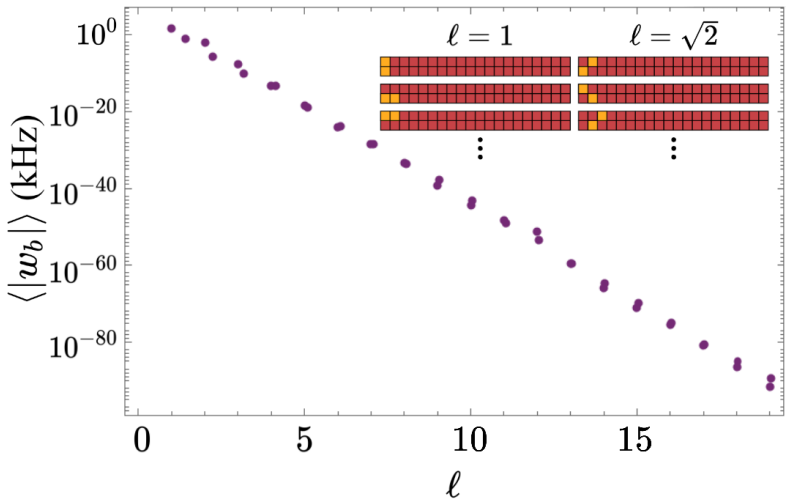

Figure 5.6: Walsh-Hadamard exponential hierarchy: Plot of averaged Walsh-Hadamard coefficients of weight 2 as a function of the correlation range ℓ for a 2×20 quasi-1D lattice. Averaging is done among Walsh-Hadamard coefficients of the same correlation range. The parameter values used here are $J = 1$ MHz, $\langle \omega \rangle = 5.4$ GHz, $\Delta = 2E_C$ and $E_C = 0.33$ GHz. The inset is a visual representation for a sample of some Walsh-Hadamard coefficients corresponding to bit-strings b with correlation range $\ell = 1$ on the lattice. Red corresponds to 0 and orange to 1 of the bitstring b.

architectures. Our new perturbation-theory scheme can be used as a guide for the properties a frequency pattern should possess or avoid. Despite the limited accuracy of our perturbation scheme, we have demonstrated that it is possible to obtain useful analytical results for the Walsh-Hadamard coefficients of large many-body systems. We believe that accuracy can ultimately be improved with a renormalized perturbation theory. Finally, we need to stress out that the results for the 2×20 lattice are well beyond the realm of what is attainable with exact diagonalization techniques. The main impediment for increasing the size further is the exponential scaling of the number of Walsh-Hadamard coefficients themselves, which is 2^N. However, if we instead restrict the calculation to only low-weight coefficients with small correlation range, then the main hurdle is the calculation of the tensors $\mathcal{S}$ and $\mathcal{D}$ which scale only polynomially with lattice size, but with a high power $\sim N^4$.

Outlook

We have observed that transmon arrays with Gaussian disorder demonstrate a transition from chaotic behavior to a MBL phase. Although the traditional diagnostics of level spacing distribution and IPR disagree on the exact location of this transition, our innovative technique utilizing the Walsh-Hadamard transformation has provided us with a basis-independent probe to showcase that quantum computation is secure only deep into the MBL phase, where the ZZ interactions can be effectively managed.

As was anticipated by MBL theory increasing the coordination number of the lattice destabilizes the MBL phase further. Furthermore, we have demonstrated that caution should be exercised when employing qubit frequency engineered patterns in the transmon architecture using the LASIQ technique. Although simple configurations such as a staggered pattern with a limited set of frequencies can still effectively localize the system, thanks to the presence of residual disorder, reducing the strength of disorder even further can bring the system uncomfortably close to the chaotic regime.

While using LASIQ to create a simple frequency pattern can be unreliable from a localization prospective, the ability to tune Josephson junctions to a higher precision, even post fabrication, opens up an intriguing avenue for designing fractal or quasi-periodic frequency patterns that mimic random disorder. We have seen that by employing a quasi-periodic pattern based on the Aubry-André model we were able to localize a quasi-1D transmon lattice. Even more astonishing was the fact that the quasi-periodic system demonstrated an even higher degree of localization from a similar system with Gaussian disorder. Furthermore, employing our perturbation theory scheme allowed us to obtain the Walsh-Hadamard coefficients for a large-scale system, comparable to experimental devices. The observed exponential hierarchy in the Walsh-Hadamard coefficients provides compelling evidence of the sustained localization of the system.

We acknowledge that our study of MBL as a protective measure against decoherence for quantum memories should be thought of as a first attempt to bridge the fields of quantum information and MBL, and it does not come without limita-

tions. For the first part of our approach we employed a purely numerical method for characterizing the system and therefore this limits the size of systems that we can study. In addition, the transmons are bosonic systems with an infinite number of eigenstates. In turn, this forces us to use a Hilbert space truncation scheme. Regardless the dimensionality of Hilbert spaces that we considered was immense by any computational standards and it suffices for the convergence of our statistics.

For the second part we relied on an effective Hamiltonian description of the system, the Bose-Hubbard approximation, which is suitable for the transmon regime, however it is only an approximate description within a finite energy window. The perturbation scheme employed there is also suffering from the pathogenies of the φ^4 theory which also limits the parameter range for which our approximation is working.

In both approaches we have not considered tunable coupling [45] which is also a reasonable approach to counter decoherence. Despite these difficulties our core message, that transmons can avoid thermalization and thus be protected from decoherence via MBL, is still valid and one that warrants further investigation.

It is important to note that our analysis thus far has focused exclusively on static systems with time-independent Hamiltonians, disregarding the dynamic aspects of the system. However, it is worth exploring how the dynamics of the system are influenced by MBL and quantum chaos, as they are dynamic phases of matter. A compelling question arises: How do MBL and quantum chaos manifest themselves in the system's dynamics, and what diagnostic tools can be employed to investigate this transition?

Finally, it is worth noting that the perturbation theory scheme we employed for obtaining the Walsh-Hadamard coefficients in the Metallic-Aubry-André model has proven valuable for studying the localization properties of large systems beyond the limitations of exact diagonalization. However, it is important to acknowledge that this perturbation theory scheme has a limited parameter range in which it can be applied effectively. To address this limitation, one intriguing solution would be to utilize a renormalized version of the perturbation theory, which is known to improve the radius of convergence in theories such as the φ^4 theory. Alternatively, one could consider employing the full form of the transmon Hamiltonian, as given in Eq. (B.13), at the moment however it remains unclear how to achieve that.

Appendices

A

Identities of Bosonic Operators

In this appendix we will prove some properties of bosonic ladder operators that we have used throughout the thesis.

Lemma 1. *For bosonic operators $a, a^\dagger$ with $[a, a^\dagger] = 1$ we have*

$$(a^\dagger a)^n a^k = a^k (a^\dagger a - k)^n \quad \textit{and} \quad (a^\dagger a)^n a^{\dagger k} = a^{\dagger k} (a^\dagger a + k)^n. \tag{A.1}$$

with $n, k \in \mathbb{N}$.

Proof. We will prove this with double induction. Once on of the two relations is proved the other follows from complex conjugation as well. First we will prove that

$$(a^\dagger a) a^k = a^k (a^\dagger a - k). \tag{A.2}$$

Assuming that this hold for $k + 1$ as well we obtain

$$\begin{aligned} (a^\dagger a) a^{k+1} &= (a^\dagger a) a^k a = a^k (a^\dagger a - k) a \\ &= a^k (a^\dagger a a - k a) = a^k (a a^\dagger a - a - k a) \\ &= a^{k+1} (a^\dagger a - k - 1) \end{aligned} \tag{A.3}$$

and the induction is complete. Now for the general case of Eq. (A.1), assuming it hold for $n + 1$ we will have

$$(a^\dagger a)^{n+1} a^k = a^\dagger a (a^\dagger a)^n a^k = a^k (a^\dagger a - k)(a^\dagger a - k)^n = a^k (a^\dagger a - k)^{n+1} \tag{A.4}$$

□

Lemma 2. *For bosonic operators $a, a^\dagger$ with $[a, a^\dagger] = 1$ we have*

$$a^{\dagger k} a^k = \prod_{m=0}^{k-1} (a^\dagger a - m) = \frac{\Gamma(a^\dagger a + 1)}{\Gamma(a^\dagger a - k + 1)}, \tag{A.5}$$

where $\Gamma(x) = (x-1)!$ is the Gamma function [B3] and $k \in \mathbb{N}$.

Proof. We will prove this inductively. Assuming Eq. (A.5) is true then

$$a^{\dagger(k+1)} a^{(k+1)} = a^{\dagger k} (a^\dagger a) a^k. \tag{A.6}$$

Using Lemma 1 we can write this as

$$a^{\dagger(k+1)} a^{(k+1)} = (a^\dagger a - k) a^{\dagger k} a^k = \prod_{m=0}^{k} (a^\dagger a - m). \tag{A.7}$$

□

Lemma 3. *For bosonic operators $a, a^\dagger$ with $[a, a^\dagger] = 1$ we have*

$$e^{i\beta a^\dagger a} a^m e^{-i\beta a^\dagger a} = e^{-i\beta m} a^m \tag{A.8}$$

with $\beta \in \mathbb{R}$ and $m \in \mathbb{N}$

Proof. We expand the second exponential to write

$$e^{i\beta a^\dagger a} a^m e^{-i\beta a^\dagger a} = e^{i\beta a^\dagger a} \sum_{k=0}^{\infty} \frac{(-i\beta)^k}{k!} a^m (a^\dagger a)^k. \tag{A.9}$$

Using again Lemma 1 we obtain

$$\begin{aligned} e^{i\beta a^\dagger a} a^m e^{-i\beta a^\dagger a} &= e^{i\beta a^\dagger a} \left(\sum_{k=0}^{\infty} \frac{(-i\beta)^k}{k!} (a^\dagger a - m)^k \right) a^m \\ &= e^{i\beta a^\dagger a} e^{-i\beta a^\dagger a} e^{-i\beta m} a^m = e^{-i\beta m} a^m. \end{aligned} \tag{A.10}$$

□

B

Second Quantization Form of the Charge Qubit Hamiltonian

Here we will derive a second quantization Hamiltonian for the transmon qubit. Starting from the Hamiltonian of Eq. (1.31) and setting $n_g = 0$ we can perform the canonical transformation of Eq. (1.37) to write

$$H_{\mathrm{CQ}} = -\sqrt{\frac{E_{\mathrm{C}}E_{\mathrm{J}}}{2}}(a^\dagger - a)^2 - E_{\mathrm{J}}\cos\left[\sqrt[4]{\frac{2E_{\mathrm{J}}}{E_{\mathrm{C}}}}(a^\dagger + a)\right] \tag{B.1}$$

We will expand the cosine again, but this time we will not truncate the expansion keeping the full series

$$\cos\varphi = \sum_{n=0}^{\infty} c_n(a^\dagger + a)^{2n} = \sum_{n=0}^{\infty} \frac{(-1)^n}{2^{n/2}(2n)!}\left(\frac{E_{\mathrm{C}}}{E_{\mathrm{J}}}\right)^{n/2}(a^\dagger + a)^{2n}. \tag{B.2}$$

Now we need to deal with the powers of the bosonic operator. In general, if we expand the $2n$-th power we will obtain 2^{2n}. We will normal order each of these terms using Wick's theorem

$$ABCD\cdots = \mathcal{N}(ABCD\dots) + \sum_{\text{1 contraction}} \mathcal{N}(\overbrace{AB}CD\dots) + \sum_{\text{2 contractions}} \mathcal{N}(\overbrace{AB}\,\overbrace{CD}\dots) + \dots \tag{B.3}$$

where $\mathcal{N}(\cdot)$ implies normal ordering and operators connected by an overline are to be contracted according to the Wick contraction rules of Eq. (3.20).

In order to do this efficiently it will prove beneficial to divide the terms of $(a^\dagger + a)^{2n}$ in three categories, terms with an equal number of creation and annihilation operators C_0^n, terms with an excess of creation operators C_+^n and terms with an excess of annihilation operators C_-^n

$$(a^\dagger + a)^{2n} = C_0^n + C_+^n + C_-^n \tag{B.4}$$

Since φ is Hermitian, the cosine in total should also be Hermitian and therefore $(C_+^n)^\dagger = C_-^n$ since C_0^n is Hermitian as well.

We treat the C_0^n terms first. Applying Wick's theorem we see that

$$C_0^n = w_{n0} a^{\dagger n} a^n + w_{n1} a^{\dagger(n-1)} a^{n-1} + \cdots + w_{nn} = \sum_{k=0}^{n} w_{nk} a^{\dagger(n-k)} a^{(n-k)} \tag{B.5}$$

with w_{nk} the combinatorial factor accounting for how many k simultaneous contractions are possible among all the permutations of the product $a^{\dagger n} a^n$.

Since we have all the permutations of $a^{\dagger n} a^n$ to consider it is obvious that all possible contractions that can appear, will appear. So we can reverse the problem by building up each term contraction by contraction. Consider the following counting problem:

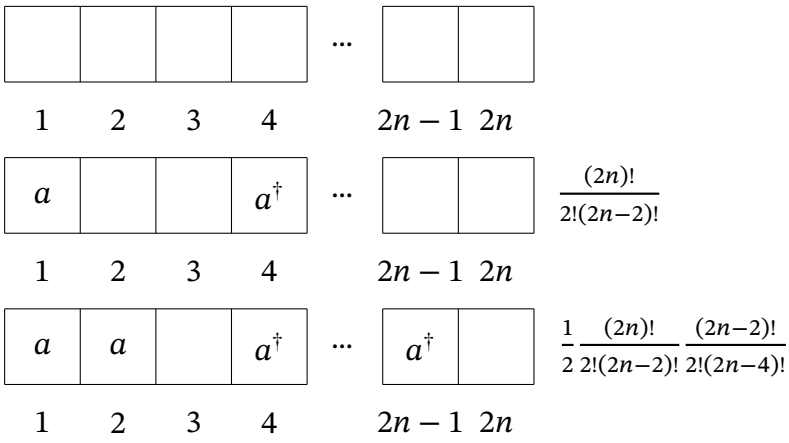

Figure B.1: Counting of Wick contractions. Graphic representation of the procedure of building up k contractions for an operator product with $2n$ ladder operators, by iteratively adding a pair and counting the possible ways to it.

Assume we start with $2n$ empty slots. For a term with k contractions we need to distribute k pairs of $a, a^\dagger$ in this order. To insert the first pair we just need to choose 2 out of $2n$ available slots, therefore we have $\binom{2n}{2}$ initial contractions and

$$\binom{2n}{2} = \frac{(2n)!}{2(2n-2)!} \tag{B.6}$$

is the binomial coefficient.

Now there are $2n-2$ slots available to place the next contraction therefore we have $\binom{2n-2}{2}$ choices and in total $\binom{2n}{2}\binom{2n-2}{2}$ choices for two pairs and so on until we place k contractions. In total we will have

$$\prod_{p=0}^{k-1}\binom{2n-2p}{2} = \frac{(2n)!}{2^k(2n-2k)!} \tag{B.7}$$

pairs of contractions. Of course in this way we have distinguished between the different permutations of the same set of contractions so we have to divide with the symmetry factor of $k!$. Finally there are $2n-2k$ positions to be filled and since we are looking at terms with an equal number of creation and annihilation operators it means we are left with $n-k$ of each. There are of course $\binom{2n-2k}{n-k}$ ways to distribute them and so in total

$$w_{nk} = \frac{(2n)!}{2^k k!(n-k)!^2}. \tag{B.8}$$

Similarly for C_+^n we will have from Wick's theorem

$$C_+^n = (C_-^n)^\dagger = \sum_{m=1}^{\infty} C_+^{(n,m)} = \sum_{m=1}^{\infty} a^{\dagger 2m} \sum_{k=0}^{n-m} w_{nk}^m a^{\dagger(n-m-k)} a^{(n-m-k)} \tag{B.9}$$

with an excess of $2m$ creation operators. The reason the excess has to be even is given by the following argument: Assume the number of annihilation operators is x and that the creation operators have an excess of y. The number of creation operators should then be $x+y$ and in total we need to have $2n$ operators per product. In other words $(x+y)+x = 2n$ and so the excess $y = 2(n-x)$ is an even number.

Now we have the Wick coefficients w_{nk}^m accounting for how many k simultaneous contractions are possible among all the permutations of the product $a^{\dagger(n+2m)}a^n$. The steps for the derivation of w_{nk}^m are identical to the ones for w_{nk} of C_0^n with the only difference in the last step. For the case of excess creation operators we be left with $n+m-k$ creation and $n-m-k$ annihilation operators to be distributed in $2n-2k$ slots thus a factor of $\binom{2n-2k}{n+m-k}$ leading to

$$w_{nk}^m = \frac{(2n)!}{2^k k!(n+m-k)!(n-m-k)!}. \tag{B.10}$$

We now combine everything back into Eq. (B.2)

$$\cos\varphi = \Lambda_0(a^\dagger a) + \sum_{m=0}^{\infty}\left(a^{\dagger 2m}\Lambda_m(a^\dagger a) + \Lambda_m(a^\dagger a)a^{2m}\right). \tag{B.11}$$

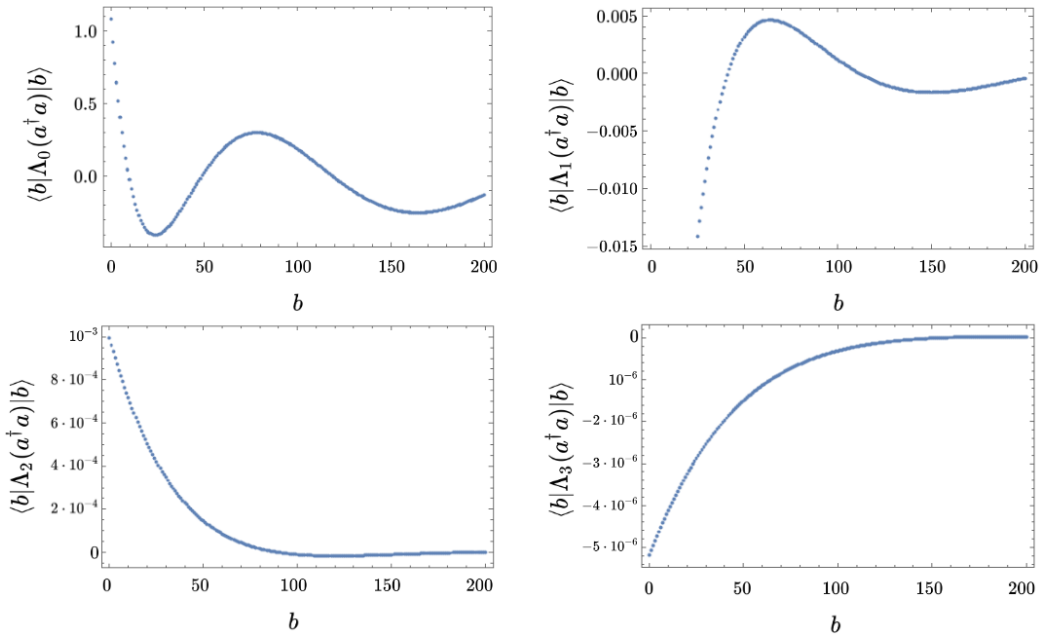

Figure B.2: Elements of the Λ functions. We plot the first 200 diagonal elements of the Λ_m function of Eq. (B.12) for $m = 0, 1, 2$ and 3. The ratio E_C/E_J is fixed at 20.

where we defined the function

$$\begin{aligned}\Lambda_m(a^\dagger a) &= \sum_{n=0}^{\infty}\sum_{k=0}^{n-m} c_n w_{nk}^m a^{\dagger(n-m-k)} a^{(n-m-k)} \\ &= (-1)^m \left(\frac{E_C}{2E_J}\right)^{m/2} e^{-\frac{1}{2}\sqrt{\frac{E_C}{2E_J}}}\, {}_1\widetilde{F}_1\left(a^\dagger a, 2m+1, \sqrt{\frac{E_C}{2E_J}}\right)\end{aligned} \tag{B.12}$$

and ${}_1\widetilde{F}_1$ is the regularized confluent hypergeometric function [B3].

In conclusion the Hamiltonian can be written in the form

$$H_{CQ} = \sqrt{2E_C E_J}\, a^\dagger a - E_J \Lambda_0(a^\dagger a) - E_J \sum_{m=0}^{\infty} \left(a^{\dagger 2m}\widetilde{\Lambda}_m(a^\dagger a) + \widetilde{\Lambda}_m(a^\dagger a) a^{2m}\right) \tag{B.13}$$

where we modified slightly the definition of the Λ_m function as

$$\widetilde{\Lambda}_m(a^\dagger a) = \Lambda_m(a^\dagger a) + \sqrt{\frac{E_C}{2E_J}}\delta_{m,1}. \tag{B.14}$$

If we employ a RWA the Hamiltonian is diagonalized in the Fock basis

$$H_{CQ} \overset{\text{RWA}}{\simeq} \sqrt{2E_C E_J}\, a^\dagger a - E_J \Lambda_0(a^\dagger a). \tag{B.15}$$

C

Moments of Polynomial Functions with Random Gaussian Variables

In this appendix we present several derivations of distributions for functions which take Gaussian random variables as arguments.

Lemma 4. *Given the random variables $X_1, X_2, \dots, X_n$ drawn from a distribution $\rho_X(x)$, the probability distribution of variable $f(X_1, X_2, \dots, X_n)$ is given by*

$$\rho_Y(y) = \int_{\mathbb{R}^n} dx_1 dx_2 \dots dx_n \rho_X(x_1)\rho_X(x_2)\dots\rho_X(x_n)\delta\left(y - f(x_1, x_2, \dots, x_n)\right) \tag{C.1}$$

Proof. Assume the variable Y which is defined as

$$Y = f(X_1, X_2, \dots, X_n). \tag{C.2}$$

The distribution of the random variable Y is related to the cumulative probability of taking a value less than why y in the following way

$$\begin{aligned}\rho_Y(y) &= \frac{d}{dy}P(Y < y) = \frac{d}{dy}P(f(X_1, X_2, \dots, X_n) < y) \\ &= \frac{d}{dy}\int_{\mathbb{R}^n} dx_1 dx_2 \dots dx_n \rho_X(x_1)\rho_X(x_2)\dots\rho_X(x_n)\theta\left(y - f(x_1, x_2, \dots, x_n)\right)\end{aligned} \tag{C.3}$$

where θ is the Heaviside function and its derivative is the Dirac delta distribution therefore we can write

$$\rho_Y(y) = \int_{\mathbb{R}^n} dx_1 dx_2 \dots dx_n \rho_X(x_1)\rho_X(x_2)\dots\rho_X(x_n)\delta\left(y - f(x_1, x_2, \dots, x_n)\right). \tag{C.4}$$

This formula offers a very intuitive definition of the distribution for the function f by integrating out all the parts of the product of the probability distributions of the individual variables that are not on the surface $f(x_1, \dots, x_n) = y$. □

Lemma 5. *For X_1 and X_2 two random variables drawn from a Gaussian distribution*

$$\rho_X(x) = \frac{1}{\sqrt{2\pi}} e^{-x^2/2}. \tag{C.5}$$

We have the following moments for the product

$$\overline{X_1^m X_2^m} = \begin{cases} 0 & m \text{ odd} \\ \left[(m-1)!!\right]^2 & m \text{ even.} \end{cases} \tag{C.6}$$

Proof. Assume a variable Y which is defined as

$$Y = X_1 X_2 \tag{C.7}$$

The probability distribution for the variable Y will be according to the result of Lemma 4

$$\rho_Y(y) = \int_{\mathbb{R}^2} dx_1 dx_2 \rho_X(x_1)\rho_X(x_2)\delta\left(y - x_1 x_2\right) \tag{C.8}$$

using the Dirac delta property

$$\delta\left(y - x_1 x_2\right) = \frac{1}{|x_1|}\delta\left(\frac{y}{x_1} - x_2\right) \tag{C.9}$$

and substituting the Gaussian distribution we obtain

$$\rho_Y(y) = \frac{1}{2\pi}\int_{\mathbb{R}} \frac{dx_1}{|x_1|} e^{-x_1^2/2} e^{-y^2/(2x_1^2)} = \frac{G_2(y^2/4)}{2\pi} \tag{C.10}$$

with $G_2(z)$ the simplified Meijer G function defined as

$$G_n(y) = \frac{1}{2\pi i}\int_{\mathbb{R}} dx \Gamma(x)^n y^{-x} \tag{C.11}$$

With the probability distribution at hand we can calculate the moments and confirm

$$\overline{Y^{2k-1}} = \overline{X_1^{2k-1}X_2^{2k-1}} = \frac{1}{2\pi}\int_{\mathbb{R}} dy\, y^{2k-1}G_2(y^2/4) = 0 \tag{C.12}$$

$$\overline{Y^{2k}} = \overline{X_1^{2k}X_2^{2k}} = \frac{1}{2\pi}\int_{\mathbb{R}} dy\, y^{2k}G_2(y^2/4) = \left[(2k-1)!!\right]^2 \tag{C.13}$$

for $k \in \mathbb{N}$ and $k \geq 1$ □

Lemma 6. *The variable*

$$Y = \frac{1}{d^m}\sum_{i,j=1}^{d} O_i O_j X_i^m X_j^m \tag{C.14}$$

with $O_1, \ldots, O_d$ some fixed real parameters and $X_1, \ldots, X_d$ a set of random variables drawn from the same Gaussian distribution

$$\rho_X(x) = \frac{1}{\sqrt{2\pi}}e^{-x^2/2}, \tag{C.15}$$

has an average value of

$$\overline{Y} = \begin{cases} \frac{(2m-1)!!}{d^{m-1}}\overline{O^2} & m \text{ odd} \\ \frac{(2m-1)!! - \left[(m-1)!!\right]^2}{d^{m-1}}\overline{O^2} + \frac{\left[(m-1)!!\right]^2}{d^{m-2}}\overline{O}^2 & m \text{ even.} \end{cases} \tag{C.16}$$

Proof. The average of Y according to the definition will be

$$\overline{Y} = \frac{1}{d^m}\sum_{i,j=1}^{d} O_i O_j \overline{X_i^m X_j^m}. \tag{C.17}$$

One might be tempted to use Lemma 5 immediately however for the summands that $i = j$ this result is not valid and these are in fact the moments of the Gaussian distribution therefore we need to separate the two cases first and then apply the lemma

$$\begin{aligned} \overline{Y} &= \frac{1}{d^m}\sum_{i=1}^{d} O_i^2 \overline{X_i^{2m}} + \frac{1}{d^m}\sum_{i\neq j=1}^{d} O_i O_j \overline{X_i^m X_j^m} \\ &= \frac{(2m-1)!!}{d^m}\sum_{i=1}^{d} O_i^2 + \frac{1}{d^m}\sum_{i\neq j=1}^{d} O_i O_j \overline{X_i^m X_j^m}. \end{aligned} \tag{C.18}$$

We now consider the two cases for m separately. For odd m the proof is completed immediately

$$\overline{Y} = \frac{(2m-1)!!}{d^m} \sum_{i=1}^{d} O_i^2 = \frac{(2m-1)!!}{d^{m-1}} \overline{O^2}. \tag{C.19}$$

While for even m we have

$$\overline{Y} = \frac{(2m-1)!!}{d^m} \sum_{i=1}^{d} O_i^2 + \frac{[(m-1)!!]^2}{d^m} \sum_{i \neq j=1}^{d} O_i O_j \tag{C.20}$$

and in order to complete the proof we add and subtract the diagonal of the second sum

$$\begin{aligned} \overline{Y} &= \frac{(2m-1)!! - [(m-1)!!]^2}{d^m} \sum_{i=1}^{d} O_i^2 + \frac{[(m-1)!!]^2}{d^m} \sum_{i,j=1}^{d} O_i O_j \\ &= \frac{(2m-1)!! - [(m-1)!!]^2}{d^{m-1}} \overline{O^2} + \frac{[(m-1)!!]^2}{d^{m-2}} \overline{O}^2 \end{aligned} \tag{C.21}$$

□

Lemma 7. *For X_1, X_2, X_3 and X_4 4 random variables drawn from a Gaussian distribution*

$$\rho_X(x) = \frac{1}{\sqrt{2\pi}} e^{-x^2/2}. \tag{C.22}$$

We have the following moments for the product

$$\overline{X_1^m X_2^m X_3^m X_4^m} = \begin{cases} 0 & m \text{ odd} \\ [(m-1)!!]^4 & m \text{ even.} \end{cases} \tag{C.23}$$

Proof. Assume the variables Y_1 and Y_2 defined as

$$Y_1 = X_1 X_2 \qquad Y_2 = X_3 X_4 \tag{C.24}$$

and their product $Z = Y_1 Y_2$ The probability distribution for the variable Z will be according to the result of Lemma 4

$$\rho_Z(z) = \int_{\mathbb{R}^2} dy_1 dy_2 \rho_Y(y_1) \rho_Y(y_2) \delta(z - y_1 y_2) \tag{C.25}$$

using the Dirac delta property

$$\delta(z - y_1 y_2) = \frac{1}{|y_1|} \delta\left(\frac{z}{y_1} - y_2\right) \tag{C.26}$$

and substituting the distribution of the Y variables from Lemma 5 we obtain

$$\rho_Y(y) = \frac{1}{4\pi^2}\int_{\mathbb{R}} \frac{dx_1}{|x_1|} G_2(y_1^2/4) G_2(z^2/(4y_1^2)) = \frac{G_4(z^2/16)}{4\pi^2} \tag{C.27}$$

With the probability distribution at hand we can calculate the moments and confirm

$$\overline{Z^{2k-1}} = \overline{X_1^{2k-1}X_2^{2k-1}X_3^{2k-1}X_3^{2k-1}} = \frac{1}{4\pi^2}\int_{\mathbb{R}} dz\, z^{2k-1} G_4(z^2/16) = 0 \tag{C.28}$$

$$\overline{Z^{2k}} = \overline{X_1^{2k}X_2^{2k}X_3^{2k}X_4^{2k}} = \frac{1}{4\pi^2}\int_{\mathbb{R}} dz\, z^{2k} G_4(z^2/16) = \left[(2k-1)!!\right]^4 \tag{C.29}$$

for $k \in \mathbb{N}$ and $k \geq 1$ □

Lemma 8. *The variable*

$$\mathrm{Z} = \frac{1}{d^{2m}} \sum_{i,j=1}^{d} O_i O_j X_i^m X_j^m Y_i^m Y_j^m \tag{C.30}$$

with $O_1, \ldots, O_d$ some fixed real parameters and $X_1, \ldots, X_d$ and $Y_1, \ldots, Y_d$ two sets of random variables drawn from the same Gaussian distribution

$$\rho_X(s) = \rho_Y(s) = \frac{1}{\sqrt{2\pi}} e^{-s^2/2}, \tag{C.31}$$

has an average value of

$$\overline{Z} = \begin{cases} \frac{\left[(2m-1)!!\right]^2}{d^{2m-1}}\overline{O^2} & m \text{ odd} \\ \frac{\left[(2m-1)!!\right]^2 - \left[(m-1)!!\right]^4}{d^{2m-1}}\overline{O^2} + \frac{\left[(m-1)!!\right]^4}{d^{2m}}\overline{O}^2 & m \text{ even.} \end{cases} \tag{C.32}$$

Proof. The average of Z according to the definition will be

$$\overline{Z} = \frac{1}{d^m} \sum_{i,j=1}^{d} O_i O_j \overline{X_i^m X_j^m Y_i^m Y_j^m}. \tag{C.33}$$

Similarly to the proof of Lemma 6 we cannot apply Lemma 7 immediately therefore we need to separate the two cases of $i = j$ and $i \neq j$ first and then apply the appropriate Lemmas

$$\begin{aligned} \overline{Z} &= \frac{1}{d^{2m}} \sum_{i=1}^{d} O_i^2 \overline{X_i^{2m} Y_i^{2m}} + \frac{1}{d^{2m}} \sum_{i,j=1}^{d} O_i O_j \overline{X_i^m X_j^m Y_i^m Y_j^m} \\ &= \frac{\left[(2m-1)!!\right]^2}{d^{2m}} \sum_{i=1}^{d} O_i^2 + \frac{1}{d^{2m}} \sum_{i\neq j=1}^{d} O_i O_j \overline{X_i^m X_j^m Y_i^m Y_j^m}. \end{aligned} \tag{C.34}$$

We now consider the two cases for m separately. For odd m the proof is completed immediately

$$\overline{Z} = \frac{\left[(2m-1)!!\right]^2}{d^{2m}} \sum_{i=1}^{d} O_i^2 = \frac{\left[(2m-1)!!\right]^2}{d^{2m-1}} \overline{O^2}. \tag{C.35}$$

While for even m we have

$$\overline{Z} = \frac{\left[(2m-1)!!\right]^2}{d^{2m}} \sum_{i=1}^{d} O_i^2 + \frac{\left[(m-1)!!\right]^4}{d^{2m}} \sum_{i \neq j=1}^{d} O_i O_j \tag{C.36}$$

and in order to complete the proof we add and subtract the diagonal of the second sum

$$\begin{aligned} \overline{Z} &= \frac{\left[(2m-1)!!\right]^2 - \left[(m-1)!!\right]^4}{d^{2m}} \sum_{i=1}^{d} O_i^2 + \frac{\left[(m-1)!!\right]^4}{d^{2m}} \sum_{i,j=1}^{d} O_i O_j \\ &= \frac{\left[(2m-1)!!\right]^2 - \left[(m-1)!!\right]^4}{d^{2m-1}} \overline{O^2} + \frac{\left[(m-1)!!\right]^4}{d^{2m}} \overline{O}^2 \end{aligned} \tag{C.37}$$

□

D

Explicit Second Order Perturbation Theory Walsh-Hadamard coefficients

We will present the Walsh-Hadamard coefficient results from perturbation theory of section 3.2 in an explicit form. We will make use of all the conventions in that section and additionally we will use a different notation for the Walsh-Hadamard coefficients. Specifically assuming some coefficient w corresponding to a bitstring of weight m with non-zero digits at positions ℓ_1 through ℓ_m, we will denote the n-th order correction to that coefficient as $w^{(n)}_{\ell_1 \ldots \ell_m}$.

Perturbation terms of the weight zero bitstrings:

$$w_0^{(0)} = \frac{E_\mu}{2} \tag{D.1}$$

$$w_0^{(1)} = \frac{1}{4}|\varepsilon_{\mu\nu}|\mathcal{E}_{\mu\nu} \tag{D.2}$$

$$w_0^{(2)} = \left(\frac{1}{4}|\varepsilon_{\alpha\beta}| + |\varepsilon_{\alpha\beta\mu}|\right)\mathcal{D}_{\alpha\beta\mu\nu} + |\varepsilon_{\alpha\beta\mu}|\mathcal{S}_{\alpha\beta\mu\nu} \tag{D.3}$$

Perturbation terms of the weight one bitstrings:

$$w_{\ell_1}^{(0)} = \frac{E_{\ell_1}}{2} \tag{D.4}$$

$$w_{\ell_1}^{(1)} = \frac{1}{2}|\varepsilon_{\mu\ell_1}|\mathcal{E}_{\mu\ell_1} \tag{D.5}$$

$$w_{\ell_1}^{(2)} = \left(\frac{1}{2}|\varepsilon_{\ell_1\beta}| + 2|\varepsilon_{\ell_1\beta\mu}| - |\varepsilon_{\ell_1\mu\nu}|\right)\mathcal{D}_{\ell_1\beta\mu\nu} + |\varepsilon_{\ell_1\beta\mu}|\left(2\mathcal{S}_{\ell_1\beta\mu\nu} + \mathcal{S}_{\beta\mu\nu\ell_1}\right) \tag{D.6}$$

Perturbation terms of the weight two bitstrings:

$$w^{(0)}_{\ell_1\ell_2} = 0 \tag{D.7}$$

$$w^{(1)}_{\ell_1\ell_2} = \frac{1}{2}\mathcal{E}_{\ell_1\ell_2} \tag{D.8}$$

$$\begin{aligned} w^{(2)}_{\ell_1\ell_2} = &\left(\frac{1}{2} + |\varepsilon_{\ell_1\ell_2\mu}|\right)\mathcal{D}_{\ell_1\ell_2\mu\nu} + 2\left(|\varepsilon_{\ell_1\ell_2\mu}| - |\varepsilon_{\ell_1\ell_2\nu}|\right)\mathcal{D}_{\mu\ell_1\ell_2\nu} \\ &+ 2|\varepsilon_{\ell_1\ell_2\mu}|\left(\mathcal{S}_{\ell_1\ell_2\mu\nu} + \mathcal{S}_{\mu\ell_1\ell_2\nu} + \mathcal{S}_{\mu\ell_2\ell_1\nu}\right) \end{aligned} \tag{D.9}$$

Perturbation terms of the weight three bitstrings:

$$w^{(0)}_{\ell_1\ell_2\ell_3} = 0 \tag{D.10}$$

$$w^{(1)}_{\ell_1\ell_2\ell_3} = 0 \tag{D.11}$$

$$w^{(2)}_{\ell_1\ell_2\ell_3} = 2\left(\mathcal{D}_{\ell_1\ell_2\ell_3\nu} + \mathcal{D}_{\ell_1\ell_3\ell_2\nu} + \mathcal{D}_{\ell_2\ell_3\ell_1\nu} + \mathcal{S}_{\ell_1\ell_2\ell_3\nu} + \mathcal{S}_{\ell_1\ell_3\ell_2\nu} + \mathcal{S}_{\ell_2\ell_3\ell_1\nu}\right) \tag{D.12}$$

References

Articles covering the presented results

A1 C. Berke, E. Varvelis, S. Trebst, A. Altland and D. P. DiVincenzo:
'Transmon platform for quantum computing challenged by chaotic fluctuations',
Nature communications **13**, 1–10 (2022).

A2 E. Varvelis and D. P. DiVincenzo:
'Perturbative analysis of quasi-periodic patterning of transmon quantum computers: enhancement of many-body localization',
arXiv preprint arXiv:2212.03805 (2022).

Books

B1 M. Nielsen and I. Chuang:
Quantum computation and quantum information,
Cambridge Series on Information and the Natural Sciences (Cambridge University Press, 2000).

B2 M. Tinkham:
Introduction to superconductivity, volume second edition,
(Dover Publications Inc., Mineola, New York, 2004).

B3 G. B. Arfken and H. J. Weber:
Mathematical methods for physicists,
(American Association of physics teachers, 1999).

B4 J. Gambetta:
Quantum Information Processing: Lecture Notes of the 44th IFF Spring School,
(Forschungszentrum Jülich, 2013).

B5 M. L. Mehta:
Random matrices,
(Elsevier, 2004).

B6 Y. A. Farkov, P. Manchanda and A. H. Siddiqi:
Introduction to Walsh Analysis and Wavelets,
(2019), pp. 1–25.

Articles, proceedings and theses

1 R. Feynman:
'Simulating physics with computers',
Int J Theor Phys **21**, 467–488 (1982).

2 P. Shor:
'Algorithms for quantum computation: discrete logarithms and factoring',
in Proceedings 35th annual symposium on foundations of computer science (1994), pp. 124–134.

3 F. Arute, K. Arya, R. Babbush, D. Bacon, J. C. Bardin, R. Barends, R. Biswas, S. Boixo, F. G. S. L. Brandao, D. A. Buell, B. Burkett, Y. Chen, Z. Chen, B. Chiaro, R. Collins, W. Courtney, A. Dunsworth, E. Farhi, B. Foxen, A. Fowler, C. Gidney, M. Giustina, R. Graff, K. Guerin, S. Habegger, M. P. Harrigan, M. J. Hartmann, A. Ho, M. Hoffmann, T. Huang, T. S. Humble, S. V. Isakov, E. Jeffrey, Z. Jiang, D. Kafri, K. Kechedzhi, J. Kelly, P. V. Klimov, S. Knysh, A. Korotkov, F. Kostritsa, D. Landhuis, M. Lindmark, E. Lucero, D. Lyakh, S. Mandrà, J. R. McClean, M. McEwen, A. Megrant, X. Mi, K. Michielsen, M. Mohseni, J. Mutus, O. Naaman, M. Neeley, C. Neill, M. Y. Niu, E. Ostby, A. Petukhov, J. C. Platt, C. Quintana, E. G. Rieffel, P. Roushan, N. C. Rubin, D. Sank, K. J. Satzinger, V. Smelyanskiy, K. J. Sung, M. D. Trevithick, A. Vainsencher, B. Villalonga, T. White, Z. J. Yao, P. Yeh, A. Zalcman, H. Neven and J. M. Martinis:
'Quantum supremacy using a programmable superconducting processor',
Nature **574**, 505–510 (2019).

4 Y. Wu, W.-S. Bao, S. Cao, F. Chen, M.-C. Chen, X. Chen, T.-H. Chung, H. Deng, Y. Du, D. Fan, M. Gong, C. Guo, C. Guo, S. Guo, L. Han, L. Hong, H.-L. Huang, Y.-H. Huo, L. Li, N. Li, S. Li, Y. Li, F. Liang, C. Lin, J. Lin, H. Qian, D. Qiao, H. Rong, H. Su, L. Sun, L. Wang, S. Wang, D. Wu, Y. Xu, K. Yan, W. Yang, Y. Yang, Y. Ye, J. Yin, C. Ying, J. Yu, C. Zha, C. Zhang, H. Zhang, K. Zhang, Y. Zhang, H. Zhao, Y. Zhao, L. Zhou, Q. Zhu, C. Y. Lu, C.-Z. Peng, X. Zhu and J.-W. Pan:
'Strong quantum computational advantage using a superconducting quantum processor',
Phys. Rev. Lett. **127**, 180501 (2021).

5 *Https://www.ibm.com/quantum-computing/.*

6 O. Bohigas, M. J. Giannoni and C. Schmit:
'Characterization of chaotic quantum spectra and universality of level fluctuation laws',
Phys. Rev. Lett. **52**, 1–4 (1984).

7 T. Orell, A. A. Michailidis, M. Serbyn and M. Silveri:
'Probing the many-body localization phase transition with superconducting circuits',
Phys. Rev. B **100**, 134504 (2019).

8 J. Eisert, M. Cramer and M. B. Plenio:
'Colloquium: area laws for the entanglement entropy',
Rev. Mod. Phys. **82**, 277–306 (2010).

9 D. Loss and D. P. DiVincenzo:
'Quantum computation with quantum dots',
Phys. Rev. A **57**, 120–126 (1998).

10 J. H. Eberly, N. B. Narozhny and J. J. Sanchez-Mondragon:
'Periodic spontaneous collapse and revival in a simple quantum model',
Phys. Rev. Lett. **44**, 1323–1326 (1980).

11 A. Blais, A. L. Grimsmo, S. M. Girvin and A. Wallraff:
'Circuit quantum electrodynamics',
Rev. Mod. Phys. **93**, 025005 (2021).

12 J. Koch, T. M. Yu, J. Gambetta, A. A. Houck, D. I. Schuster, J. Majer, A. Blais, M. H. Devoret, S. M. Girvin and R. J. Schoelkopf:
'Charge-insensitive qubit design derived from the Cooper pair box',
Phys. Rev. A **76**, 042319 (2007).

13 D. Zeuch, F. Hassler, J. J. Slim and D. P. DiVincenzo:
'Exact rotating wave approximation',
Annals of physics **423**, 168327 (2020).

14 N. Ullah:
'Invariance hypothesis and higher correlations of hamiltonian matrix elements',
Nuclear Physics **58**, 65–71 (1964).

15 J. M. Deutsch:
'Quantum statistical mechanics in a closed system',
Phys. Rev. A **43**, 2046–2049 (1991).

16 M. Srednicki:
'The approach to thermal equilibrium in quantized chaotic systems',
Journal of Physics A: Mathematical and General **32**, 1163 (1999).

17 P. W. Anderson:
'Absence of Diffusion in Certain Random Lattices',
Phys. Rev. **109**, 1492–1505 (1958).

18 E. Abrahams, P. W. Anderson, D. C. Licciardello and T. V. Ramakrishnan:
'Scaling theory of localization: absence of quantum diffusion in two dimensions',
Phys. Rev. Lett. **42**, 673–676 (1979).

19 D. A. Huse, R. Nandkishore and V. Oganesyan:
'Phenomenology of fully many-body-localized systems',
Phys. Rev. B **90**, 174202 (2014).

20 M. Serbyn, Z. Papi ć and D. A. Abanin:
'Local conservation laws and the structure of the many-body localized states',
Phys. Rev. Lett. **111**, 127201 (2013).

21 J. Z. Imbrie:
'Diagonalization and many-body localization for a disordered quantum spin chain',
Phys. Rev. Lett. **117**, 027201 (2016).

22 J.-y. Choi, S. Hild, J. Zeiher, P. Schauß, A. Rubio-Abadal, T. Yefsah, V. Khemani, D. A. Huse, I. Bloch and C. Gross:
'Exploring the many-body localization transition in two dimensions',
Science **352**, 1547–1552 (2016).

23 I. Aleiner, B. Altshuler and G. Shlyapnikov:
'A finite-temperature phase transition for disordered weakly interacting bosons in one dimension',
Nature Physics **6**, 900–904 (2010).

24 T. B. Wahl, A. Pal and S. H. Simon:
'Signatures of the many-body localized regime in two dimensions',
Nature Physics **15**, 164–169 (2019).

25 S. W. Kim, G. De Tomasi and M. Heyl:
'Real-time dynamics of one-dimensional and two-dimensional bosonic quantum matter deep in the many-body localized phase',
Phys. Rev. B **104**, 144205 (2021).

26 Y. Y. Atas, E. Bogomolny, O. Giraud and G. Roux:
'Distribution of the ratio of consecutive level spacings in random matrix ensembles',
Phys. Rev. Lett. **110**, 084101 (2013).

27 W.-L. You, Y.-W. Li and S.-J. Gu:
'Fidelity, dynamic structure factor, and susceptibility in critical phenomena',
Phys. Rev. E **76**, 022101 (2007).

28 P. Plötz, M. Lubasch and S. Wimberger:
'Detection of avoided crossings by fidelity',
Physica A: Statistical Mechanics and its Applications **390**, 1363–1369 (2011).

29 S.-J. Gu and H.-Q. Lin:
'Scaling dimension of fidelity susceptibility in quantum phase transitions',
Europhysics Letters **87**, 10003 (2009).

30 I. V. Beloussov:
'Another formulation of the Wick's theorem. Farewell, pairing?',
Special Matrices **3**, 169–174 (2015).

31 M. C. Smith:
'The inerter: a retrospective',
Annual Review of Control, Robotics, and Autonomous Systems **3**, 361–391 (2020).

32 O. Bohigas, M. Giannoni and C. Schmit:
'Spectral properties of the laplacian and random matrix theories',
Journal de Physique Lettres **45**, 1015–1022 (1984).

33 P. Jurcevic and L. C. Govia:
'Effective qubit dephasing induced by spectator-qubit relaxation',
Quantum Science and Technology **7**, 045033 (2022).

34 N. Macé, F. Alet and N. Laflorencie:
'Multifractal scalings across the many-body localization transition',
Phys. Rev. Lett. **123**, 180601 (2019).

35 J. Ku, X. Xu, M. Brink, D. C. McKay, J. B. Hertzberg, M. H. Ansari and B. L. T. Plourde:
'Suppression of unwanted zz interactions in a hybrid two-qubit system',
Phys. Rev. Lett. **125**, 200504 (2020).

36 E. Magesan and J. M. Gambetta:
'Effective hamiltonian models of the cross-resonance gate',
Phys. Rev. A **101**, 052308 (2020).

37 N. Sundaresan, I. Lauer, E. Pritchett, E. Magesan, P. Jurcevic and J. M. Gambetta:
'Reducing unitary and spectator errors in cross resonance with optimized rotary echoes',
PRX Quantum **1**, 020318 (2020).

38 J. B. Hertzberg, E. J. Zhang, S. Rosenblatt, E. Magesan, J. A. Smolin, J.-B. Yau, V. P. Adiga, M. Sandberg, M. Brink, J. M. Chow et al.:
'Laser-annealing josephson junctions for yielding scaled-up superconducting quantum processors',
npj Quantum Information **7**, 129 (2021).

39 R. Versluis, S. Poletto, N. Khammassi, B. Tarasinski, N. Haider, D. J. Michalak, A. Bruno, K. Bertels and L. DiCarlo:
'Scalable quantum circuit and control for a superconducting surface code',
Phys. Rev. Appl. **8**, 034021 (2017).

40 A. D. Córcoles, A. Kandala, A. Javadi-Abhari, D. T. McClure, A. W. Cross, K. Temme, P. D. Nation, M. Steffen and J. M. Gambetta:
'Challenges and Opportunities of Near-Term Quantum Computing Systems',
Proceedings of the IEEE **108**, 1338–1352 (2020).

41 C. K. Andersen, A. Remm, S. Lazar, S. Krinner, N. Lacroix, G. J. Norris, M. Gabureac, C. Eichler and A. Wallraff:
'Repeated quantum error detection in a surface code',
Nature Physics **16**, 875–880 (2020).

42 A. G. Fowler, M. Mariantoni, J. M. Martinis and A. N. Cleland:
'Surface codes: towards practical large-scale quantum computation',
Phys. Rev. A **86**, 032324 (2012).

43 A. C. Potter, R. Vasseur and S. A. Parameswaran:
'Universal Properties of Many-Body Delocalization Transitions',
Phys. Rev. X **5**, 031033 (2015).

44 L. DiCarlo, J. M. Chow, J. M. Gambetta, L. S. Bishop, B. R. Johnson, D. Schuster, J. Majer, A. Blais, L. Frunzio, S. Girvin et al.:
'Demonstration of two-qubit algorithms with a superconducting quantum processor',
Nature **460**, 240–244 (2009).

45 F. Yan, P. Krantz, Y. Sung, M. Kjaergaard, D. L. Campbell, T. P. Orlando, S. Gustavsson and W. D. Oliver:
'Tunable Coupling Scheme for Implementing High-Fidelity Two-Qubit Gates',
Phys. Rev. Applied **10**, 054062 (2018).

46 X. Xu and M. Ansari:
'ZZ Freedom in Two-Qubit Gates',
Phys. Rev. Applied **15**, 064074 (2021).

47 F. Evers and A. D. Mirlin:
'Anderson transitions',
Rev. Mod. Phys. **80**, 1355–1417 (2008).

48 S. Aubry and G. André:
'Analyticity breaking and Anderson localization in incommensurate lattices',
Ann. Israel Phys. Soc **3**, 18 (1980).

49 Y. E. Kraus, Y. Lahini, Z. Ringel, M. Verbin and O. Zilberberg:
'Topological States and Adiabatic Pumping in Quasicrystals',
Phys. Rev. Lett. **109**, 106402 (2012).

50 G. Roati, C. D'Errico, L. Fallani, M. Fattori, C. Fort, M. Zaccanti, G. Modugno, M. Modugno and M. Inguscio:
'Anderson localization of a non-interacting Bose–Einstein condensate',
Nature **453**, 895–898 (2008).

51 Szabó, Attila and Schneider, Ulrich:
'Mixed spectra and partially extended states in a two-dimensional quasiperiodic model',
Phys. Rev. B **101**, 014205 (2020).

52 D. Johnstone, P. Öhberg and C. W. Duncan:
'The mean-field Bose glass in quasicrystalline systems',
Journal of Physics A: Mathematical and Theoretical **54**, 395001 (2021).

53 M. Gonçalves, B. Amorim, E. V. Castro and P. Ribeiro:
'Hidden dualities in 1D quasiperiodic lattice models',
SciPost Phys. **13**, 046 (2022).

54 V. W. de Spinadel:
'The metallic means family and multifractal spectra',
Nonlinear Analysis: Theory, Methods & Applications **36**, 721–745 (1999).

55 T. Proctor, K. Rudinger, K. Young, E. Nielsen and R. Blume-Kohout:
'Measuring the capabilities of quantum computers',
Nature Physics **18**, 75–79 (2022).

56 Møller, Chr. and Plesset, M. S.:
'Note on an Approximation Treatment for Many-Electron Systems',
Phys. Rev. **46**, 618–622 (1934).

57 J. A. Pople, J. S. Binkley and R. Seeger:
'Theoretical models incorporating electron correlation',
International Journal of Quantum Chemistry **10**, 1–19 (1976).